Supplementary Information

Consequences of Encapsulated vs Covalently Attached Pd-NHC Amphiphilic Polymeric Nanocatalysts in Bioorthogonal Catalysis

Lieke de Jonge, Ibai Hazenberg, Harshit Singh, Tessa Loman, A. P. Prakasham*, and Anja R. A. Palmans*

Department of Chemical Engineering & Chemistry and Institute for Complex Molecular Systems, Eindhoven University of Technology, P.O. Box 513, 5600 MB Eindhoven, The Netherlands.

E-mail: a.palmans@tue.nl, a.p.prakasham@tue.nl

Table of Contents

1. General information

All commercial chemicals were purchased from Merck, TCI, Thermo Fisher Scientific, Alfa Aesar, Aaron chemicals and used without further purification. All solvents were purchased from Biosolve. Dry solvents were obtained with an MBRAUN solvent purification system. Deuterated solvents ($CDCl_3$ from Cambridge Isotope Laboratories, DMSO-d_6 from Deutero GmbH) were purchased and used as received. L-Pyroglutamic acid, $PdBr_2$, NaN_3 and dibenzocyclooctyne-amine from Merck, trimethyloxonium tetrafluoroborate from Thermoscientific, pentafluorophenyl acrylate from ABCR GmbH (acrylate monomer was first filtered with neutral alumina column to remove inhibitor and afterwards used), Jeffamine M1000 was purchased from Huntsman Holland BV (pre-dried over P_2O_5 in vacuum oven overnight before using). The 6-8 kDa molecular weight cut-off spectra/por 1 dialysis tubing was purchased from repligen. Gibco Dulbecco's Modified Eagle Medium, (DMEM, D-Glucose concentration 4.5 g/L, with L-Glutamine, without Pyruvate) and Gibco Roswell Park Memorial Institute, (RPMI, D-glucose concentration 4.5 g/L, HEPES buffer concentration 2.383 g/L, with sodium bicarbonate concentration 1.5 g/L, with sodium pyruvate concentration 110 mg/L, and with L-glutamine) were purchased from Fischer Scientific. Cell Counting Kit-8 (CCK-8) kit was obtained from Sigma-Aldrich, live cell imaging solution was obtained from Thermo Fisher scientific and used directly. (*S*)-5-(Azidomethyl)pyrrolidin-2-one (**s5**),[1] amphiphilic 80 % Jeffamine®M1000 and 20 % dodecyl amine polymer[2] were synthesized using a modified procedure from the literature. NMR spectra were recorded on Bruker Avance III 400 MHz spectrometer. ^1H and $^{13}C\{^1H\}$ NMR signals are reported in ppm downfield from TMS. ^1H signals are referenced to the residual proton of a deuterated solvent 7.26 ppm for $CDCl_3$. $^{13}C\{^1H\}$ signals are referenced to the solvent signal at 39.52 ppm for DMSO-d_6. ^1H NMR peaks are labelled as singlet (s), doublet (d), triplet (t), broad (br), quartet (q), sextet, septet (sept), doublet of doublets (dd), triplet of triplets (tt) and multiplet (m). Matrix-assisted laser desorption/ionization time-of-flight followed by mass spectrometry (MALDI-ToF-MS) measurements were performed on a Bruker Autoflex Speed using α-cyano-4-hydroxycinnamic acid (CHCA) and trans-2-[3-(4-tert-butylphenyl)-2-methyl-2- propenylidene]malononitrile (DCTB) as matrices. Infra-red (IR) spectroscopy was performed on a Shimadzu IRTracer 100, using a KBr pellet. UV-Vis measurements were performed on Agilent Cary 3500 multicell UV-Vis spectrophotometer using 1 cm pathlength quartz cuvettes and disposable cuvettes. Fluorescence measurements were performed on Agilent Cary eclipse fluorescence spectrophotometer using 1 cm × 1 cm pathlength quartz cuvettes. Dynamic light scattering (DLS) experiments were performed with a Malvern Zetasizer nano μV with a 830 nm laser at an angle of scattering at 90°. Size-exclusion chromatography (SEC) measurements were carried out on a Shimadzu system. High performance liquid chromatography (HPLC) – UV experiments were performed using Shimadzu UFLC-XR with PDA detector. Cell viability visualization absorbance was recorded at Tecan SPARK microplate reader. Inductively coupled plasma-optical emission spectroscopy (ICP-OES) was performed on thermo scientific icap pro X instrument. SAXS was measured on beamline BM29 (BioSAXS) at the European Synchrotron Radiation Facility.

2. Experimental section

2.1. Synthesis of pre-NHC ligand (1)

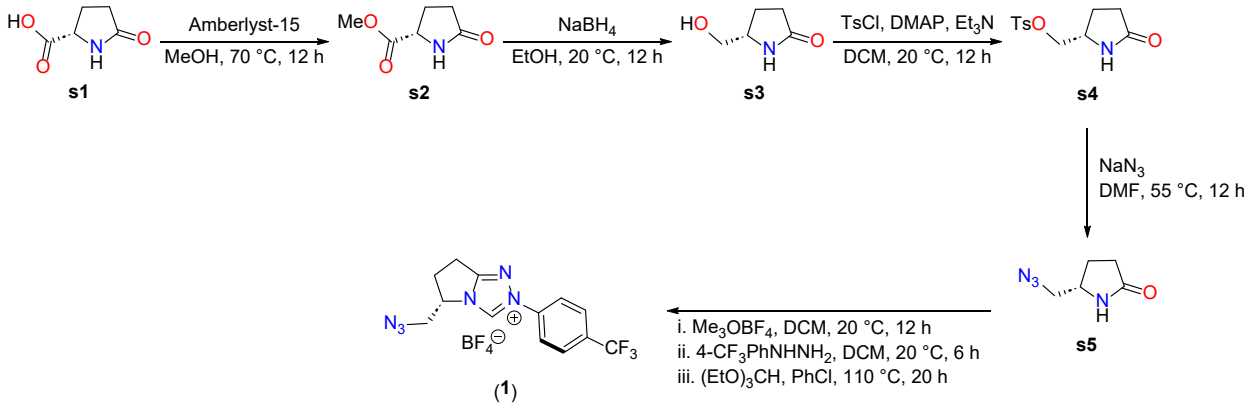

Scheme S1. Synthesis of pre-NHC ligand (**1**).

To a DCM solution (*ca*. 15 mL, anhydrous) of (*S*)-5-(azidomethyl)pyrrolidin-2-one (**s5**) (1.00 g, 7.14 mmol) in a 100 mL RB, Meerwein's salt (trimethyloxonium tetrafluoroborate, rapidly decomposes upon exposure to atmospheric moisture) (1.16 g, 7.85 mmol) was added and the reaction mixture was stirred at room temperature for 12 hours under Ar atmosphere. Subsequently, 4-(trifluoromethyl)phenylhydrazine (1.57 g, 8.92 mmol) was added as a DCM (*ca*. 2 mL) solution to the reaction mixture and continued stirring for another 6 hours. Then the DCM was evaporated under vacuum through the Schlenk line. Thus obtained residue was redissolved in chlorobenzene (*ca*. 15 mL) in the same RB and triethylorthoformate (5.29 g, 35.68 mmol) was added and the reaction mixture was heated at 110 °C for 20 hours under Ar atmosphere. After the reaction, all the volatiles were evaporated under reduced pressure and the obtained solid was triturated with DCM/Et_2O and further washed with Et_2O to get the precarbene ligand (**1**) as a brown solid (2.34 g) in 83 % yield. ^{1}H NMR (400 MHz, $CDCl_3$, 25 °C, δ ppm): 10.18 (s, 1H, NC*H*N), 7.99 (d, J = 8.0 Hz, 2H), 7.78 (d, J = 8.0 Hz, 2H), 5.16 (sextet, J = 4.0 Hz, 1H), 4.21 (dd, J = 16.0 Hz and 4.0 Hz, 1H), 3.80 (dd, J = 16.0 Hz and 4.0 Hz, 1H), 3.29-3.24 (m, 2H), 3.11-3.01 (m, 1H), 2.69-2.60 (m, 1H). ^{13}C{^{1}H} NMR (100 MHz, DMSO-d_6, 25 °C, δ ppm): 162.74 (C_q), 139.27 (N*C*HN), 138.43 (quat, C_q, J_{CF} = 1 Hz), 130.34 (quat, $^2J_{CF}$ = 33 Hz), 127.57 (quat, $^3J_{CF}$ = 4 Hz), 123.58 (quat, $^1J_{CF}$ = 271 Hz, *C*F_3), 121.53 (2 × *C*H_{Ar}), 59.68, 51.91, 30.10, 21.01.[3] ^{19}F{^{1}H} NMR (376 MHz, $CDCl_3$, 25 °C, δ ppm): −61.25 (C*F*$_3$), −148.40 (^{10}B*F*$_4$), −148.46 (^{11}B*F*$_4$). MALDI-ToF-MS: *m/z* calcd. for $C_{13}H_{12}N_6F_3^+$: 309.11, found: 309.11 $[M-BF_4]^+$.

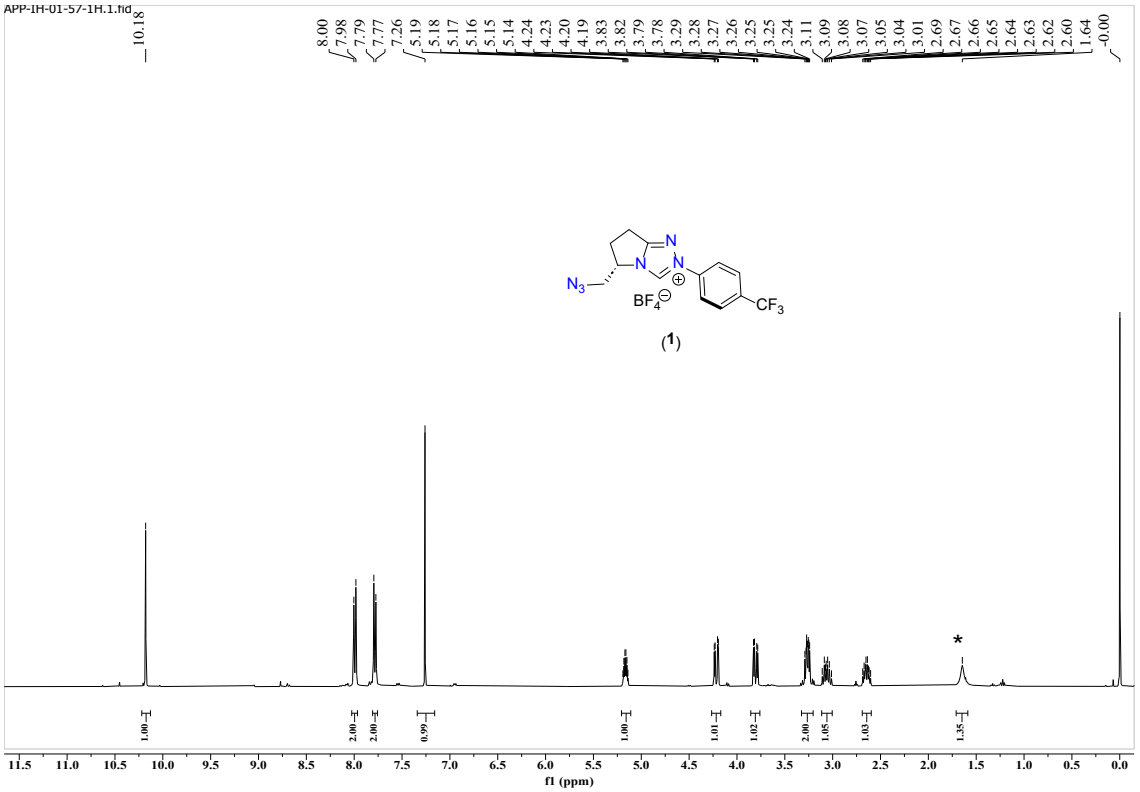

Figure S1. ^{1}H NMR of pre-NHC ligand (**1**) in $CDCl_3$. * H_2O.

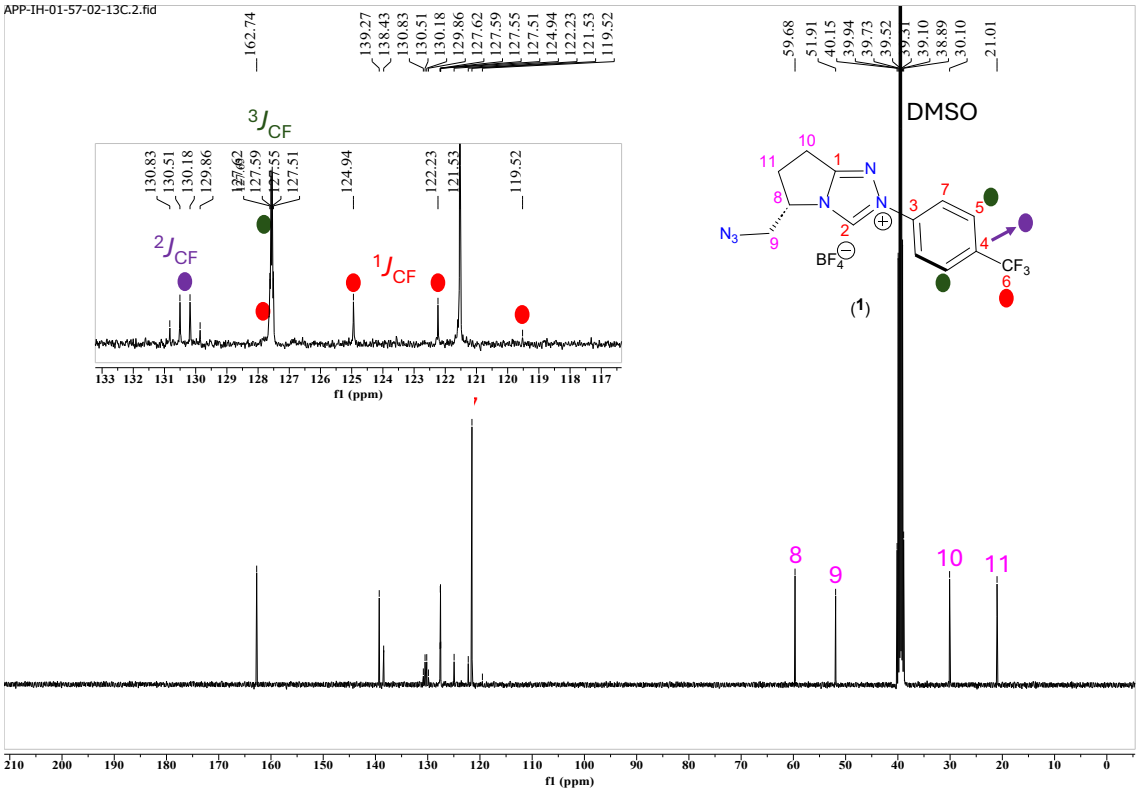

Figure S2. $^{13}C\{^{1}H\}$ NMR of pre-NHC ligand (**1**) in DMSO-d_6, inset showing C-F coupling.

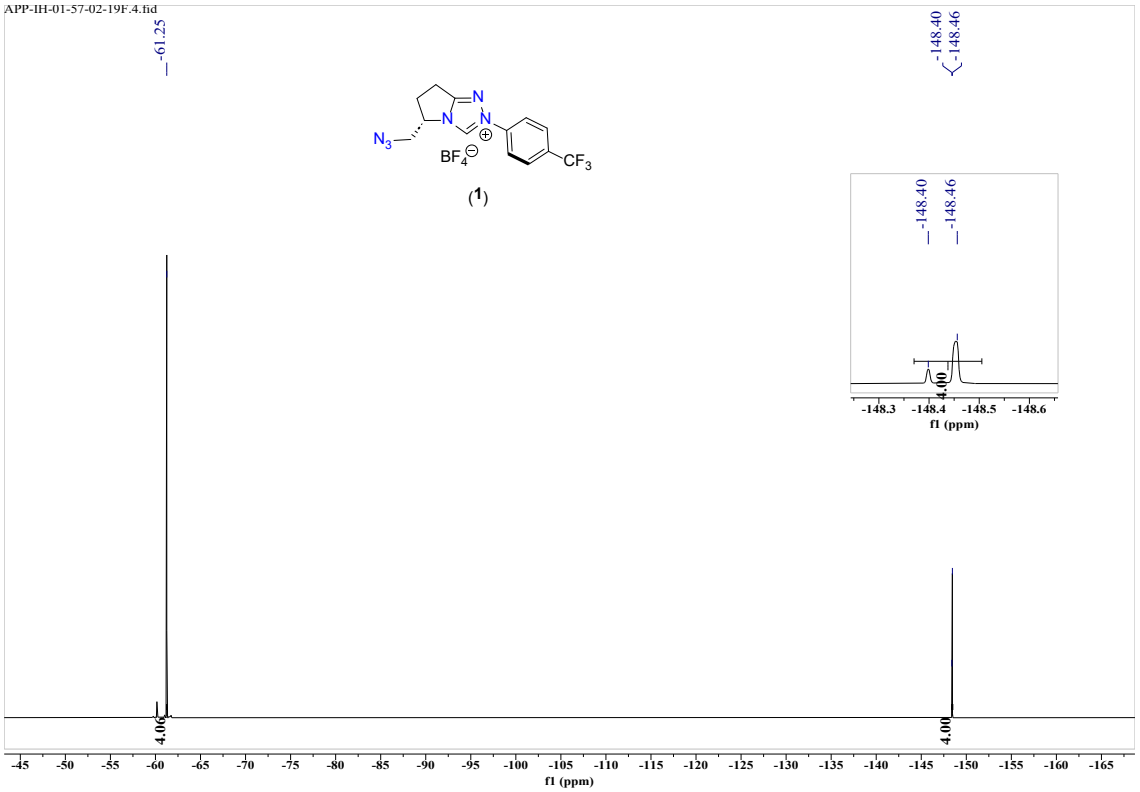

Figure S3. $^{19}F\{^{1}H\}$ NMR of pre-NHC ligand (**1**) in $CDCl_3$, inset $^{11}B\underline{F}_4$ and $^{10}B\underline{F}_4$ isotopes.

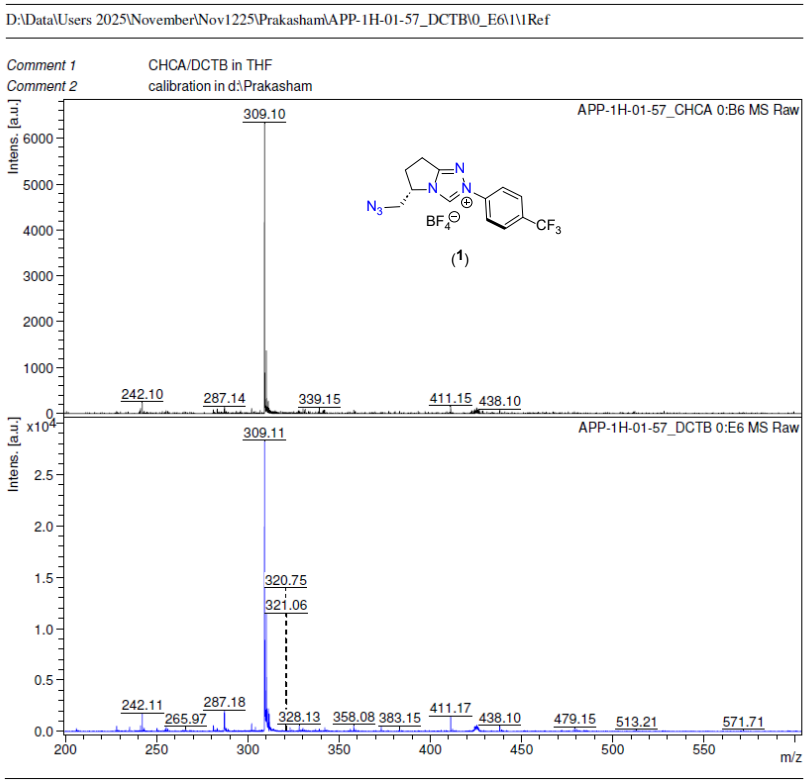

Figure S4. MALDI-ToF-MS spectra of pre-NHC ligand (**1**).

2.2. Synthesis of Pd-NHC complex (2)

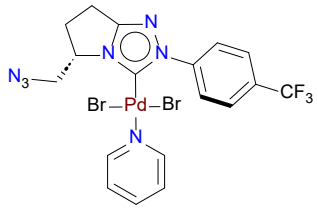

(2)

The pre-NHC ligand (**1**) (0.250 g, 0.631 mmol), $PdBr_2$ (0.168 g, 0.631 mmol), K_2CO_3 (0.131 g, 0.947 mmol), and KBr (0.075 g, 0.631 mmol) were added to an oven dried round bottom flask and to which pyridine (*ca*. 5 mL) was added. The RB was connected to a water condenser and was placed in a pre-heated oil bath at 110 °C and left stirring for 16 h under argon atmosphere. After completion of the reaction, the reaction mixture was cooled to room temperature, diluted with chloroform (*ca*. 20 mL) filtered over celite under vacuum, and further washed with chloroform (*ca*. 30 mL). The combined organic fraction was evaporated using rotatory evaporator under reduced pressure. The crude product was further purified by silica gel column chromatography using heptane/DCM as an eluent, and further increasing the polarity with ethylacetate (5%). The product was obtained as an yellow/orange powder (0.290 g, 70% yield). ^{1}H NMR (400 MHz, $CDCl_3$, 25 °C, δ ppm): 8.97-8.95 (m, 2H, $NC_5\underline{H}_5$), 8.60 (d, J = 8.0 Hz, 2H, $C_6\underline{H}_4$), 7.84 (d, J = 8.0 Hz, 2H, $C_6\underline{H}_4$), 7.79 (tt, J = 8.0 Hz and 4.0 Hz, 1H, $NC_5\underline{H}_5$), 7.38-7.34 (m, 2H, $NC_5\underline{H}_5$), 5.07-5.02 (m, 1H), 4.96 (dd, J = 12.0 Hz and 4.0 Hz, 1H), 4.21 (dd, J = 12.0 and 4.0 Hz, 1H), 3.27-3.19 (m, 1H), 3.08-2.91 (m, 2H), 2.70-2.64 (m, 1H). ^{13}C{^{1}H} NMR (100 MHz, $CDCl_3$, 25 °C, δ ppm): 161.91 (C_q), 153.23 (Pd−$\underline{C}$), 152.80 (*o*-$N\underline{C}_5H_5$), 142.32 (quat, J_{CF} = 2 Hz, C_q), 138.40 (*p*-$N\underline{C}_5H_5$), 130.90 (quat, $^{2}J_{CF}$ = 33 Hz), 126.40 (quat, $^{3}J_{CF}$ = 4 Hz), 124.93 (*m*-$N\underline{C}_5H_5$), 124.64 (2 × $\underline{C}H_{Ar}$), 123.85 (quat, $^{1}J_{CF}$ = 271 Hz, $\underline{C}F_3$), 57.66, 53.46, 30.46, 21.58. ^{19}F{^{1}H} NMR (376 MHz, $CDCl_3$, 25 °C, δ ppm): δ −62.51 (s, $C\underline{F}_3$). IR data (cm^{-1}) KBr pellet: 2115 (s) N_3-stretch. MALDI-ToF-MS: m/z calcd. for $C_{18}H_{17}BrF_3N_7Pd$: 574.97, found 575.31 $[M-Br+H]^+$.

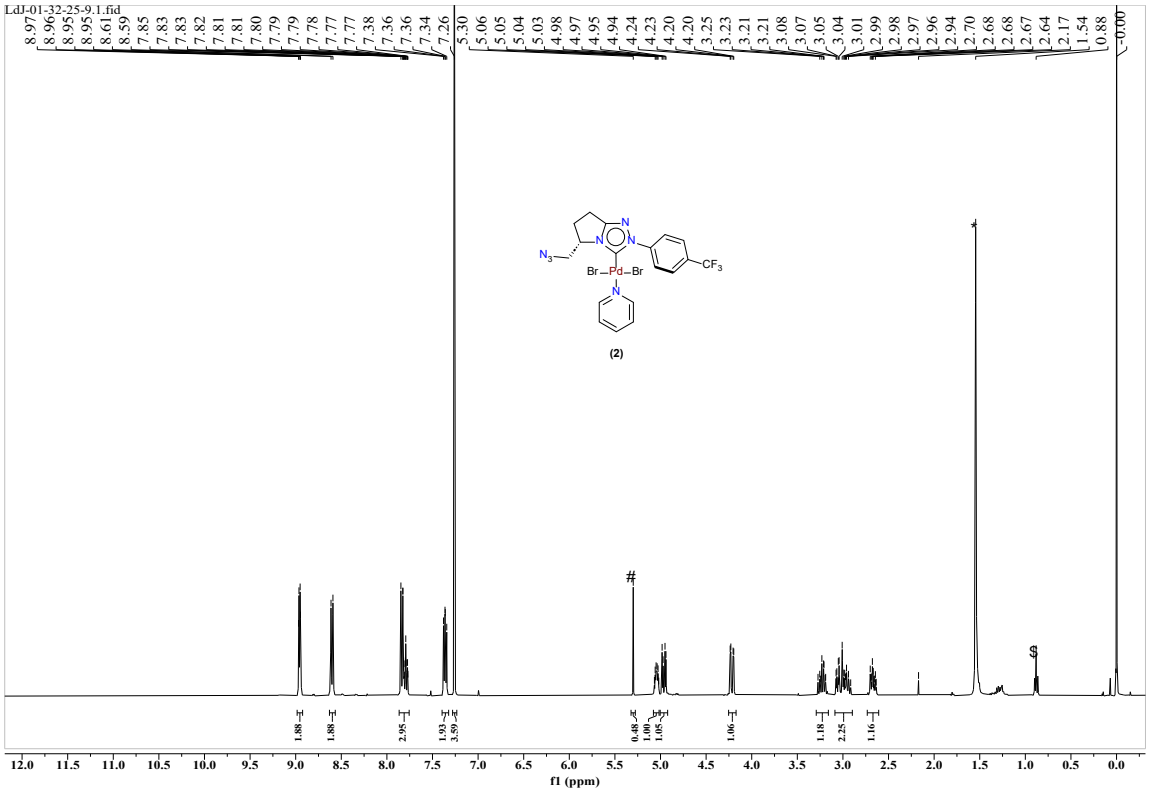

Figure S5. ^{1}H NMR of Pd-NHC complex (**2**) in $CDCl_3$. # DCM, * H_2O, $ heptane.

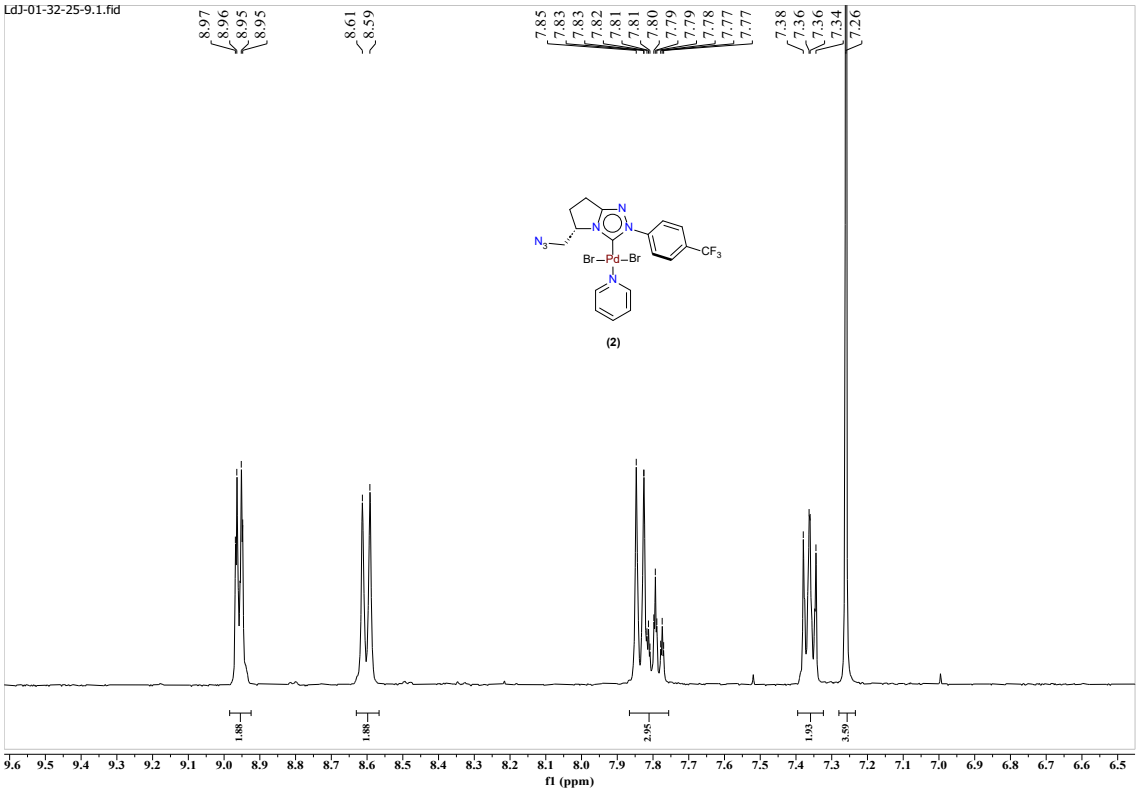

Figure S6. Expanded ^{1}H NMR of Pd-NHC complex (**2**) in $CDCl_3$.

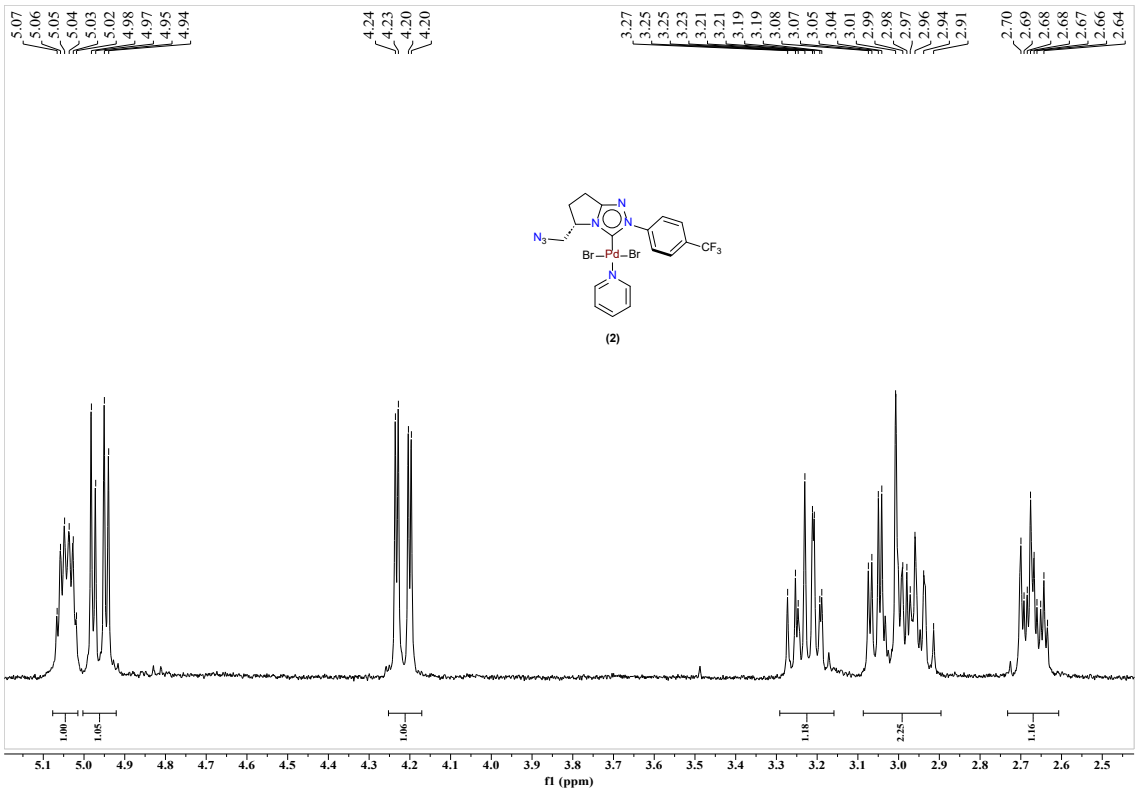

Figure S7. Expanded ^{1}H NMR of Pd-NHC complex (**2**) in $CDCl_3$.

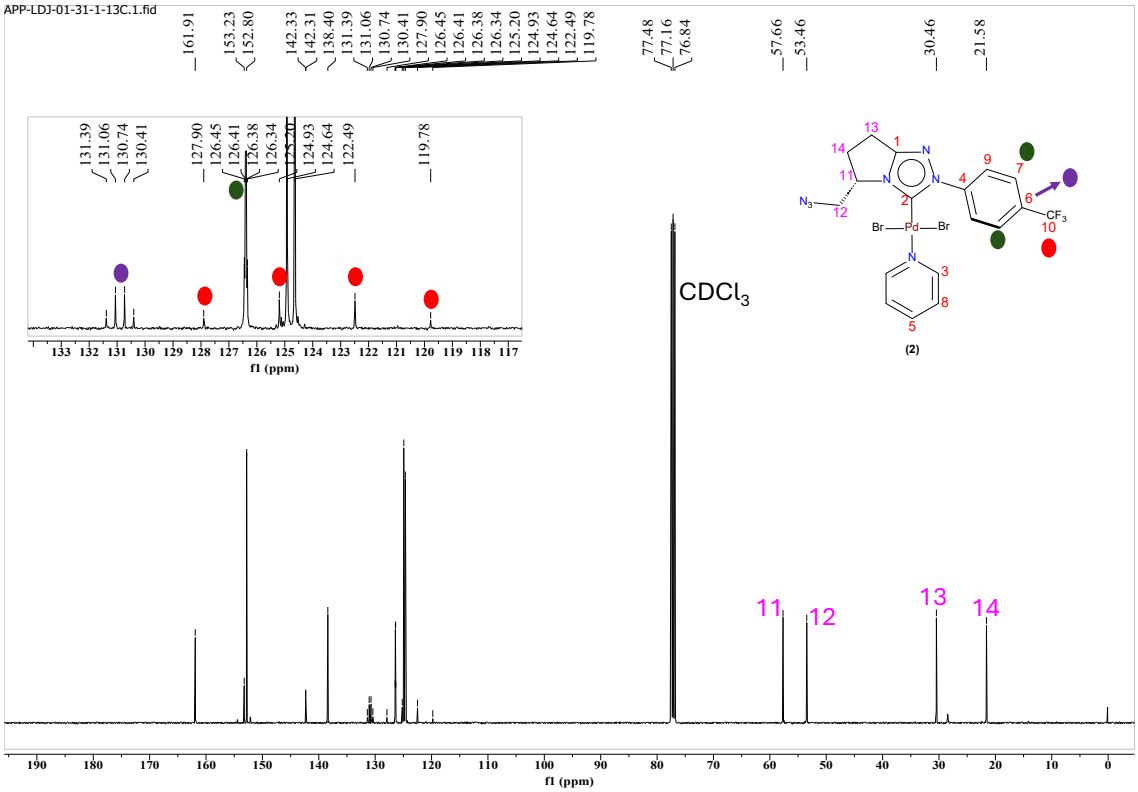

Figure S8. ^{13}C{^{1}H} NMR of Pd-NHC complex (**2**) in $CDCl_3$, inset showing C-F coupling.

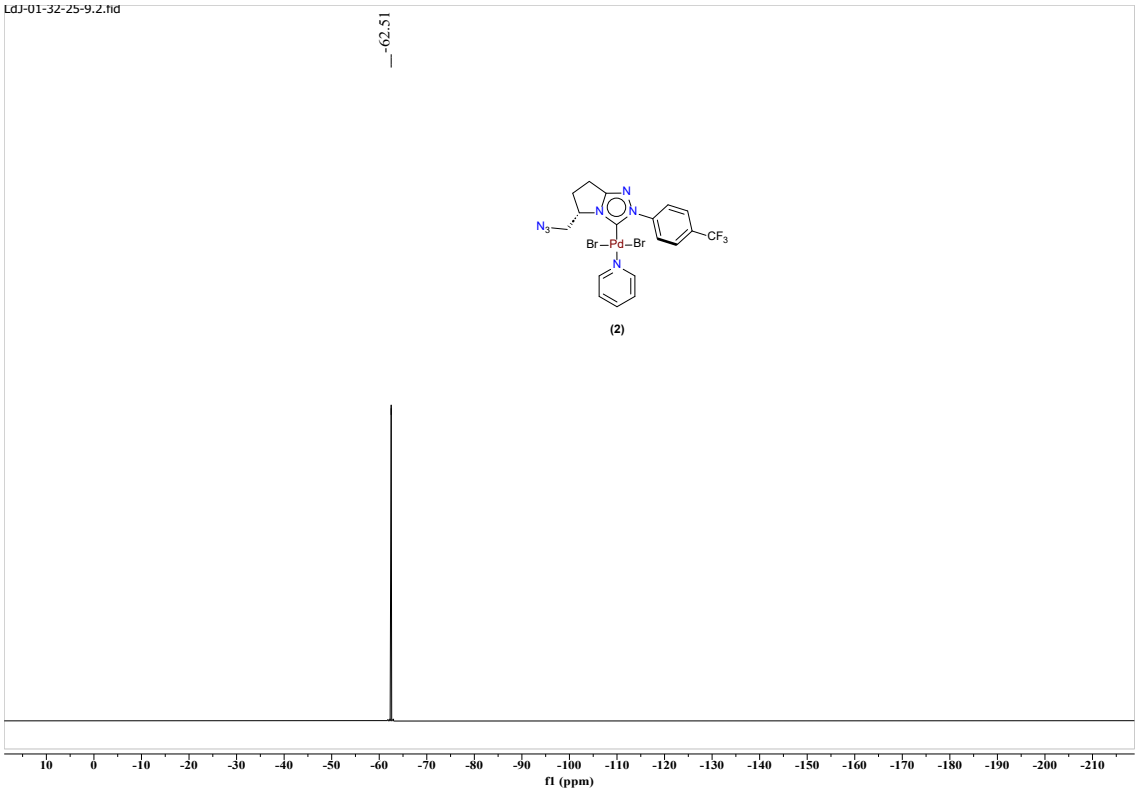

Figure S9. $^{19}F\{^{1}H\}$ NMR of Pd-NHC complex (**2**) in $CDCl_3$.

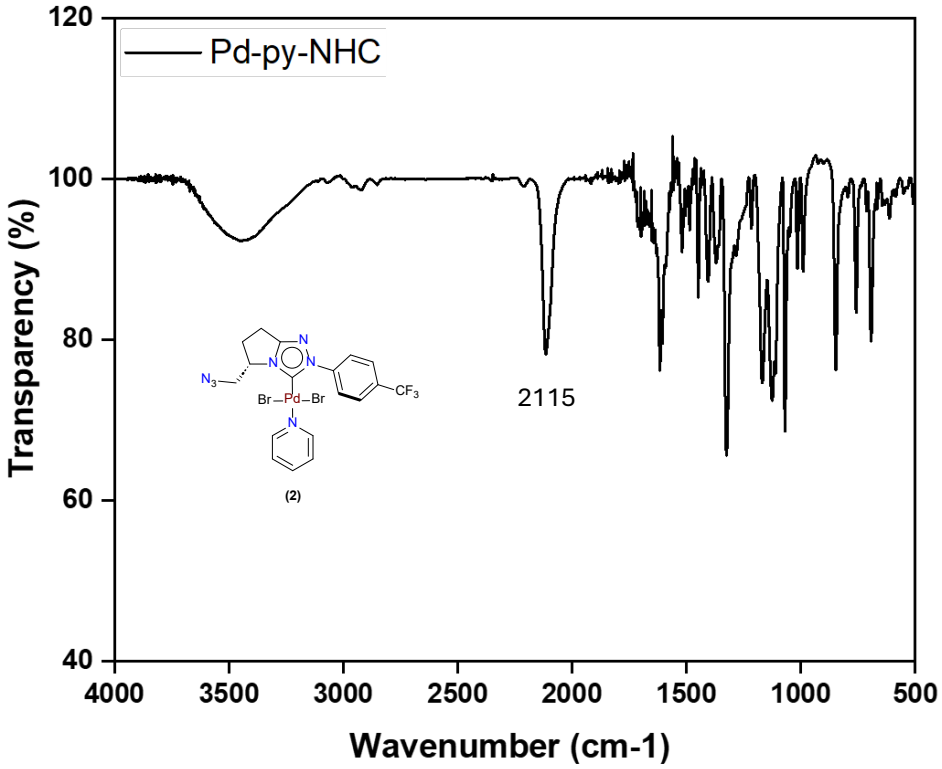

Figure S10. Infrared spectrum of Pd-NHC complex (**2**) in KBr pellet.

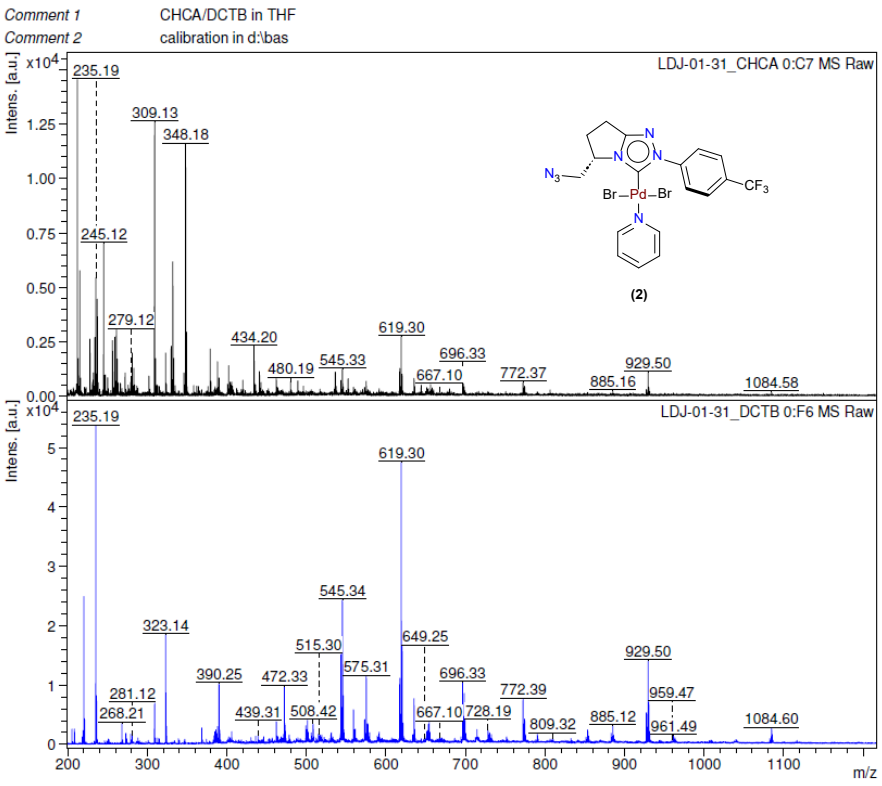

Figure S11. MALDI-ToF-MS spectra of Pd-NHC complex (**2**).

2.3. Synthesis of Pd-NHC complex (3)

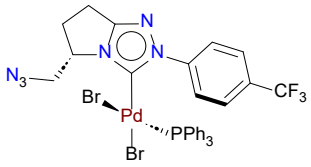

(3)

The Pd-NHC complex (**2**) (0.214 g, 0.328 mmol) and triphenylphosphine (0.086 mg, 0.328 mmol) were added to an oven dried Schlenk flask and dissolved in dry DCM (*ca*. 10 mL). The reaction was left stirring for 1 h at room temperature under argon atmosphere. After the reaction, the solvent was evaporated without exposing the reaction mixture to air using Schlenk line. The obtained crude solid was purified by trituration where it was redissolved in minimal amount of dry DCM (*ca*. 0.2 mL) and precipitated using dry cold diethyl ether (*ca*. 5 mL), then the solvent was removed by syringe after the product precipitated. This trituration process was repeated for 4 times. Finally the product was dried under inert atmosphere, to get the pure Pd-NHC complex (**3**) as an yellow powder (0.204 g, 74% yield). ^{1}H NMR (400 MHz, $CDCl_3$, 25 °C, δ ppm): 8.52 (d, J = 8.0 Hz, 2H, $C_6\underline{H}_4$), 7.73 (d, J = 8.0 Hz, 2H, $C_6\underline{H}_4$), 7.45-7.37 (m, 10H, $P(C_6\underline{H}_5)_3$), 7.32-7.27 (m, 5H, $P(C_6\underline{H}_5)_3$), 4.87 (dd, J = 12.0 and 4.0 Hz, 1H), 4.11 (dd, J = 12.0 and 4.0 Hz, 1H), 4.04-4.00 (m, 1H), 3.09-3.00 (m, 1H), 2.55-2.48 (m, 1H), 2.43-2.36 (m, 1H), 2.27-2.17 (m, 1H). ^{13}C{^{1}H} NMR (100 MHz, $CDCl_3$, 25 °C, δ ppm): 166.54 (Pd−$\underline{C}$), 162.01 (C_q), 141.63 (quat, J_{CF} = 1 Hz, C_q), 133.92 (d, J_{CP} = 10 Hz, *o*-$\underline{C}_6H_5$), 131.36 (d, J_{CP} = 3 Hz, *p*-$\underline{C}_6H_5$), 130.86 (quat, $^{2}J_{CF}$ = 33 Hz), 129.87 (d, J_{CP} = 53 Hz, *ipso*-$\underline{C}_6H_5$), 128.61 (d, J_{CP} = 11 Hz, *m*-$\underline{C}_6H_5$), 126.42 (quat, $^{3}J_{CF}$ = 4 Hz), 124.05 (2 × $\underline{C}H_{Ar}$), 123.65 (quat, $^{1}J_{CF}$ = 271 Hz, $\underline{C}F_3$), 57.86, 52.85, 30.65, 21.22. ^{19}F{^{1}H} NMR (376 MHz, $CDCl_3$, 25 °C, δ ppm): −62.59 (s, $C\underline{F}_3$). ^{31}P{^{1}H} NMR (162 MHz, $CDCl_3$, 25 °C, δ ppm): 26.20 (s, Pd-$\underline{P}(C_6H_5)_3$). IR data (cm^{-1}) KBr pellet: 2113 (s). MALDI-ToF-MS: *m/z* calcd. for $C_{31}H_{26}BrF_3N_6PPd$: 757.01, found 757.03 $[M-Br]^+$, 729.01 $[M-Br-N_2]^+$.

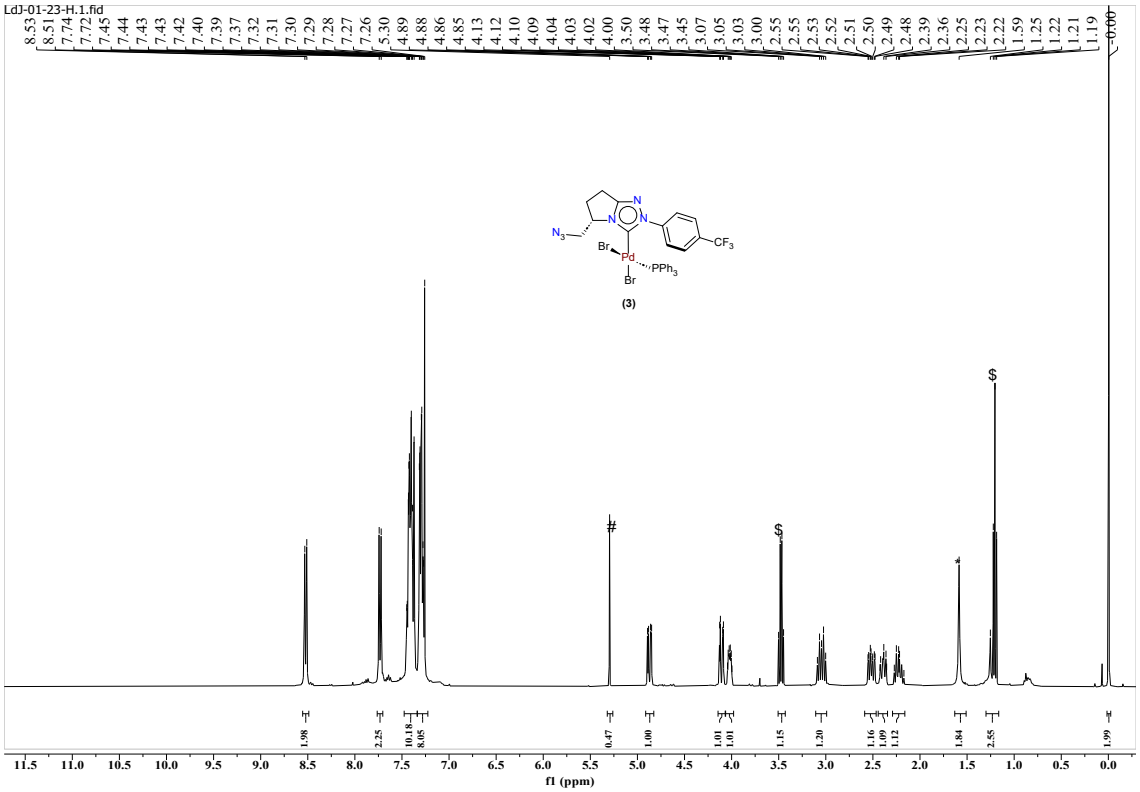

Figure S12. ^{1}H NMR of Pd-NHC complex (**3**) in $CDCl_3$. # DCM, * H_2O, $ diethyl ether.

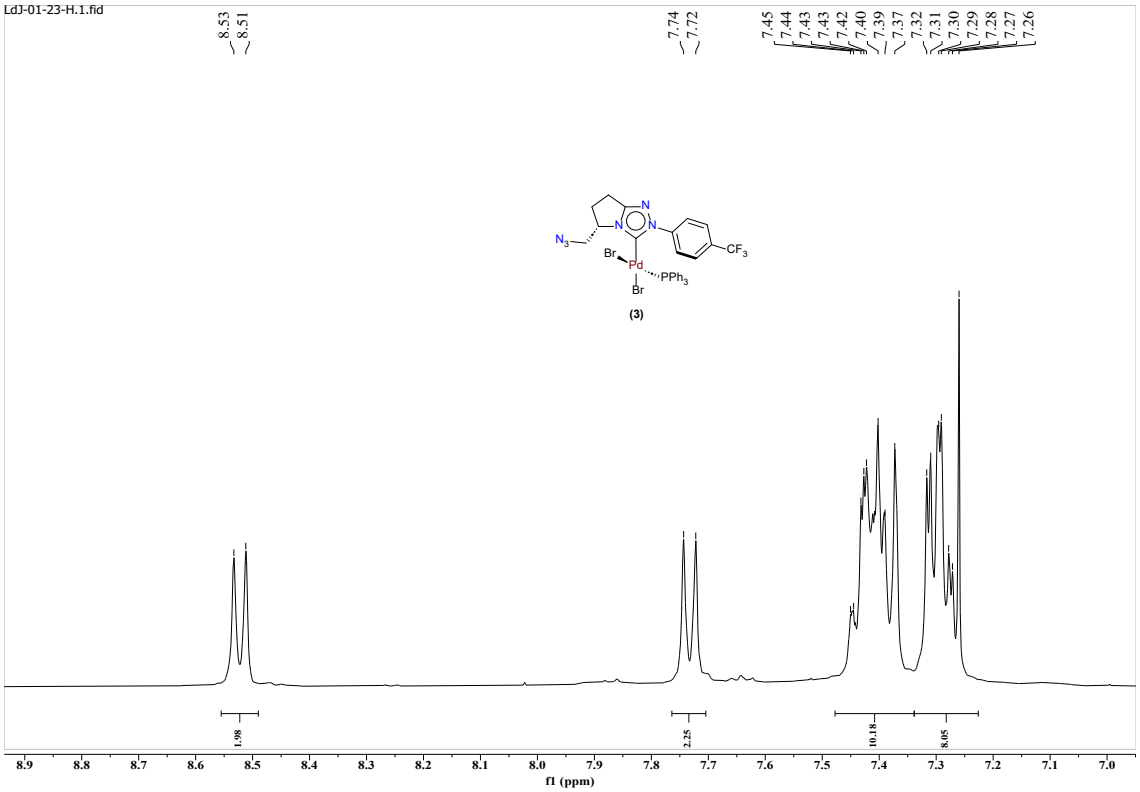

Figure S13. Expanded ^{1}H NMR of Pd-NHC complex (**3**) in $CDCl_3$.

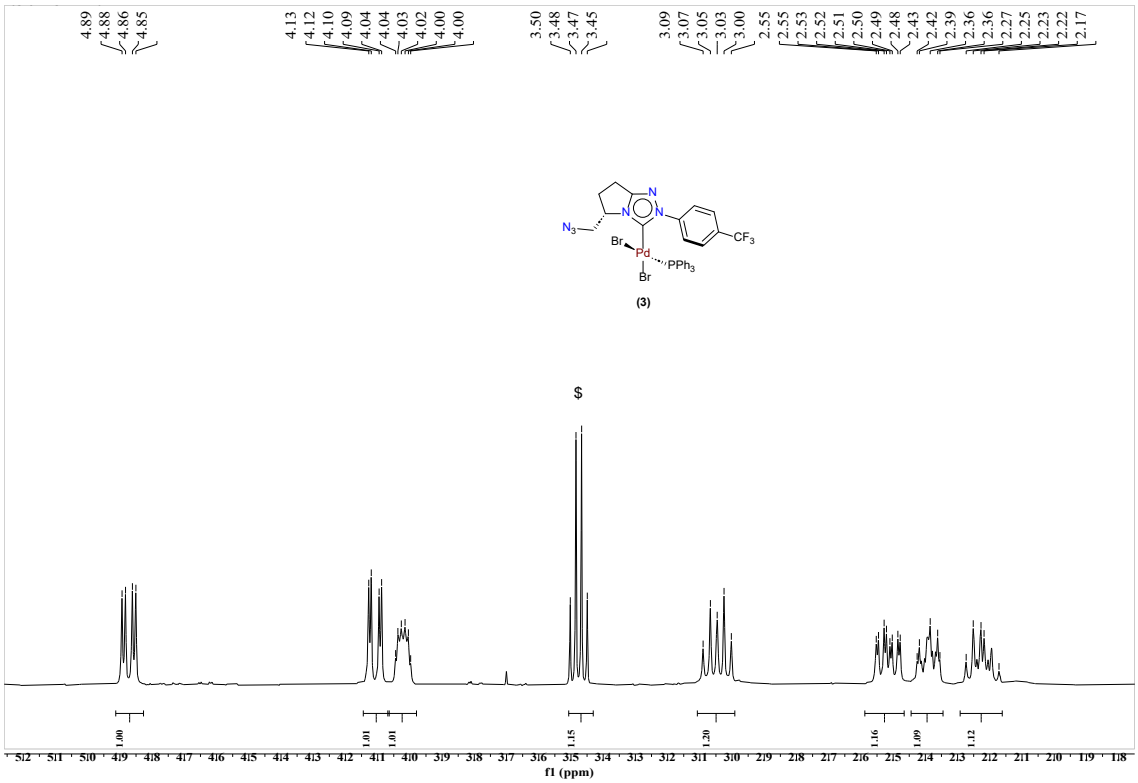

Figure S14. Expanded ^{1}H NMR of Pd-NHC complex (**3**) in $CDCl_3$. $ diethyl ether.

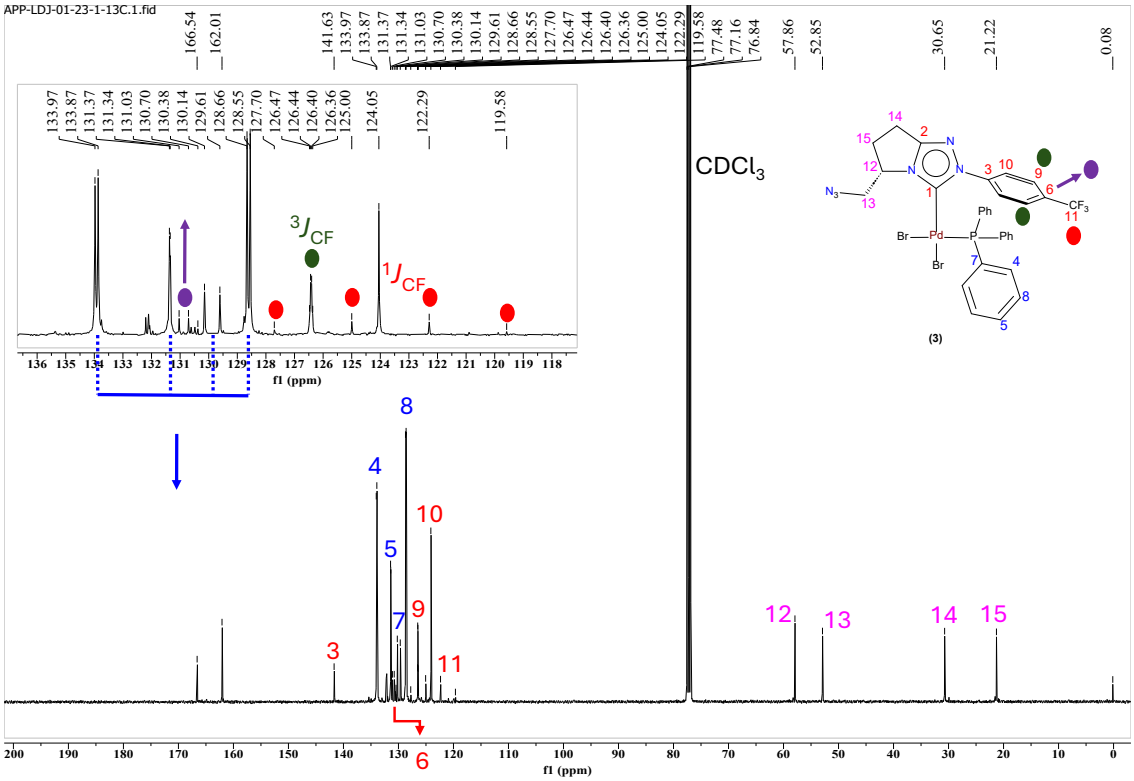

Figure S15. $^{13}C\{^{1}H\}$ NMR of Pd-NHC complex (**3**) in $CDCl_3$, inset showing C-F/C-P coupling.

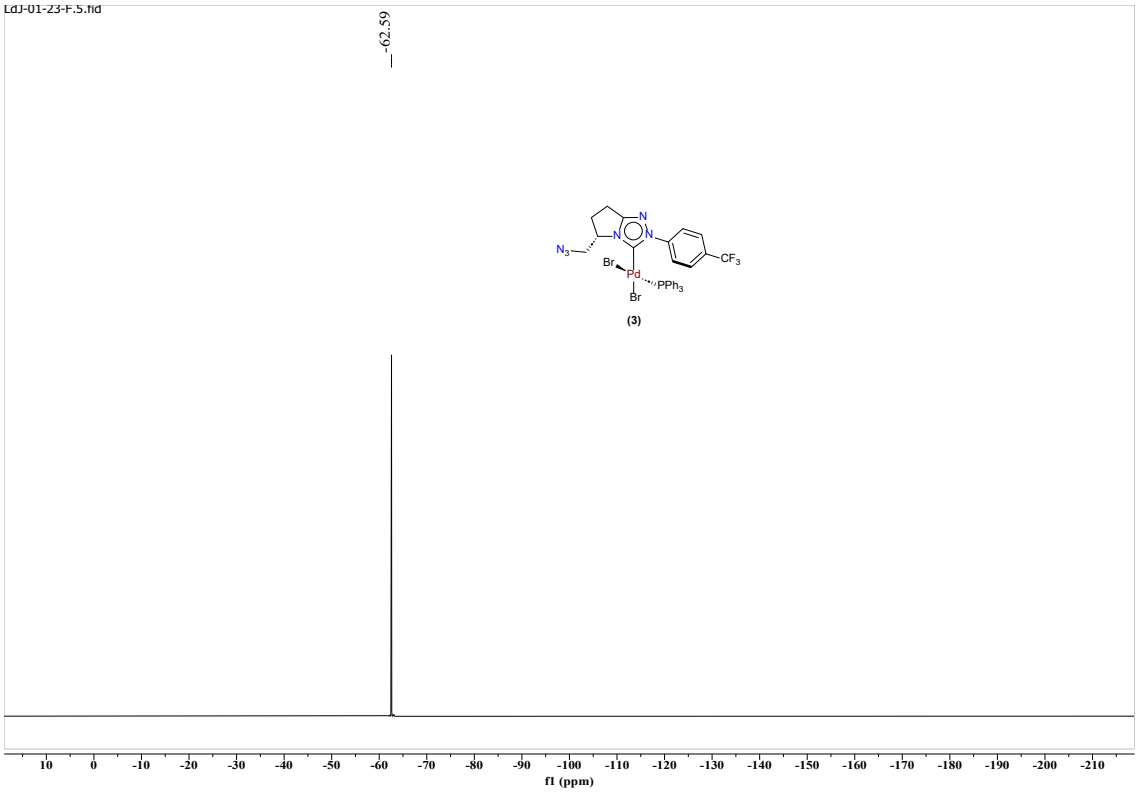

Figure S16. $^{19}F\{^{1}H\}$ NMR of Pd-NHC complex (**3**) in $CDCl_3$.

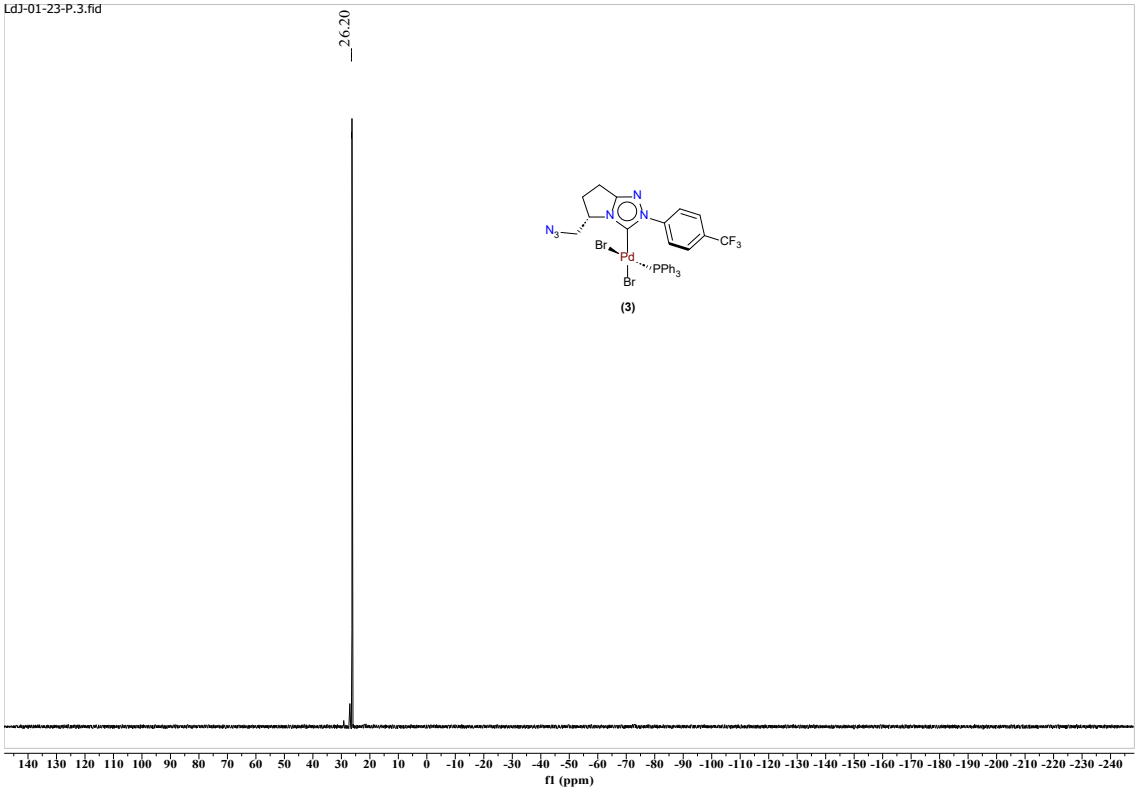

Figure S17. $^{31}P\{^{1}H\}$ NMR of Pd-NHC complex (**3**) in $CDCl_3$.

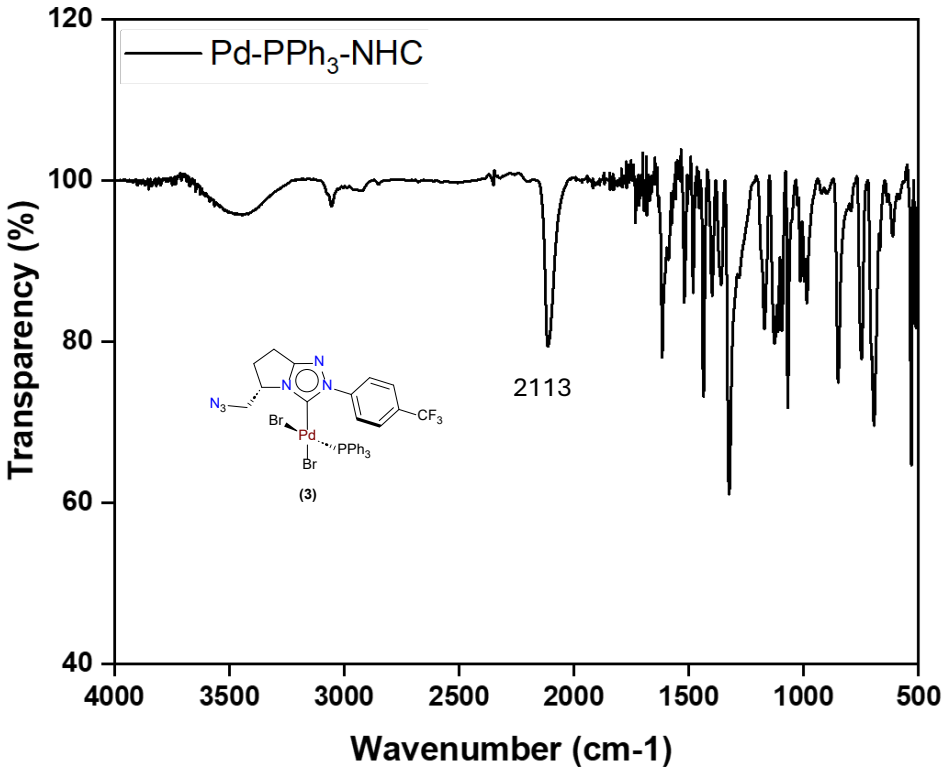

Figure S18. Infrared spectrum of Pd-NHC complex (**3**) in KBr pellet.

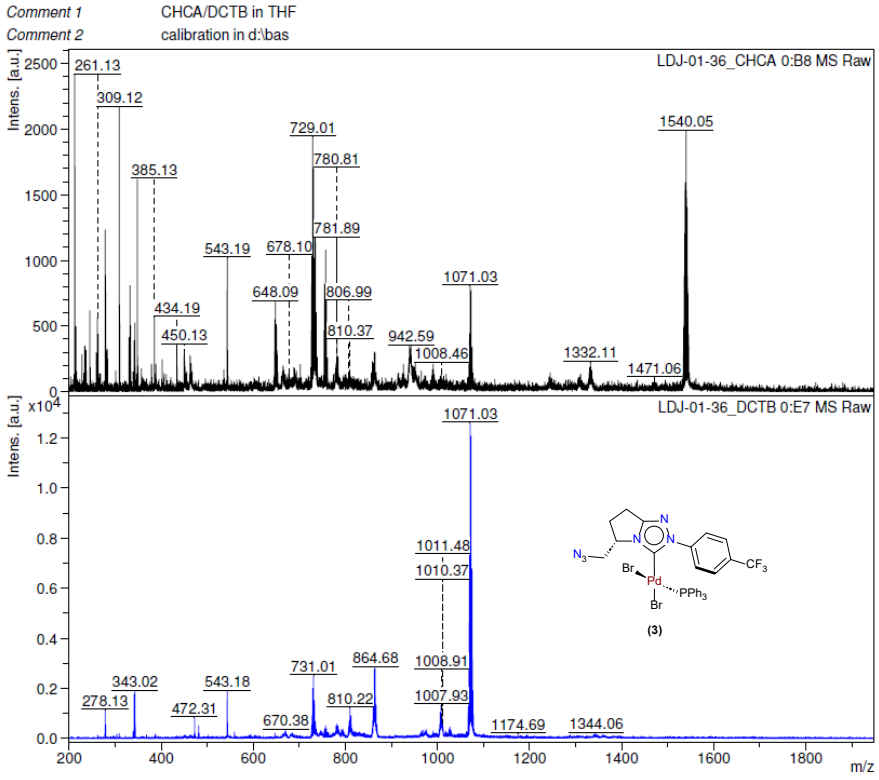

Figure S19. MALDI-ToF-MS spectra of Pd-NHC complex (**3**).

2.4. Synthesis of amphiphilic polymers P1 and P2

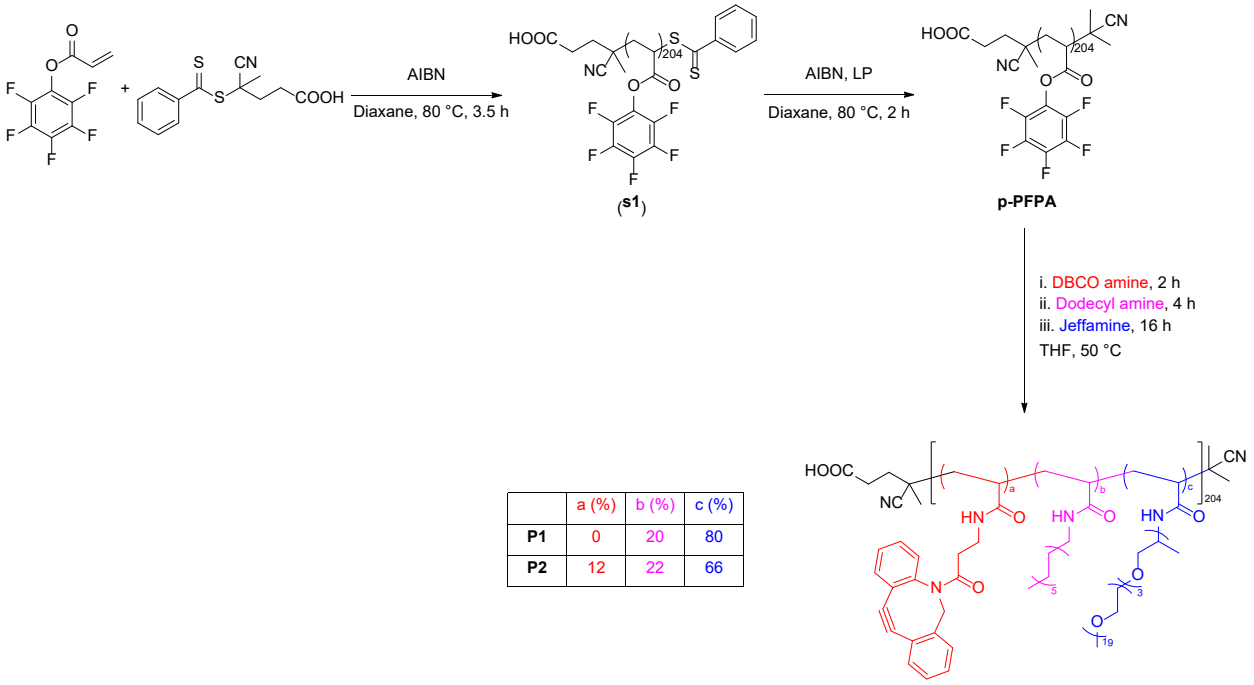

	a (%)	b (%)	c (%)
P1	0	20	80
P2	12	22	66

Scheme S2. Synthesis of amphiphilic polymers **P1** and **P2**.

2.4.1. Synthesis of poly(pentafluorophenyl) acrylate polymer (s1)

4-Cyano-4-(phenyl-carbonothioylthio)pentanoic acid (12.23 mg, 43.77 µmol) and azobis(isobutyronitrile) (AIBN) (0.870 mg, 5.30 µmol) were dissolved in dry 1,4-dioxane (*ca*. 2 mL) and added to an oven dried Schlenk tube containing pentafluorophenyl acrylate (3.00 g, 12.599 mmol). The reaction mixture was thoroughly degassed with argon for 1 h, after which the reaction mixture was placed in a pre-heated oil bath at 80 °C. The conversion of the polymerization was monitored periodically using ^{19}F-NMR and after 3.5 h, the conversion was determined to be 70.9%. The polymerization reaction was immediately quenched by submerging the Schlenk tube in liquid nitrogen. The reaction mixture was brought to room temperature and was dissolved in DCM (*ca*. 2 mL) and was purified by precipitating in cold pentane (*ca*. 50 mL). The formed solid was filtered, redissolved in DCM (*ca*. 3 mL) and precipitated again in cold pentane (*ca*. 80 mL) two more times. Finally, the polymer was filtered out and dried using rotatory evaporator. The RAFT polymer (**s1**) was obtained as a pink powder (1.51 g, 71% yield). The degree of polymerization DP = $[M]_{PFPA}$ / $[M]_{RAFT}$ × 70.9 % = 12.599 / 0.04377 × 0.709 = 204. The theoretical number-average molecular weight Mn = DP × $M.wt_{(PFPA)}$ + $M.wt_{(RAFT)}$ = 204 × 238.11 + 279.38 = 48854. ^{1}H NMR (400 MHz, $CDCl_3$, 25 °C, δ ppm): 3.09 (br), 2.51 (br), 2.12 (br). ^{19}F{^{1}H} NMR (376 MHz, $CDCl_3$, 25 °C, δ ppm): −153.24 (2F), −156.78 (1F), −162.18 (2F).

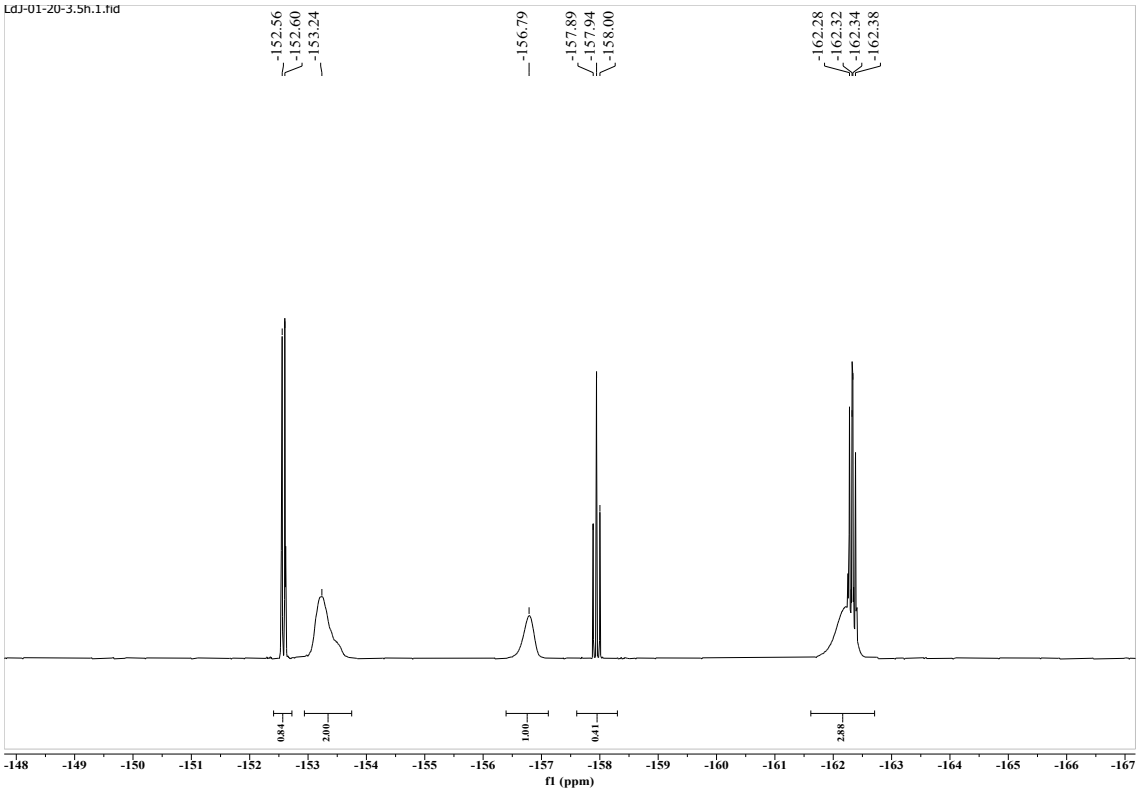

Figure S20. RAFT polymer conversion (**s1**) by ^{19}F NMR spectrum in $CDCl_3$.

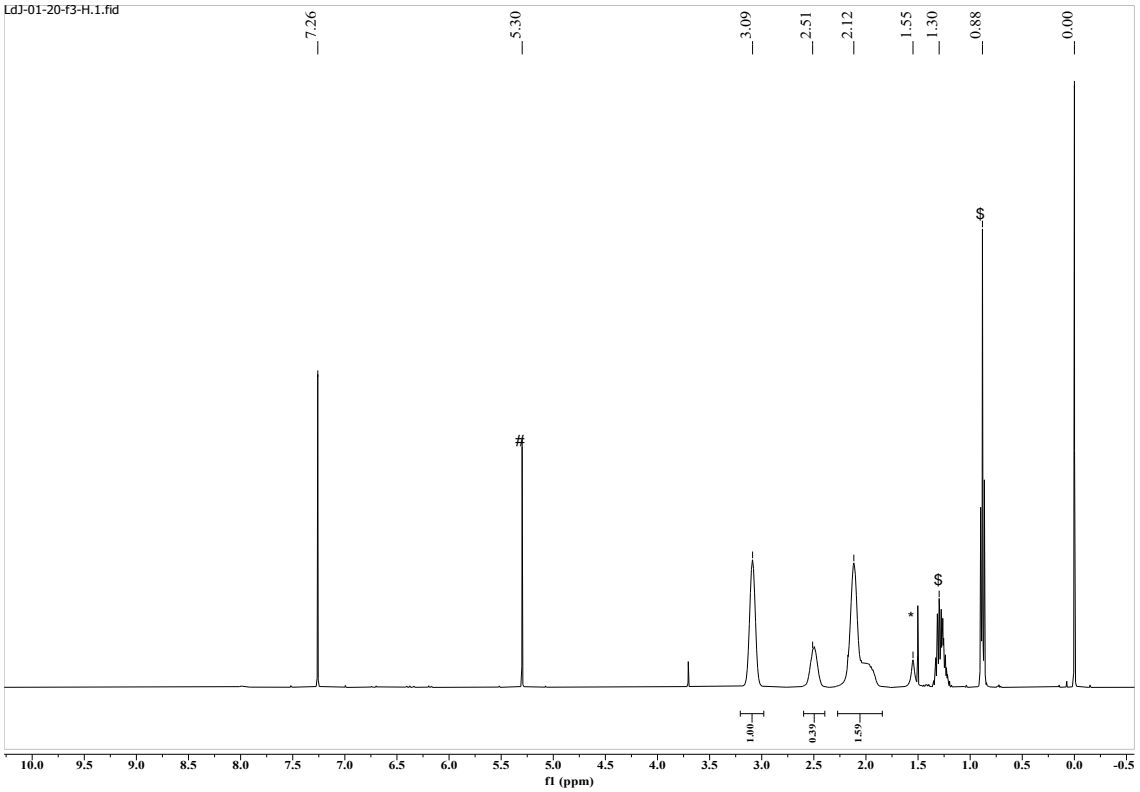

Figure S21. ^{1}H NMR of RAFT polymer (**s1**) in $CDCl_3$. # DCM, * H_2O, $ pentane.

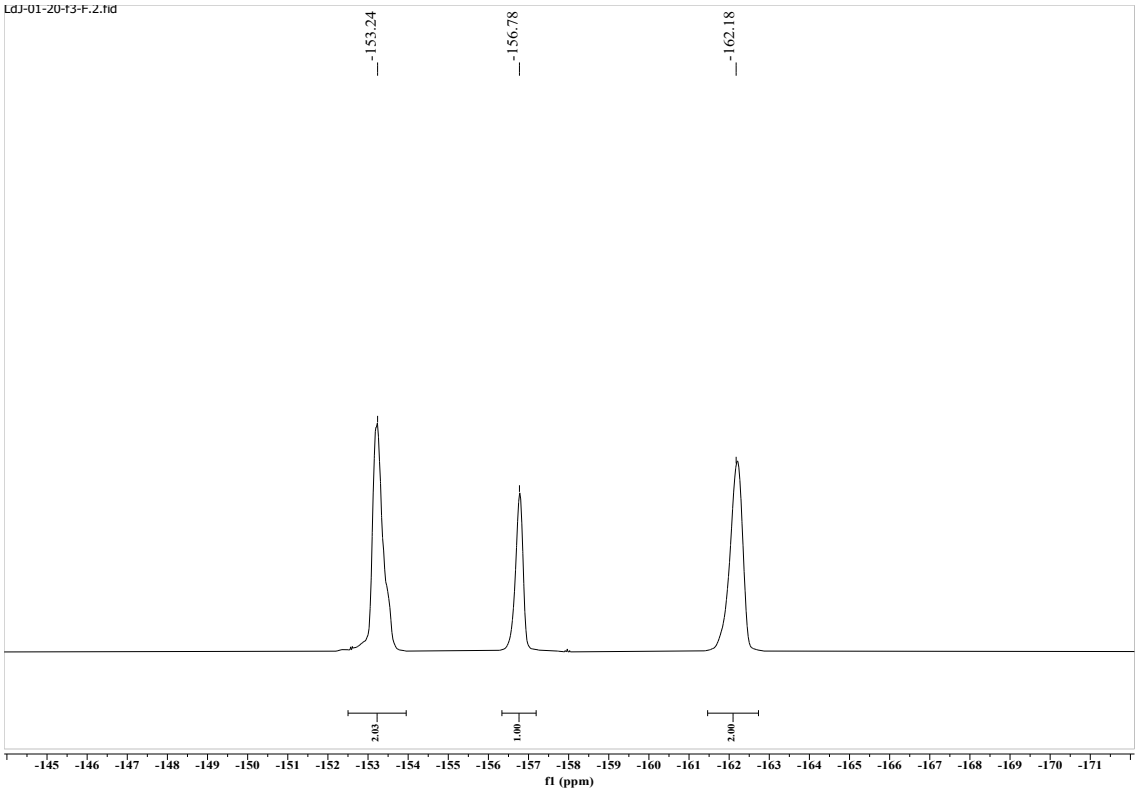

Figure S22. ^{19}F NMR of RAFT polymer (**s1**) in $CDCl_3$.

2.4.2. Synthesis of end group modified poly(pentafluorophenyl) acrylate polymer (p-PFPA)

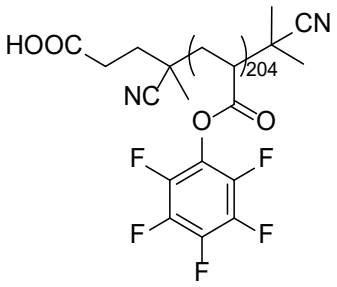

p-PFPA

Polymer (**s1**) (1.513 g, 30.97 μmol), lauryl peroxide (24.8 mg, 62.3 μmol), and AIBN (100.3 mg, 0.61 mmol) were dissolved in dry 1,4-dioxane (*ca*. 15 mL) and added to a dried Schlenk tube. The reaction mixture was thoroughly degassed with argon for 1 hour, after which the Schlenk tube was placed in an oil bath at 80 °C under Argon atmosphere and left stirring for 5 hours during which the pink color reaction mixture turned colorless. The reaction mixture was quenched with liquid nitrogen. The solvent was removed using rotatory evaporator and the mixture was redissolved in DCM (*ca*. 3 mL) and precipitated with cold pentane (*ca*. 50 mL) (3x) and afterwards dried using rotatory evaporator. The product (**p-PFPA**) was a colorless powder (1.034 g, 68% yield). The theoretical number-average molecular weight Mn = DP × M.wt(PFPA) + M.wt(end group) = 204 × 238.11 + 194.23 = 48769. ^{1}H NMR (400 MHz, $CDCl_3$, 25 °C, δ ppm): 3.09 (br), 2.50 (br), 2.12 (br). ^{19}F{^{1}H} NMR (376 MHz, $CDCl_3$, 25 °C, δ ppm): −153.24 (2F), −156.79 (1F), −162.20 (2F). Size-exclusion chromatography (SEC) (1 mg / mL THF): PDA detector: Mn = 27.96 kDa, Mw = 36.76 kDa, Đ = 1.31. RI detector: Mn = 31.56 kDa, Mw = 37.43 kDa, Đ = 1.18.

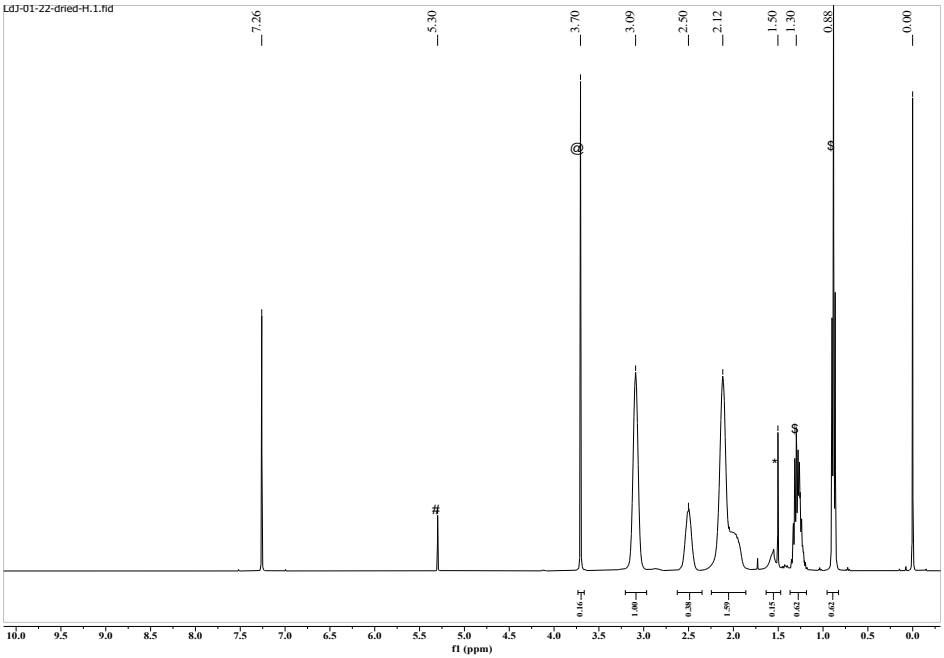

Figure S23. ^{1}H NMR of end group modified (**p-PFPA**) in $CDCl_3$. # DCM, @ 1,4-dioxane, * H_2O, $ pentane.

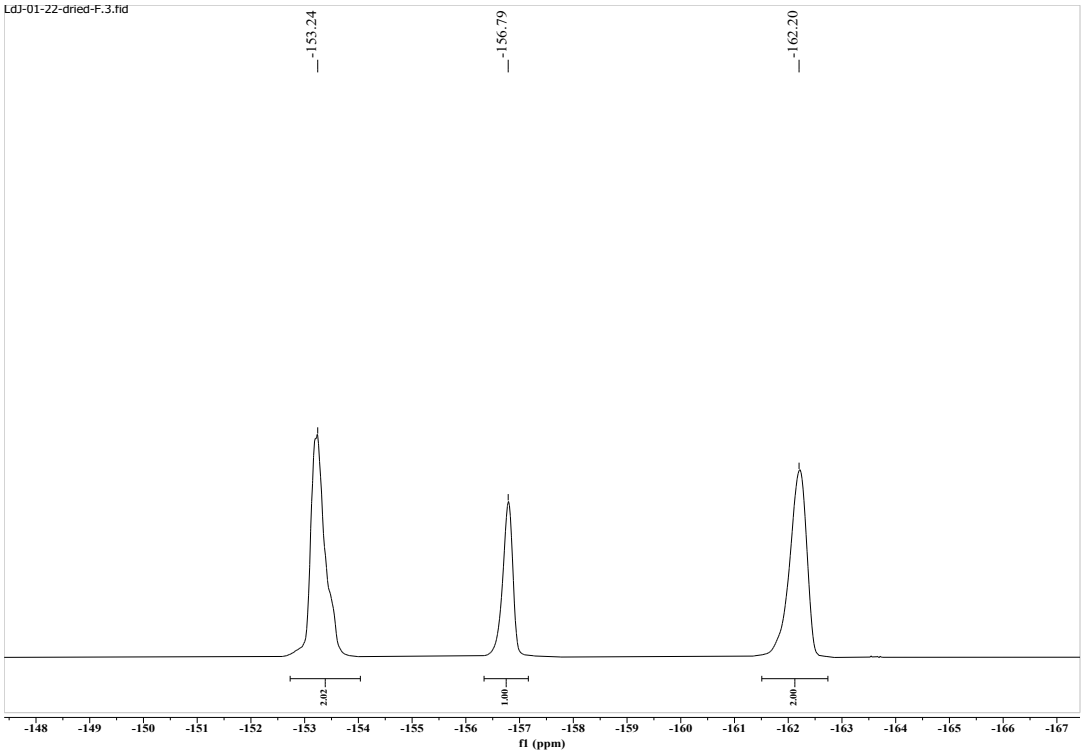

Figure S24. ^{19}F NMR of end group modified (**p-PFPA**) in $CDCl_3$.

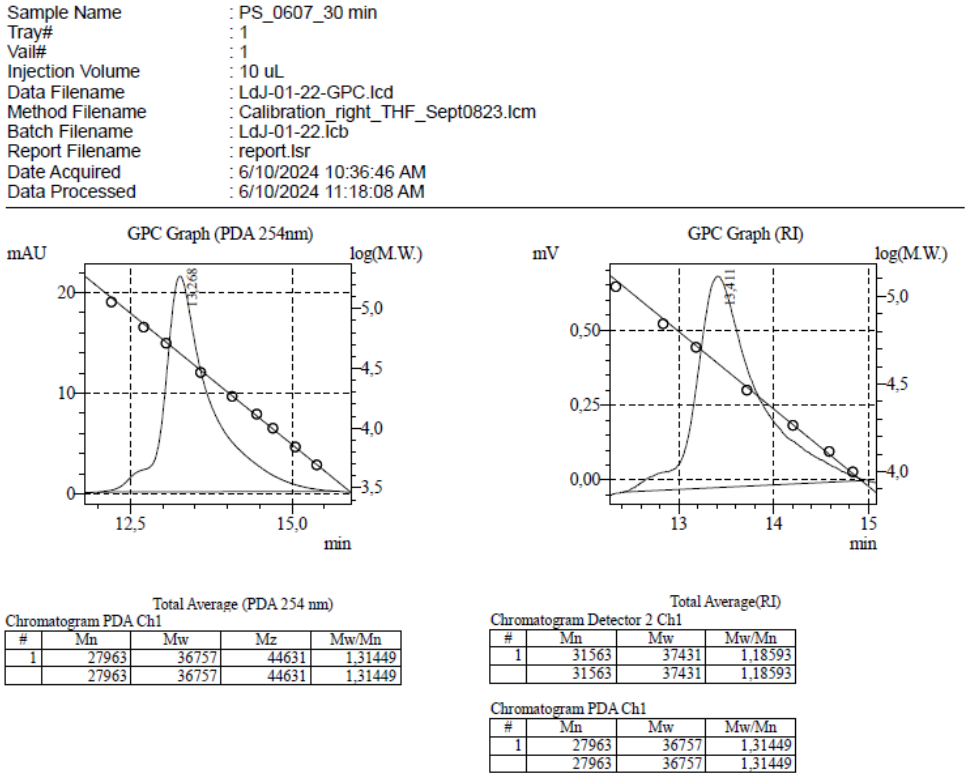

Figure S25. SEC trace of end group modified (**p-PFPA**) in THF.

2.4.3. Synthesis of amphiphilic polymer (P1)

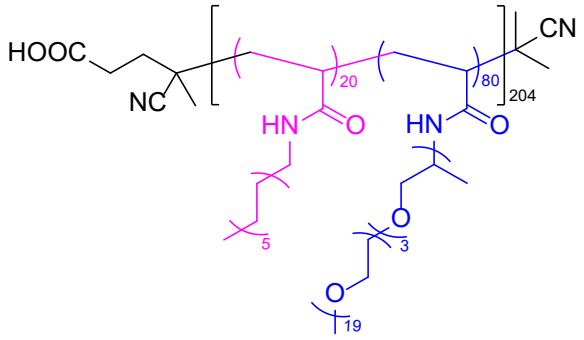

(**P1**)

In an oven dried Schlenk flask, end group modified (**p-PFPA**) (0.200 g, 4.1 µmol) and dodecyl amine (31.0 mg, 0.167 mmol) were dissolved in dry THF (*ca*. 5 mL) under argon atmosphere. The flask was placed in a pre-heated oil bath at 50 °C and left stirring until the dodecyl amine was fully incorporated into the polymer by replacing pentafluorophenolic group (4 hour), monitored periodically via ^{19}F-NMR. Next, an excess of pre-dried (at 50 °C over P_2O_5 in a vacuum oven overnight), Jeffamine 1000 M (1.392 g, 1.335 mmol) was added to the reaction mixture and the reaction was kept overnight to ensure complete incorporation of Jeffamine 1000 M. After full conversion, the reaction mixture was purified via dialysis (2 x 1 L methanol, 2 x 1 L THF) for 4 days by replacing the solvent every 24 hour and the polymer was afterwards dried using rotatory evaporator. The **P1** polymer was obtained as a colorless viscous solid (0.450 g, 58% yield). $M_{theoretical}$ = 189 kDa, $M_{n,\ SEC\text{-}PBS}$ = 43.4 kDa, $M_{w,\ SEC\text{-}PBS}$ = 73.5 kDa. Đ = 1.69. ^{1}H NMR (400 MHz, $CDCl_3$, 25 °C, δ ppm): 3.71-3.44 (m), 3.35 (br), 1.23 (br), 1.10 (br).

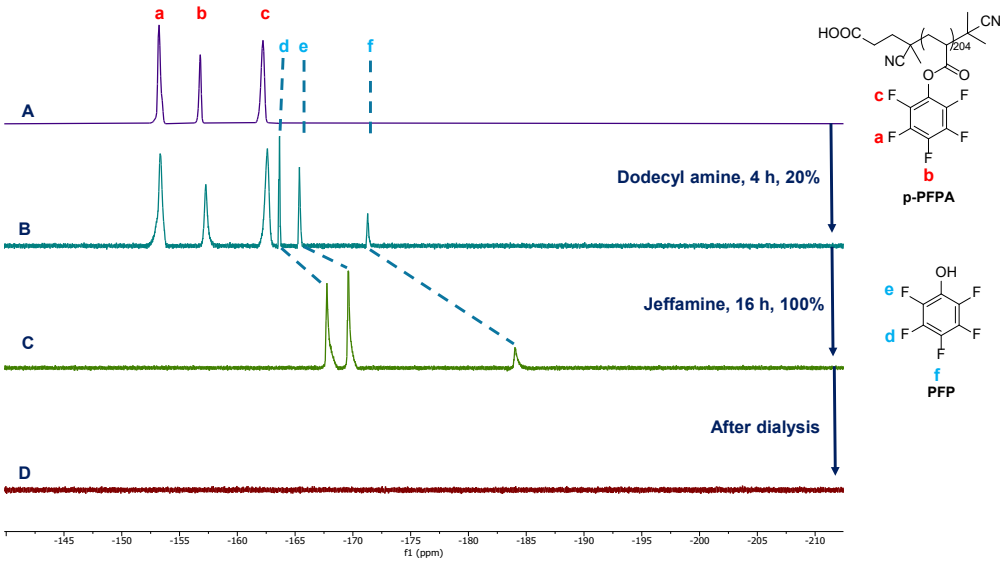

Figure S26. Conversion of **P1** monitored by ^{19}F-NMR in $CDCl_3$ of the post-functionalization of (**p-PFPA**). A) ^{19}F-NMR of (**p-PFPA**), B) 4 hours after the addition of n-dodecyl amine, C) 16 hours after the addition of Jeffamine M-1000, and D) after dialysis.

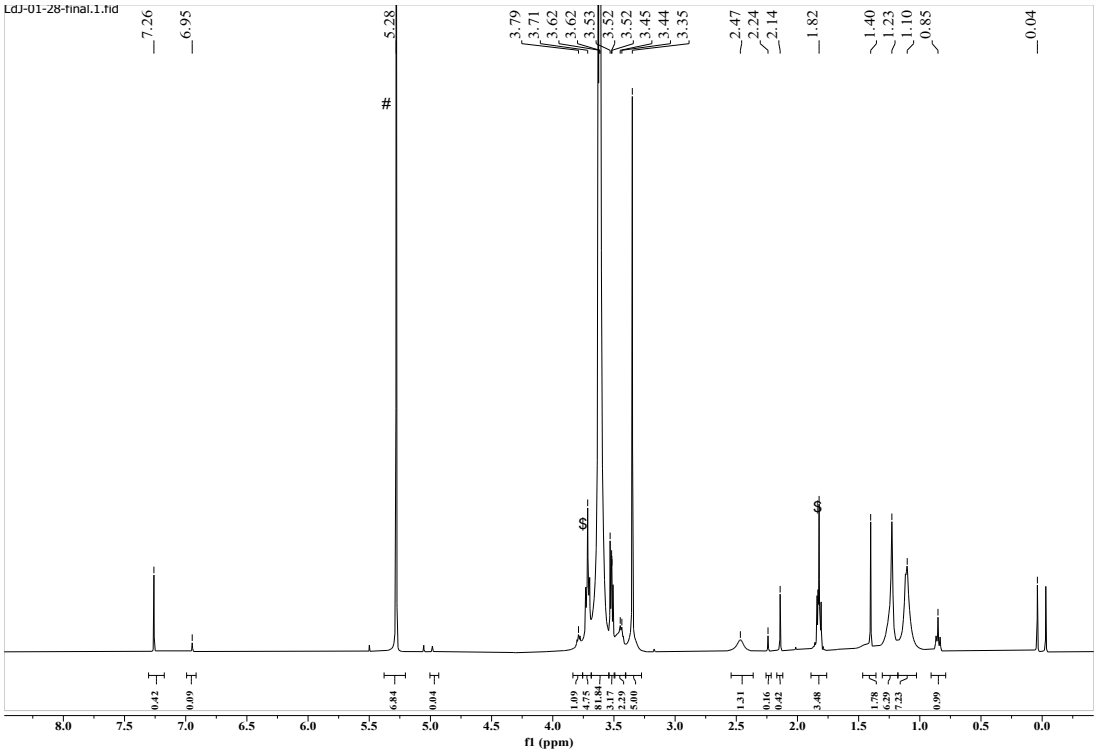

Figure S27. ^{1}H NMR of (**P1**) in $CDCl_3$. # DCM, $ THF.

Sample Name	: LdJ-01-P1
Tray#	: 1
Vail#	: 20
Injection Volume	: 50 uL
Data Filename	: LdJ-01-P1.lcd
Method Filename	: Shodex_08mL@min_Oct0421.lcm
Batch Filename	: 1b.lcb
Report Filename	: DEFAULT.lsr
Date Acquired	: 2/25/2025 11:24:41 AM
Data Processed	: 2/25/2025 1:06:02 PM

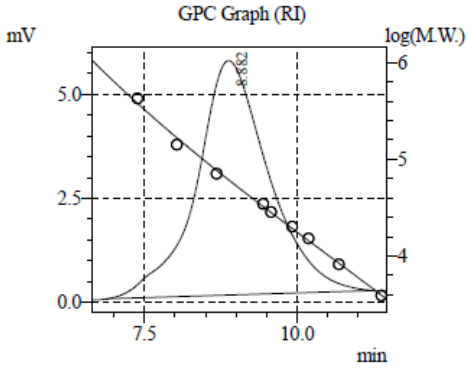

Total Average(RI)

Chromatogram Detector 2 Ch1

#	Mn	Mw	Mw/Mn
1	43404	73542	1.69436
	43404	73542	1.69436

Figure S28. SEC trace of (**P1**) in PBS.

2.4.4. Synthesis of DBCO tagged amphiphilic polymer (P2)

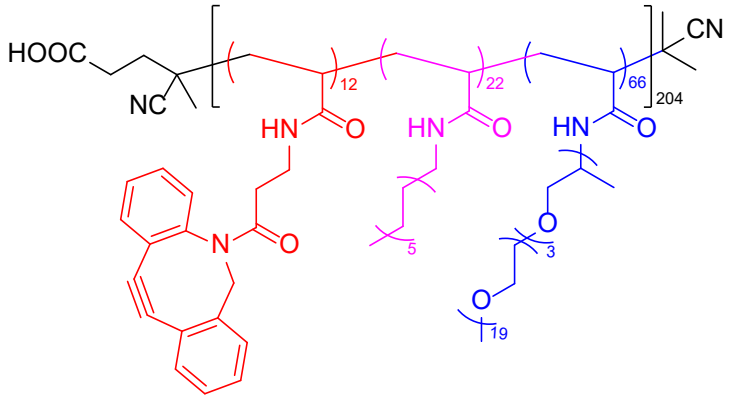

(**P2**)

In an oven dried Schlenk flask, (**p-PFPA**) (0.173 g, 3.55 µmol) and dibenzocyclooctyne-amine (DBCO amine) (20 mg, 0.072 mmol) were dissolved in dry THF (*ca*. 5 mL) under argon atmosphere. The flask was placed in a pre-heated oil bath at 50 °C and left stirring until the DBCO amine was fully incorporated into the polymer (2h), and monitored periodically via ^{19}F-NMR. Next, dodecyl amine (26.8 mg, 0.144 mmol) was added to the Schlenk flask and the reaction was continued until the dodecyl amine was fully incorporated into the polymer (4h), and lastly an excess of pre-dried (at 50 °C over P_2O_5 in a vacuum oven overnight), Jeffamine 1000 M (1.60 g, 1.535 mmol) was added to the reaction mixture and the reaction was kept overnight to ensure complete incorporation of Jeffamine 1000 M. After full conversion, the reaction mixture was purified via dialysis (2 x 1 L methanol, 2 x 1 L THF) for 4 days by replacing the solvent every 24h and the polymer was afterwards dried using rotatory evaporator. The polymer **P2** was a light yellow viscous solid (0.448 g, 76% yield). $M_{theoretical}$ = 166 kDa, $M_{n,\ SEC\text{-}PBS}$ = 40.8 kDa, $M_{w,\ SEC\text{-}PBS}$ = 125.2 kDa. Đ = 3.07. ^{1}H NMR (400 MHz, $CDCl_3$, 25 °C, δ ppm): 3.80-3.45 (m), 3.36 (br), 2.32 (br), 1.24 (br), 1.11 (br).

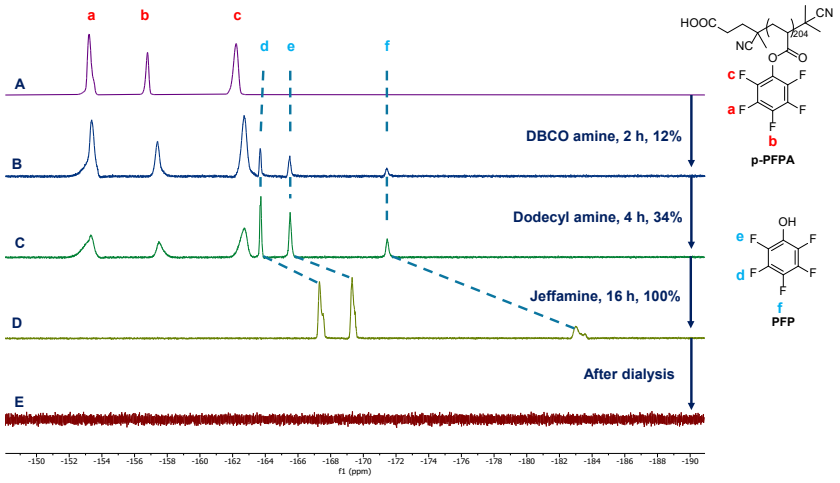

Figure S29. Conversion of **P2** monitored by ^{19}F-NMR in $CDCl_3$ of the post-functionalization of (**p-PFPA**). A) ^{19}F-NMR of (**p-PFPA**), B) 2 hours after DBCO amine, C). 4 hours after the addition of n-dodecyl amine, D) 16 hours after the addition of Jeffamine M-1000, and E) after dialysis.

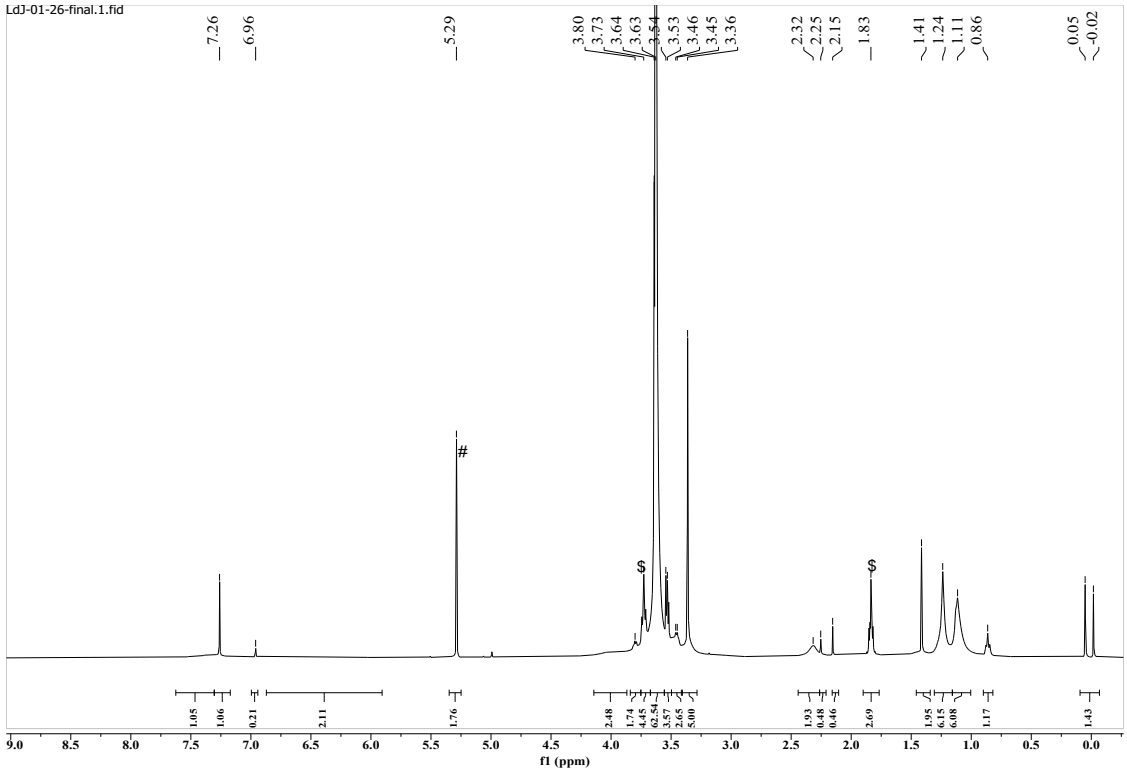

Figure S30. ^{1}H NMR of (**P2**) in $CDCl_3$. # DCM, $ THF.

Sample Name	: LdJ-01-P2
Tray#	: 1
Vail#	: 21
Injection Volume	: 50 uL
Data Filename	: LdJ-01-P2.lcd
Method Filename	: Shodex_08mL@min_Cal_April0423.lcm
Batch Filename	: 1b.lcb
Report Filename	: DEFAULT.lsr
Date Acquired	: 2/25/2025 12:25:29 PM
Data Processed	: 2/25/2025 1:05:03 PM

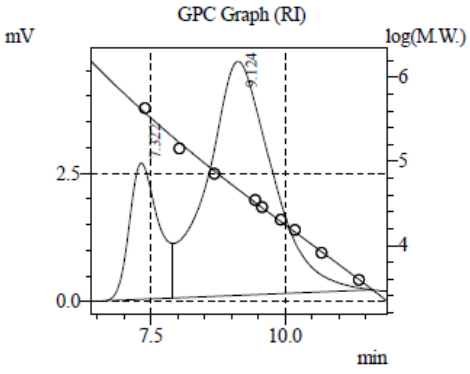

Total Average(RI)

Chromatogram Detector 2 Ch1

#	Mn	Mw	Mw/Mn
1	40803	125207	3.06855
	40803	125207	3.06855

Figure S31. SEC trace of (**P2**) in PBS (peak around 7.3 min is aggregation due to increased hydrophobicity).

2.4.5. Synthesis of 12% Pd-Py-NHC functionalized amphiphilic polymer (P2@12% Pd-Py)

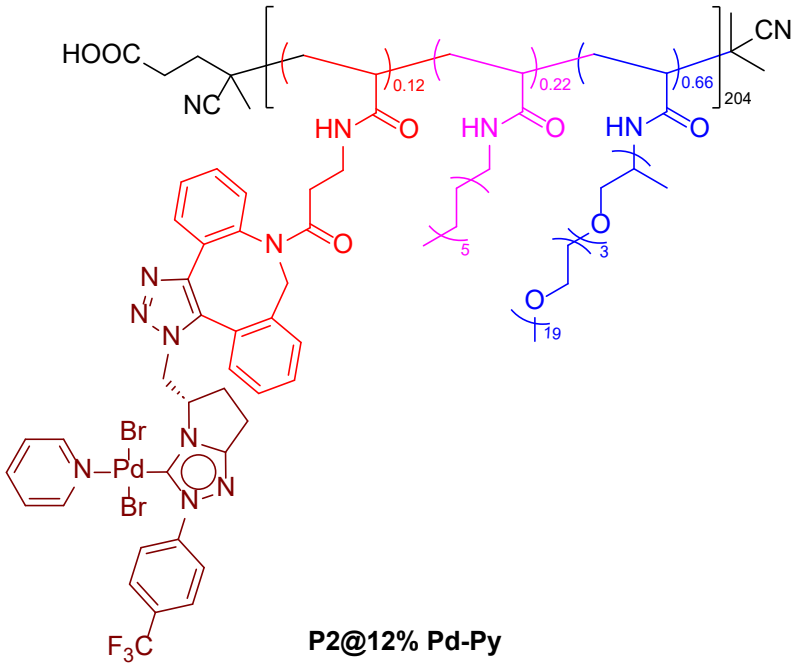

P2@12% Pd-Py

Polymer **P2** (55 mg, 0.33 µmol) and Pd-NHC complex (**2**) (5.3 mg, 8 µmol*) were dissolved in dry THF (*ca*. 2 mL) in an oven dried round bottom flask. The RB was placed in a pre-heated oil bath at 40 °C and left stirring for 8 hours under argon atmosphere. The reaction mixture was purified via dialysis (2 × 1 L THF, 2 × 1 L methanol) for 4 days by replacing the solvent every 24 hours and finally the solvent in the dialysis bag containing the Pd-NHC functionalized polymer was evaporated under reduced pressure in rotatory evaporator. The **P2@12% Pd-Py** polymer was obtained as an yellow viscous solid. $M_{theoretical}$ = 183 kDa, $M_{n,\ SEC\text{-}PBS}$ = 50.6 kDa, $M_{w,\ SEC\text{-}PBS}$ = 185.3 kDa. Đ = 3.66. ^{1}H NMR (400 MHz, $CDCl_3$, 25 °C, δ ppm): 3.93-3.47 (m), 3.37 (br), 1.24 (br), 1.12 (br). ^{19}F{^{1}H} NMR (376 MHz, $CDCl_3$, 25 °C, δ ppm): −62.52 ($C\underline{F}_3$).

*1 Equiv. with respect to DBCO graft present = 0.33 µmol × 204 × 0.12 = 8 µmol.

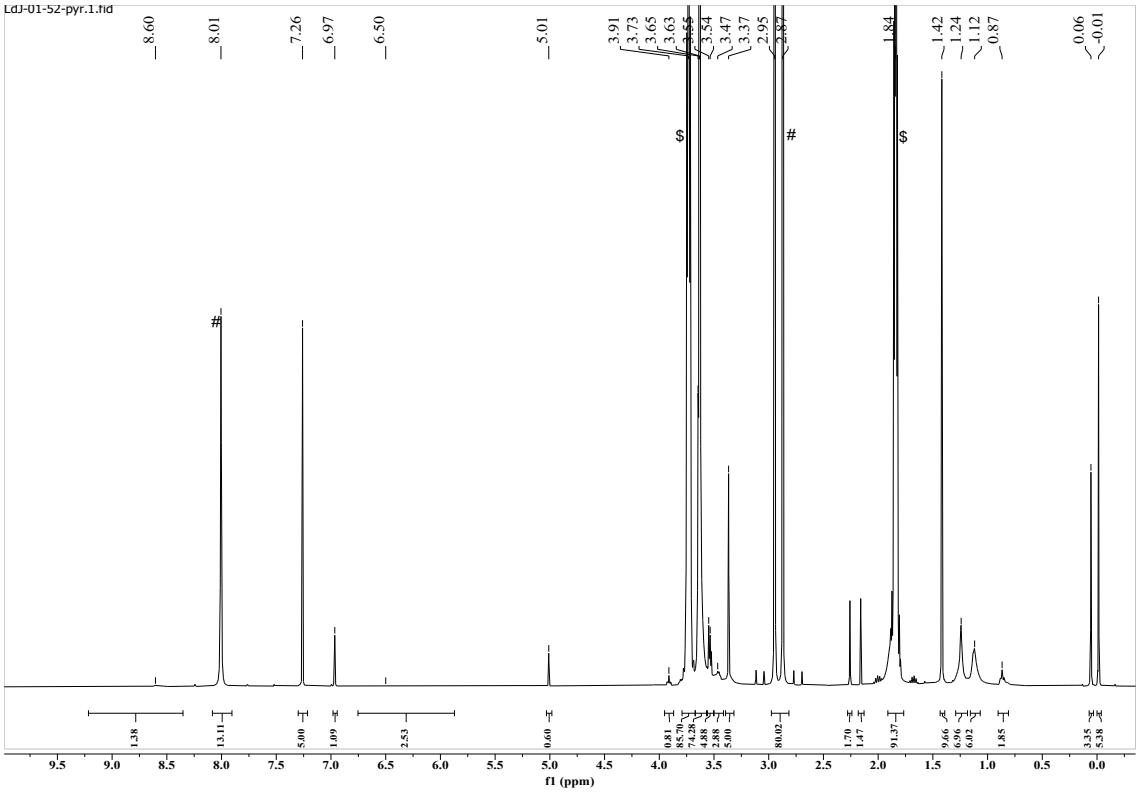

Figure S32. ^{1}H NMR of **P2@12% Pd-Py** in $CDCl_3$. # DMF, $ THF.

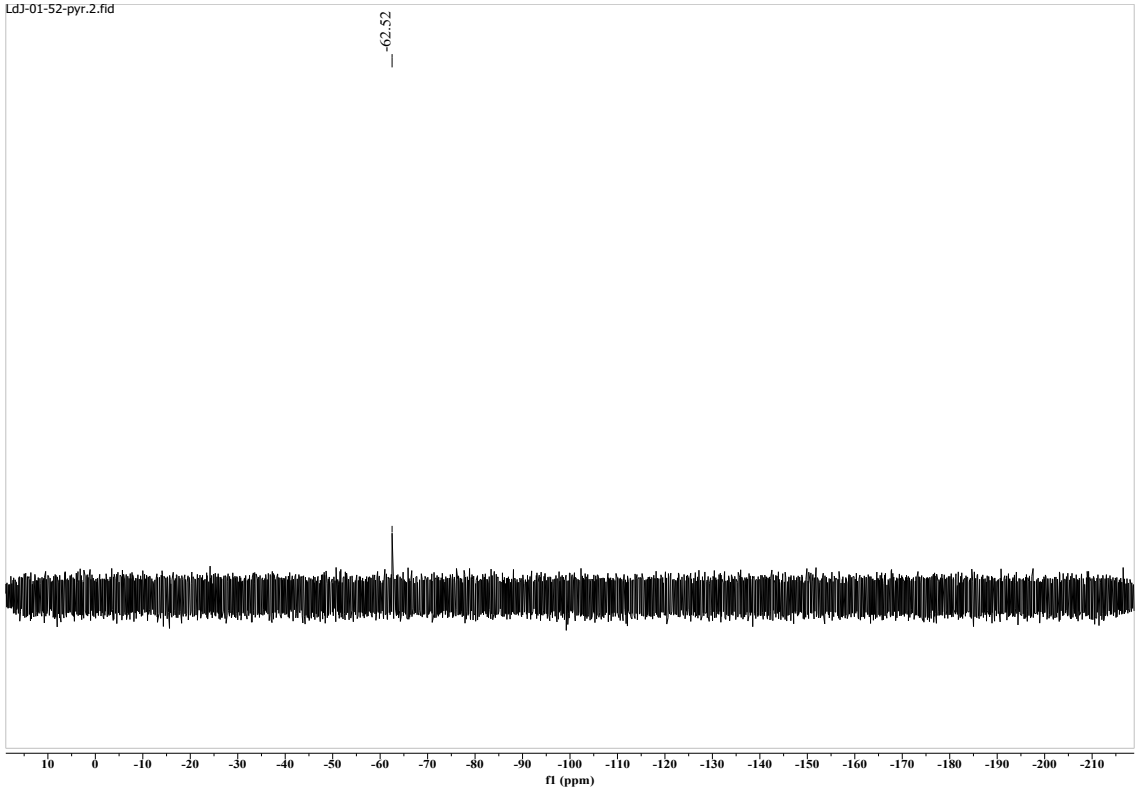

Figure S33. ^{19}F{^{1}H} NMR of **P2@12% Pd-Py** in $CDCl_3$.

Sample Name	: LdJ-01-P2@12%-pyr
Tray#	: 1
Vail#	: 21
Injection Volume	: 50 uL
Data Filename	: LdJ-01-P2@12%-pyr.lcd
Method Filename	: Shodex_08mL@min_Cal_April0423.lcm
Batch Filename	: 1b.lcb
Report Filename	: report.lsr
Date Acquired	: 2/18/2025 11:13:40 AM
Data Processed	: 2/19/2025 9:40:28 AM

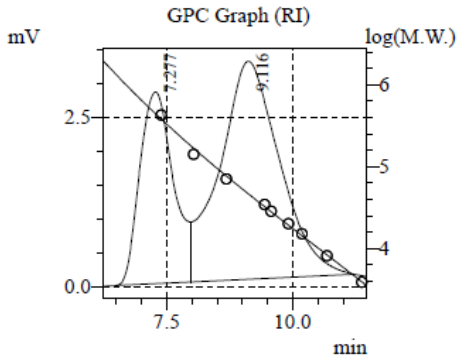

Total Average(RI)

Chromatogram Detector 2 Ch1

#	Mn	Mw	Mw/Mn
1	50650	185334	3.65912
	50650	185334	3.65912

Figure S34. SEC trace of **P2@12% Pd-Py** in PBS (peak around 7.3 min is aggregation due to increased hydrophobicity).

2.4.6. Synthesis of 12% Pd-PPh$_3$-NHC functionalized amphiphilic polymer (P2@12% Pd-PPh$_3$)

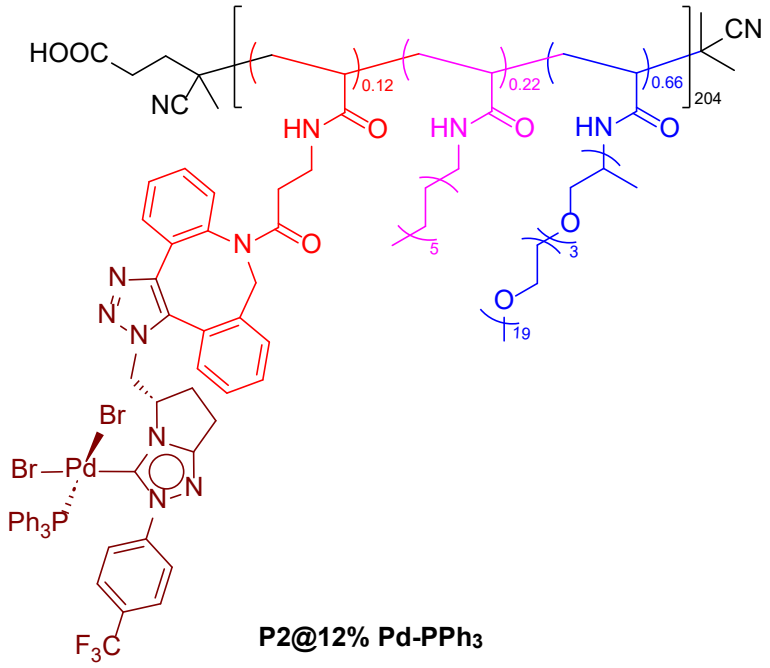

P2@12% Pd-PPh$_3$

Polymer **P2** (100 mg, 0.60 µmol) and Pd-NHC complex (**3**) (12.3 mg, 14.7 µmol*) were dissolved in dry THF (*ca*. 2 mL) in an oven dried round bottom flask. The RB was placed in a pre-heated oil bath at 40 °C and left stirring for 8 hours under argon atmosphere. The reaction mixture was purified via dialysis (2 × 1 L THF, 2 × 1 L methanol) for 4 days by replacing the solvent every 24 hours and the solvent in the dialysis bag containing the polymer was evaporated under reduced pressure in rotatory evaporator. The **P2@12% Pd-PPh$_3$** polymer was obtained as an yellow viscous solid. $M_{theoretical}$ = 187 kDa, $M_{n,\ SEC\text{-}PBS}$ = 35.5 kDa, $M_{w,\ SEC\text{-}PBS}$ = 114.3 kDa. Đ = 3.22. ^{1}H NMR (400 MHz, $CDCl_3$, 25 °C, δ ppm): 8.53 (br), 7.69-7.36 (m), 6.98 (br), 6.58 (br), 4.03 (br), 3.66 (br), 3.64 (br), 3.56-3.46 (m), 3.38 (br), 1.25 (br), 1.13 (br). ^{19}F{^{1}H} NMR (376 MHz, $CDCl_3$, 25 °C, δ ppm): −62.48 (C*F*$_3$). ^{31}P NMR (162 MHz, $CDCl_3$, 25 °C, δ ppm): δ 26.69 (Pd-*P*Ph$_3$).

The [Pd] quantified using ICP-OES measurement was slightly higher (3.12 ppm) than the actual value (2.78 ppm). The detected excess Pd likely arises from strongly associated or physically trapped Pd species that are not fully removed under the dialysis conditions employed which may slightly affect the actual Pd concentration in catalysis runs.

*1 Equiv. with respect to DBCO graft present = 0.60 µmol × 204 × 0.12 = 14.7 µmol.

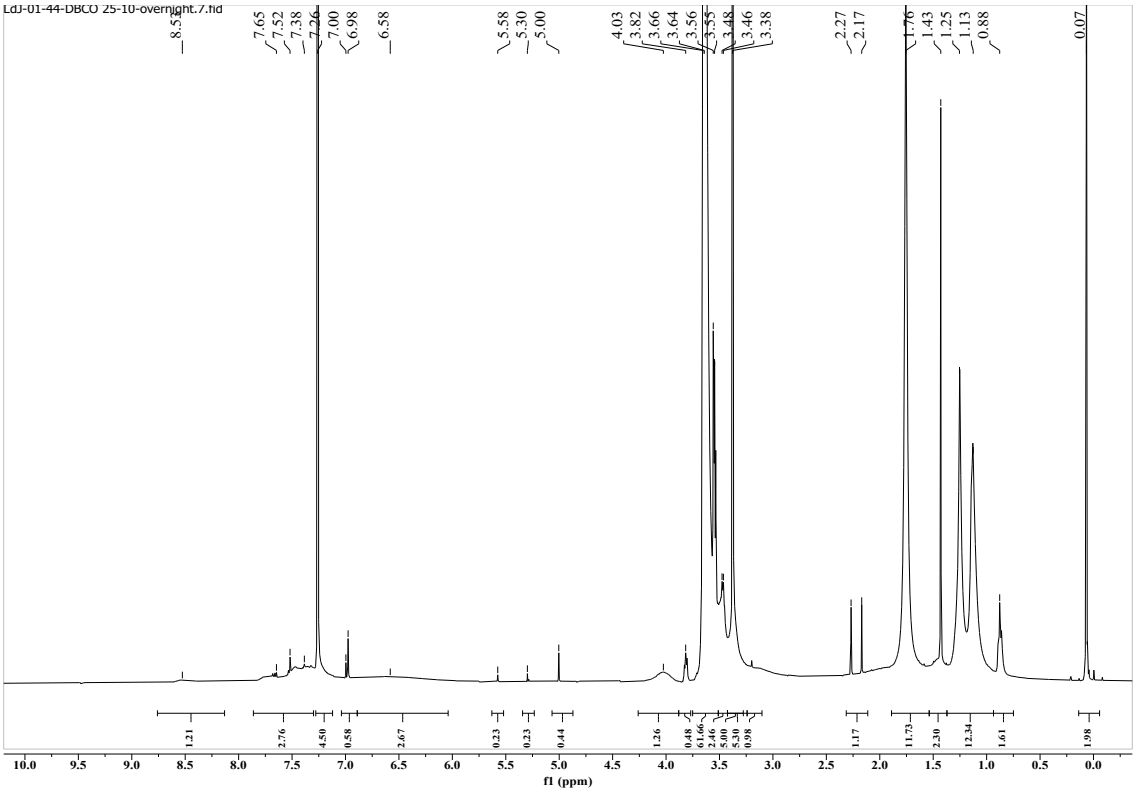

Figure S35. ^{1}H NMR of **P2@12% Pd-PPh3** in $CDCl_3$.

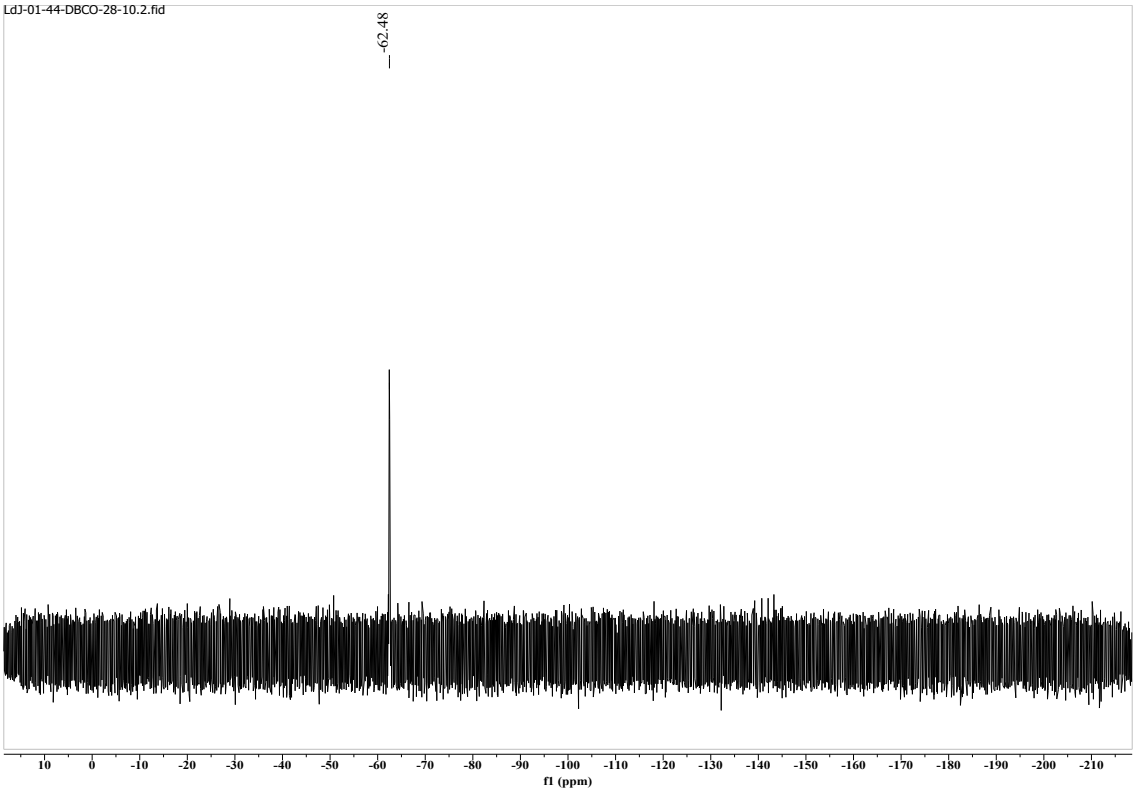

Figure S36. $^{19}F\{^{1}H\}$ NMR of **P2@12% Pd-PPh3** in $CDCl_3$.

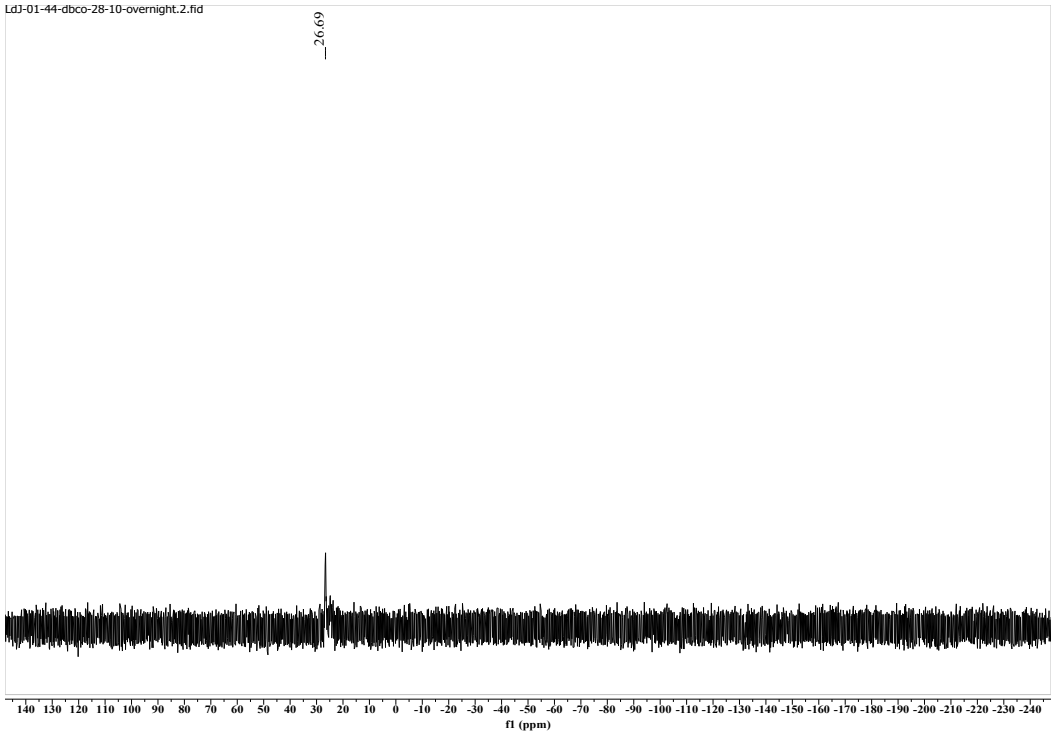

Figure S37. $^{31}P\{^{1}H\}$ NMR of **P2@12% Pd-PPh3** in $CDCl_3$.

Sample Name	: LdJ-01-P2@12%-pph3
Tray#	: 1
Vail#	: 20
Injection Volume	: 50 uL
Data Filename	: LdJ-01-P2@12%-pph3.lcd
Method Filename	: Shodex_08mL@min_Cal_April0423.lcm
Batch Filename	: 1b.lcb
Report Filename	: report.lsr
Date Acquired	: 2/18/2025 10:12:52 AM
Data Processed	: 2/19/2025 9:40:13 AM

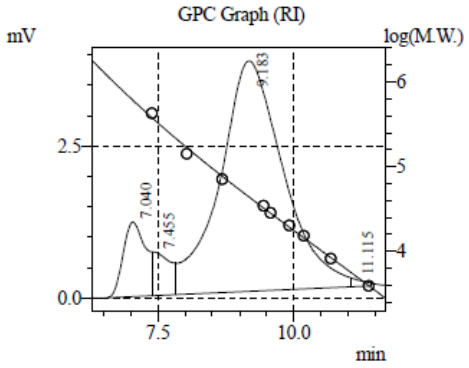

Total Average(RI)

Chromatogram Detector 2 Ch1

#	Mn	Mw	Mw/Mn
1	35535	114281	3.21604
	35535	114281	3.21604

Figure S38. SEC trace of **P2@12% Pd-PPh3** in PBS (peak around 7.0 min is aggregation due to increased hydrophobicity).

2.4.7. Synthesis of 6% Pd-PPh$_3$-NHC functionalized amphiphilic polymer (P2@6% Pd-PPh$_3$)

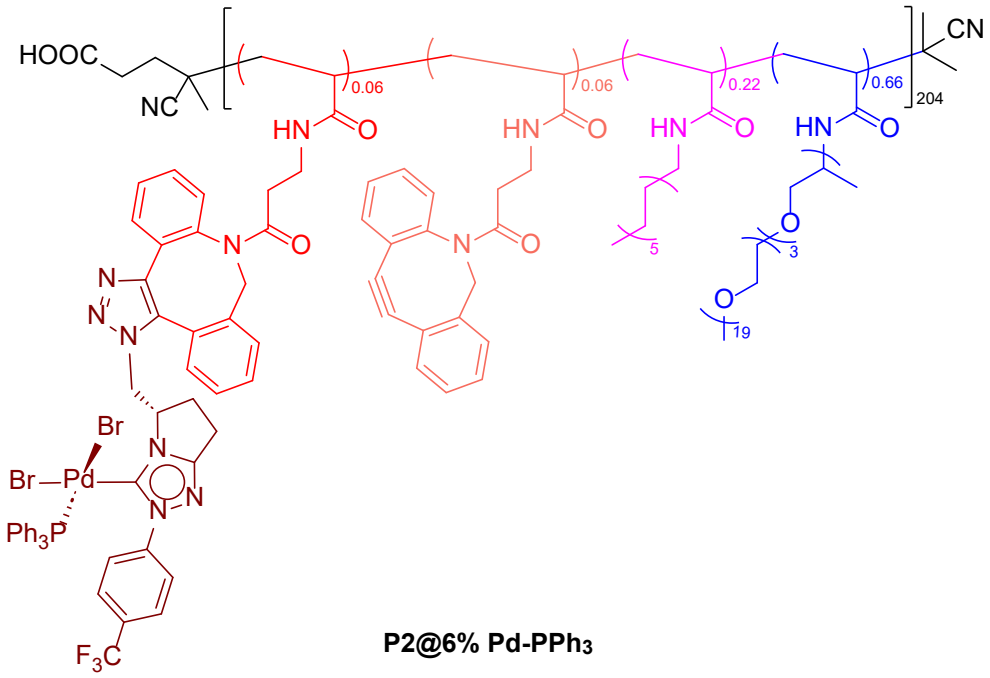

P2@6% Pd-PPh$_3$

Polymer **P2** (75 mg, 0.45 µmol) and Pd-NHC complex (**3**) (4.61 mg, 5.5 µmol*) were dissolved in dry THF (*ca*. 2 mL) in an oven dried round bottom flask. The RB was placed in a pre-heated oil bath at 40 °C and left stirring for 8 hours under argon atmosphere. The reaction mixture was purified via dialysis (2 × 1 L THF, 2 × 1 L methanol) for 4 days by replacing the solvent every 24 hours and the solvent in the dialysis bag containing the polymer was evaporated under reduced pressure in rotatory evaporator. The **P2@6% Pd-PPh$_3$** polymer was obtained as an yellow viscous solid. $M_{theoretical}$ = 177 kDa. ^{1}H NMR (400 MHz, $CDCl_3$, 25 °C, δ ppm): 7.64-7.47 (m), 6.98 (br), 4.05 (br), 3.82-3.48 (m), 3.38 (br), 1.25 (br), 1.13 (br). ^{19}F{^{1}H} NMR (376 MHz, $CDCl_3$, 25 °C, δ ppm): −62.42.

*0.5 Equiv. with respect to DBCO graft present = 0.45 µmol × 204 × 0.06 = 5.5 µmol.

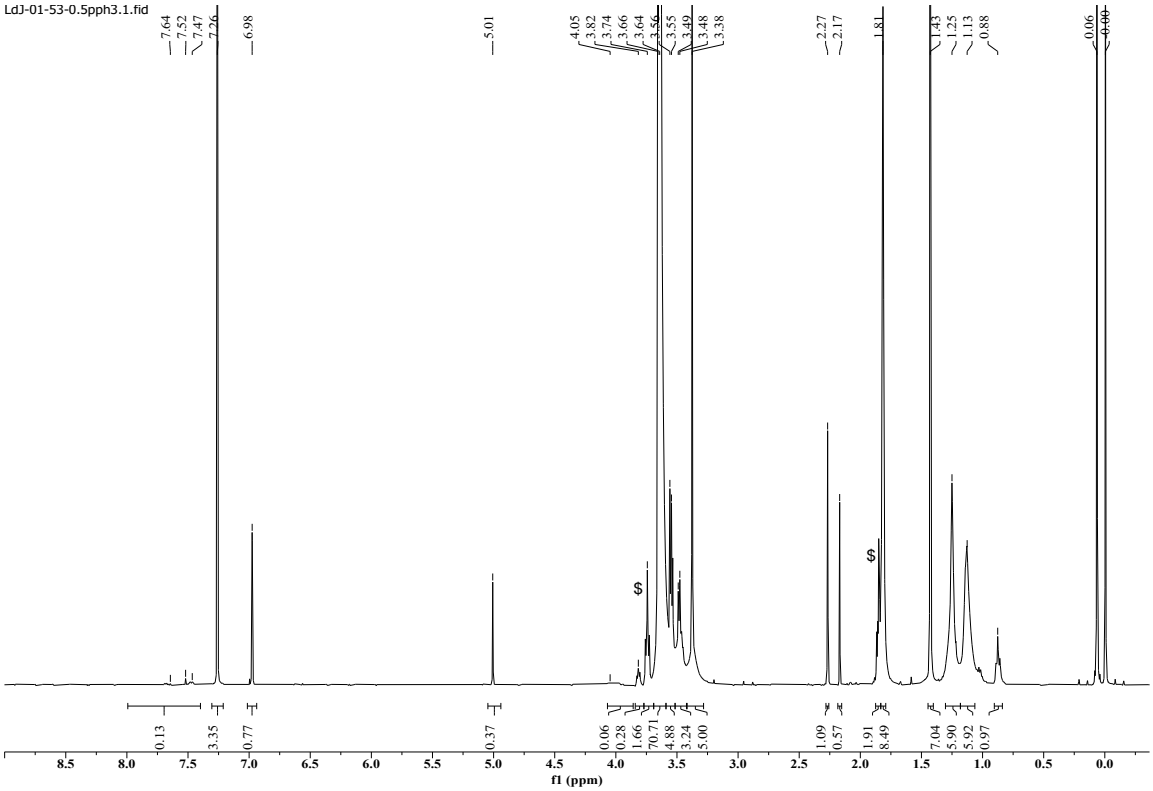

Figure S39. ^{1}H NMR of **P2@6% Pd-PPh3** in $CDCl_3$. $ THF.

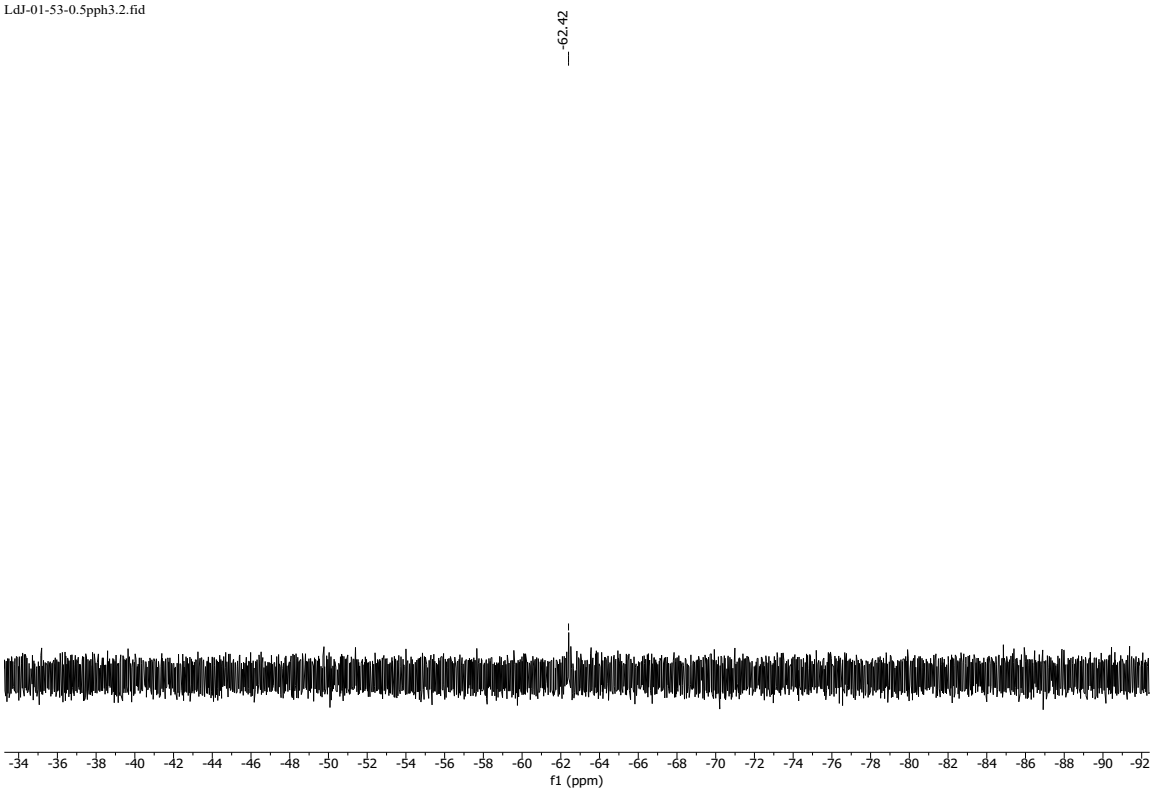

Figure S40. ^{19}F{^{1}H} NMR of **P2@6% Pd-PPh3** in $CDCl_3$.

3. General procedure for the nanoparticle formulation

3.1. Encapsulation of Pd-NHC in amphiphilic polymer (P1)

Method A: Polymer (**P1**) and Pd-NHC complexes (**2**)/(**3**) were co-dissolved in DCM in a glass vial. Depending on the analysis or experiments Pd concentrations were used. For cell studies, 1:10 P:Pd ratio, for catalysis runs 1 mg polymer per mL and 30 μM Pd concentrations were used. DCM was gently evaporated by argon gas flow, which resulted a thin film on the glass vial. The film was dried in a vacuum oven at 40 °C for 1 h. This thin film was dissolved in water by vortex, sonicated for 45 min and left to equilibrate for 30 min.

Method B:

P1-Pd-Py

Polymer (**P1**) was pre-dissolved in water. Stock solutions of Pd-NHC complex (**2**) was prepared in DMSO (10 mg / mL). **P1-Pd-Py** nanoparticles were prepared, for e.g., for catalysis runs, to a 3 mg of **P1** polymer in 2.988 mL water (1 mg / mL), 5.88 μL DMSO stock of Pd-NHC complex (**2**) was added (for 30 μM Pd) vortexed and sonicated. Then, 6.0 μL DMSO stock of pro-DNP (**4**) or 6.0 μL DMSO stock of pro-cou (**6**) was added quickly, mixed and kinetics measurements were performed immediately at a preset 37 °C using UV-Vis or fluorescence spectrophotometer. The DMSO content was 0.4 % *v/v* in the final water solution.

P1-Pd-PPh$_3$

Polymer (**P1**) was pre-dissolved in water. Stock solutions of Pd-NHC complex (**3**) was prepared in DMSO (10 mg / mL). **P1-Pd-PPh$_3$** nanoparticles were prepared, for e.g., for catalysis runs, to a 3 mg of **P1** polymer in 2.987 mL water (1 mg / mL), 7.53 μL DMSO stock of Pd-NHC complex (**3**) was added (for 30 μM Pd) vortexed and sonicated. Then, 6.0 μL DMSO stock of pro-DNP (**4**) or 6.0 μL DMSO stock of pro-cou (**6**) was added quickly, mixed and kinetics measurements were performed immediately at a preset 37 °C using UV-Vis or fluorescence spectrophotometer. The DMSO content was 0.4 % *v/v* in the final water solution.

3.2. P2 particles

The weighed samples of **P2@12% Pd-Py**, **P2@12% Pd-PPh$_3$** and **P2@6% Pd-PPh$_3$** polymers were directly dissolved in water, vortexed, sonicated for 45 min and left to equilibrate for 30 min.

4.1. Gel permeation chromatography (GPC) measurements

In order to have an insight about the polymers molecular weight distribution we performed GPC measurements in PBS (aqueous). All samples were dissolved at a concentration of 1 mg polymer per 1 mL solvent. Prepolymers were dissolved in THF, vortexed thoroughly and filtered using 0.45 μm PVDF filter before measuring. Amphiphilic polymers were dissolved in PBS, vortexed and sonicated for 30 minutes and filtered using 0.45 μm PVDF filter before measuring.

Size exclusion chromatography (SEC) measurements of poly(pentafluorophenyl) acrylate were performed on a Shimadzu LC-2030C 3D system equipped with an RID-20 refractive index detector and a PDA detector. Tetrahydrofuran (THF) was used as the eluent at a flow rate of 1 $mL \cdot min^{-1}$ on Agilent Mixed-C and Mixed-D columns connected in series and maintained at 40 °C (exclusion limit: 2.000.000 $g \cdot mol^{-1}$; 7.5 mm i.d. × 300 mm). Calibration was carried out using polystyrene standards (Polymer Laboratories).

SEC measurements in PBS (pH 7.4) were performed on a Shimadzu CBM-20A system at 25 °C equipped with a Shimadzu RID-10A refractive index detector and a PDA detector. A Shodex OHpak SB-804 HQ column (exclusion limit: 1000 kDa; 0.8 cm i.d. × 300 mm) coupled to a Shodex OHpak SB-G 6B – F6709430 guard column (0.6 cm i.d. × 40 mm) was used, with PBS as the eluent at a constant flow rate of 0.8 $mL \cdot min^{-1}$. Calibration was performed using PEO standards (Polymer Laboratories).

4.2. Dynamic light scattering (DLS) measurements

The size distribution of the formulated nanoparticles were studies by measuring the hydrodynamic radius using DLS. The polymers (0.1/0.3/0.5/1 mg per mL) were dissolved in Milli-Q water, vortexed and sonicated for 30 minutes and kept 1 hour for equilibration. Then samples were filtered using an 0.2 µm PVDF filter before measuring.

Dynamic light scattering (DLS) measurements were performed on a Malvern Zetasizer µV (λ = 830 nm) using Sarstedt disposable cuvettes. Samples were filtered prior to analysis to remove dust, and measurements were conducted at 20 °C. Scattering intensity was recorded in triplicate at a fixed scattering angle of 90°. Fluctuations in scattering intensity were analyzed using the built-in CUMULANT algorithm to obtain the intensity-, volume-, and number-weighted particle size distributions. The apparent hydrodynamic radius (R_H) was calculated from the particle diffusion coefficient (D) as $R_H = k_BT / (6\pi\eta D)$, where k_B is the Boltzmann constant, T is the solution temperature (K), and η is the solvent viscosity (η = 1.0016 mPa s). The final R_H value was taken from the intensity-weighted distribution as the average of the three measurements. The intensity, volume and number distributions of the hydrodynamic radius R_H as determined via DLS are shown in figure S41.

S.No	Polymer	Hydrodynamic radius (R_H) nm			
		0.1 mg/mL	**0.3 mg/mL**	**0.5 mg/mL**	**1.0 mg/mL**
1	**P1**		11.6		
2	**P1-Pd-Py**		9.0		
3	**P1-Pd-PPh_3**		11.4		
4	**P2**		9.2		
5	**P2@12% Pd-Py**			6.6	
6	**P2@12% Pd-PPh_3**	6.5		6.7	7.6
7	**P2@6% Pd-PPh_3**			11.0	

Table S1. Hydrodynamic radius (R_H) determined from intensity distributions.

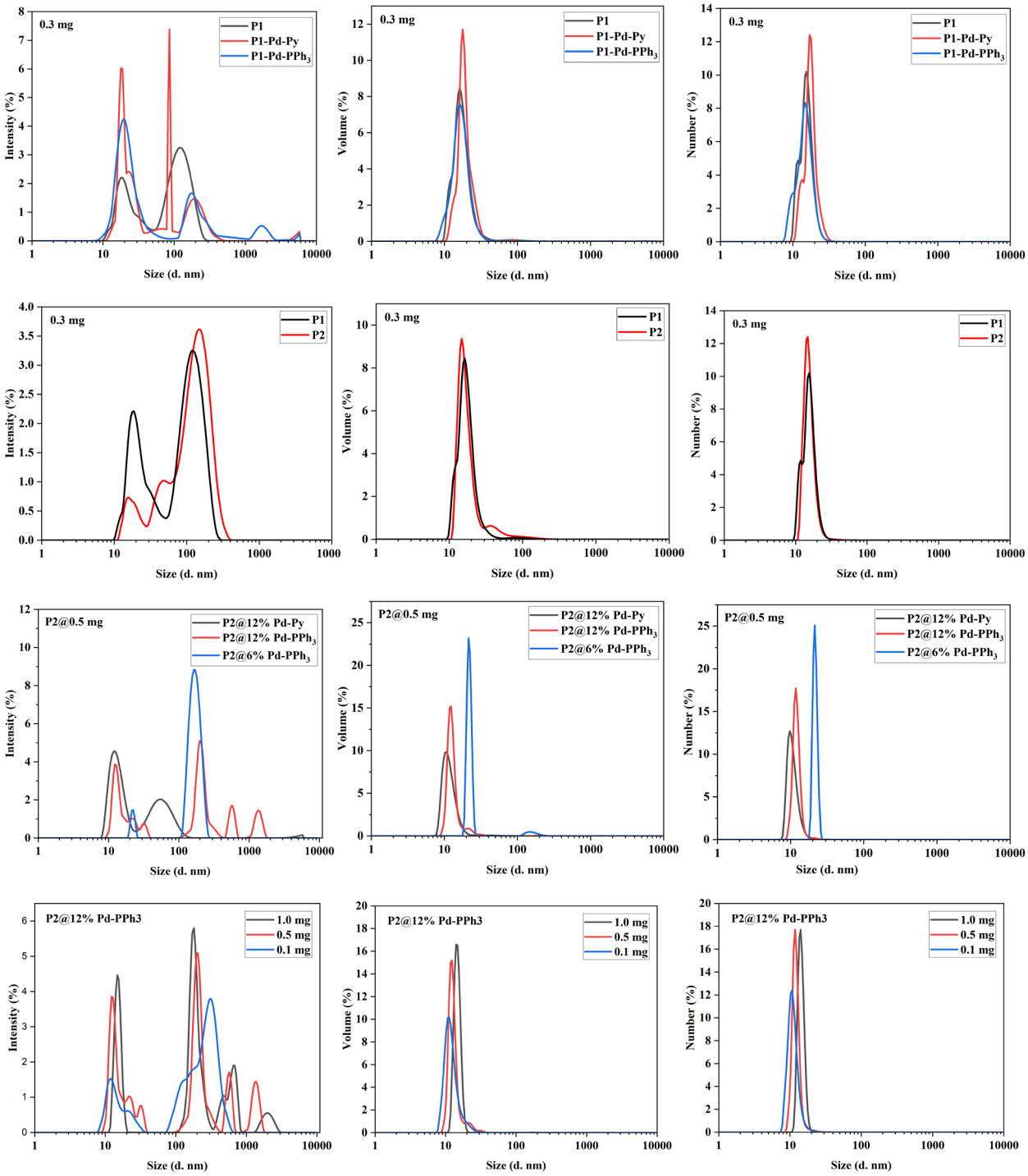

Figure S41. Dynamic light scattering (DLS) studies of **P1**, **P2** particles; left column – intensity distribution; center column – volume distribution; right column – number distributions; **P1**, **P2**, **P1-Pd-Py**, and **P1-Pd-PPh3** measured at 0.3 mg/mL; **P2@12% Pd-Py**, **P2@12% Pd-PPh3** and **P2@6% Pd-PPh3** measured at 0.5 mg/mL; **P2@12% Pd-PPh3** at 0.1, 0.5, 1 mg/mL in water at 25 °C.

4.3. Quantification of Pd concentration through ICP-OES

The actual Pd concentration in the polymeric nanoparticles were calculated using inductively coupled plasma - optical emission spectrometry (ICP-OES). 1000 mg/l Pd standard solution was used to determine the calibration curves for quantification. Pd containing polymer samples were prepared around 1-3 ppm range in 4 mL solutions. The samples were prepared in milli Q and also in milli Q with 2% THF to ensure complete dissolution of samples in the measurement.

S.No	Polymer	Expected Pd (ppm)	Measured Pd in polymer (ppm)
1	**P1-Pd-Py***	1.06	0.852
2	**P1-Pd-PPh_3***	1.06	0.972
3	**P2@12% Pd-Py#**	2.85	2.471
4	**P2@12% Pd-PPh_3#**	2.78	3.117$
5	**P2@6% Pd-PPh_3#**	1.48	1.059

Table S2. Pd concentration (ppm) in polymer samples measured using ICP-OES, * measured in milli Q, **#** measured in milli Q containing 2% THF; $ the detected excess Pd likely arises from strongly associated or physically trapped Pd species that are not fully removed under the dialysis conditions employed which may slightly affect the actual Pd concentration in catalysis runs.

Two calibration curves were measured, one in Milli Q water and another in Milli Q containing 2 % THF (*v/v*) in order to quantify the Pd concentration in the polymeric nanoparticles.

S.No	Expected Pd (ppm)	Measured Pd in standard solution (ppm)	
		Milli Q	**Milli Q + 2 % *v/v* THF**
1	0.0	0.0	0.0
2	0.5	0.635	
3	1.0	0.998	1.123
4	1.5	1.570	1.503
5	2.0	1.996	1.844
6	2.5	2.513	2.574
7	3.0	2.935	

Table S3. Calibration curves using standard Pd solution for ICP-OES measurements.

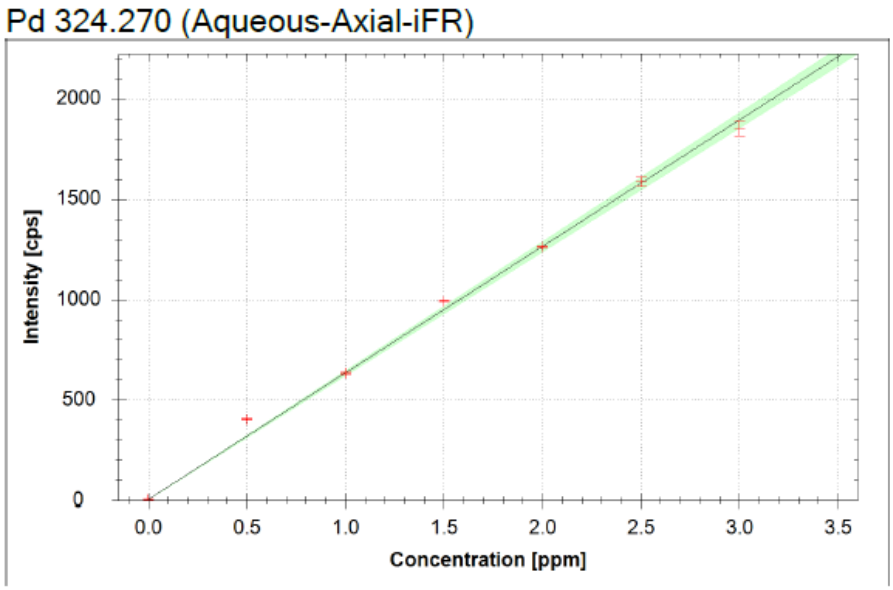

f(x) = 630.5148*x + 4.1168
R^2 = 0.9958
BEC = 0.007 ppm
LoD = 0.0052 ppm

Figure S42. Calibration curve using standard Pd solution in Milli Q for ICP-OES.

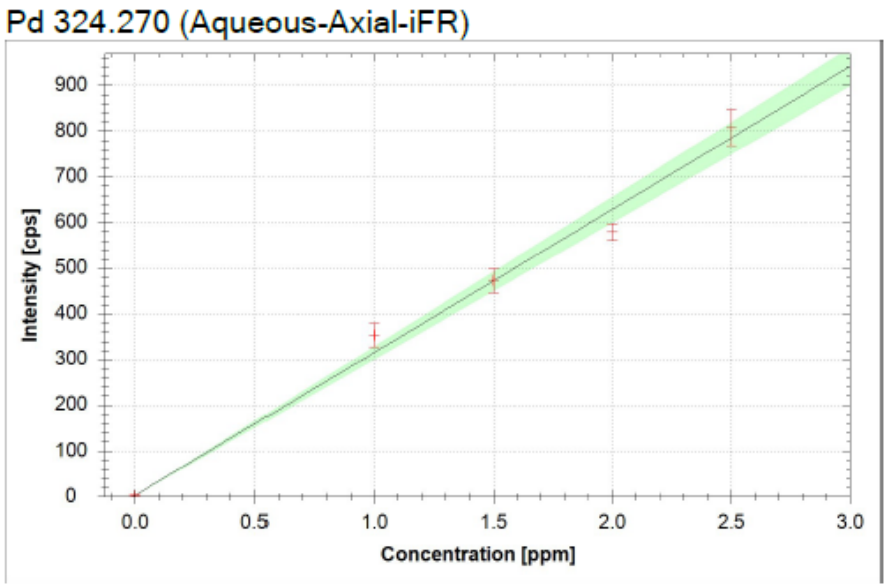

f(x) = 312.9079*x + 2.4102
R^2 = 0.9876
BEC = 0.008 ppm
LoD = 0.0069 ppm

Figure S43. Calibration curve using standard Pd solution in Milli Q water containing 2 % THF *(v/v)* for ICP-OES.

4.4. Small-angle X-ray scattering (SAXS) measurements

SAXS was measured on beamline BM29 (BioSAXS) at the European Synchrotron Radiation Facility. The scattering intensity I(q) was recorded as a function of the scattering vector q over the range of 0.08-5.85 nm^{-1} using monochromatic X-rays with an energy of 12.5 keV. The scattered x-rays were recorded on a Pilatus3 2M detector in vacuum. Samples were measured for 10 frames of 1 second in a quartz capillary with a 1 mm diameter at 20 °C using the sample changer mode. The corresponding buffer was measured after each sample. ATSAS primus was used for frame averaging and background subtraction. Form-factor fitting was performed in SasView 5.0.6. The fitting was truncated at q = 2 nm^{-1} to mitigate fitting of the noise. Additionally, for all **P2** polymeric systems measured a more significant contribution from aggregation was observed as there is an upturn at low q values. For **P2@12% Pd-Py**, the fitting range was adjusted to q = 0.17-2 nm^{-1}, the full curve is subsequently calculated. For **P2@Pd-PPh3** a custom additive model of the shape independent power law and the flexible cylinder model was used, where the power law accounts for the presence of aggregates.

Sample preparation:

P1 particles

Polymer (**P1**) was pre-dissolved in water. Stock solutions of Pd-NHC complex (**2**) and (**3**) was prepared in DMSO (10 mg / mL). For **P1-Pd-Py**: to a 0.25 mg of **P1** polymer in 0.499 mL water (0.5 mg / mL), 0.98 µL DMSO stock of Pd-NHC complex (**2**) was added (for 30 µM Pd) vortexed and sonicated for 45 min and left to equilibrate for 30 min. The DMSO content is 0.2 % *v/v* in the final water solution. For **P1-Pd-PPh3**: to a 0.25 mg of **P1** polymer in 0.499 mL water (0.5 mg / mL), 1.26 µL DMSO stock of Pd-NHC complex (**3**) was added (for 30 µM Pd) vortexed and sonicated for 45 min and left to equilibrate for 30 min. The DMSO content is 0.2 % *v/v* in the final water solution.

P2 particles

The weighed samples of **P2@12% Pd-Py**, **P2@12% Pd-PPh3** and **P2@6% Pd-PPh3** polymers (0.25 mg) were directly dissolved in 0.5 mL water (0.5 mg / mL), vortexed, sonicated for 45 min and left to equilibrate for 30 min.

Polymer	L[a] (nm)	l_k (nm)	r	Power law	χ^2
P1-Pd-Py	83	9.7 ± 0.7	2.6 ± 0.04	-	1.1
P1-Pd-PPh3	83	8.3 ± 0.4	2.5 ± 0.03	-	0.96
P2@12% Pd-Py	83	9.4 ± 0.6	2.8 ± 0.04	-	1.2
P2@12% Pd-PPh3	83	15.8 ± 0.5	2.6 ± 0.02	4.9	1.9
P2@6% Pd-PPh3	83	8.3 ± 0.3	2.4 ± 0.02	4.3	1.8

Table S4. Results of the form-factor fits to the flexible cylinder model for the studied polymers; a) Fixated at the theoretical value of 83 nm.

The theoretical contour length was calculated as the contour length of the polymeric backbone and twice the contour length of the hydrophilic side-grafts, according to $L = L_{bb}N_{bb}Đ_{bb} + 2L_{sc}N_{sc} =$

83 nm. L_{bb} = 2*0.154*cos(70.5/2) = 0.252 nm corresponds to the length of a monomer backbone, N_{bb} = 204 corresponding to the amount of monomers in the backbone and $Đ_{bb}$ = 1.31 is the polymeric backbone dispersity. Lsc = 3*0.1464*cos(68/2) = 0.364 nm is the average length of a PEG monomer and Nsc = 22 is the amount of monomer units in Jeffamine M1000. During the fitting process, we decided to fixate the contour length L to the theoretically calculated value of 83 nm (see experimental section for details on the calculation). Leaving this parameter free, led to unphysically long contour lengths. We attribute this to the relatively low signal-to-noise ratio of the data.

Due to solubility issues of the SCPNs, only a single concentration of 0.5 mg/mL was measured for each of the tested polymers. We tested five different polymers, where **P1** was used to physically encapsulate two Pd-catalysts. In **P2**, the Pd-catalysts were added via a SPAAC click reaction, to covalently link the Pd-catalysts to the polymeric backbone. The level of functionalization is different for each of the compositions and 2 different Pd-catalysts (**Pd-Py** and **Pd-PPh$_3$**) were incorporated. The polymers were measured in MilliQ, (**P1** samples were measured in MilliQ with 0.2 vol% DMSO. Background subtraction for these samples was thus performed with a different matching buffer.

The obtained scattering curves of all polymers are in shape very similar to what we expect for a 20 mol% dodecyl and 80 mol% Jeffamine polymer. We observed (approach to) a scattering plateau at low q and a gradual decrease with one inflection point at higher q values (~0.6 nm^{-1}). This is in agreement with the scattering curves of a semi-flexible polymer chain. The lack of the clear inflection point at lower q values is attributed to the low signal-to-noise ratio. We were not able to perform a Guinier analysis to obtain a value for R_G, we attribute this to the relatively low signal to noise ratio and the presence of an upturn at low q, indicative of some aggregation present.

Next we performed form factor fitting on the scattering curves. We know from previous studies that similar polymeric systems can be well described as semi-flexible polymer chains and the currently obtained scattering curves are in line with this expectation. Therefore, we fit the obtained scattering curves with the flexible cylinder model in SasView 5.0.6. This model describes the polymer chains as a semi-flexible cylinder with length L with a certain flexibility described in the Kuhn length l_k and a radius of the cylinder r. We have included error bars on the fitted parameters. As indicated in the Table S4, the Kuhn length showed relatively larger uncertainty compared to r. This is attributed to suboptimal data quality.

All SAXS curves are offset for clarity purposes. The form factor fits for **P1** with the two different Pd-catalysts are shown in Figure 1C. The fits and obtained parameters can be found in Table S4. We observed a visually good agreement between the experimental data and the fit, which is also corroborated by the low $\chi 2$ values. The radius of the polymers is mainly dictated by the Jeffamine M1000 side grafts, and is almost the same for both polymers with a value of 2.5-2.8 nm. Interestingly, we observed a difference in the Kuhn length, i.e. the distance over which the polymer is rigid, which is smaller for **P1-Pd-PPh$_3$**, (8.3 nm) suggesting a more compact polymer. The obtained parameters are in line with previously obtained values for a 20 mol% dodecyl, 80 mol% Jeffamine SCPN, where a l_k of 8.5 nm and an r of 2.5 nm were found.[4]

For the **P2** particles, we see some interesting features in the scattering curves. Most prominently, all curves exhibit an upturn at low q, indicative of aggregation. This effect is especially pronounced in the **P2@Pd-PPh$_3$** systems. The scattering curve obtained for **P2@12% Pd-Py** closely resembles that of **P1-Pd-Py**, both in shape and in the derived fit parameters. Aside from slightly

increased aggregation in the covalently attached system, appears to be minimal difference between the physical encapsulation and covalent attachment for **Pd-Py**.

Both **P2@Pd-PPh3** (12% and 6%) polymers display a very distinct low-q upturn in their scattering curves, again pointing to aggregation. To account for this, we adapted our fitting strategy by combining a power-law model with the flexible cylinder model. The power-law component captures the low-q behaviour association with the aggregates, while the flexible cylinder model describes the polymeric nanoparticles. This approach yielded good fits, as indicated by the low $\chi 2$ values.

As expected, r stays very similar across the **Pd-PPh3**-containing polymers (both **P1** and **P2**); this dimension is mainly governed by the size of the Jeffamine side-grafts. However, we observed clear differences in the obtained Kuhn lengths. For **P2@12% Pd-PPh3**, the Kuhn length increases significantly to 14 nm, suggesting a more rigid and less compact polymer. In contrast, lower functionalization in **P2@6% Pd-PPh3** results in a lower Kuhn length of 8.3 nm, equal to that of the physically encapsulated system. We attribute these differences to the nature of the PPh_3 group, which is a bulky, hydrophobic moiety capable of π–π stacking and thus inducing compaction. However, the spatial demands of the PPh_3 group may also limit the compaction of the polymeric backbone sterically. It therefore seems that the 12 mol% incorporation is overcrowding the polymeric backbone, where the lower side graft incorporation of 6 mol% does allow for some compaction of the polymeric backbone.

5. General procedure for the kinetic experiments

5.1. Pro-DNP (4) activation by UV-Vis spectroscopy

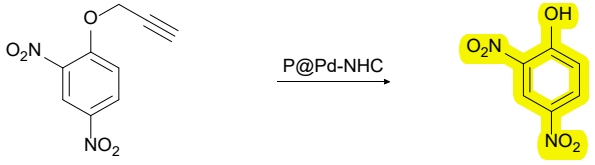

Pro-DNP (**4**) DNP (**5**)

Pro-DNP = (propargyl) protected 2,4-dinitro phenol; DNP = 2,4-dinitro phenol; UV-Vis (ultraviolet-visible light) spectroscopy

S.No	Nanoparticles	Concentration in 3 mL		P to Pd molar ratio (P:Pd)	Polymer Wt. in 3 mL (mg)
		Polymer (μM)	Pd (μM)		
1	**P1-Pd-Py**	5.29	30	1:5.7	3
2	**P1-Pd-PPh3**	5.29	30	1:5.7	3
3	**P2@12% Pd-Py**	1.23	30	1:24.4	0.675
4	**P2@12% Pd-PPh3**	1.23	30	1:24.4	0.69
5	**P2@6% Pd-PPh3**	2.45	30	1:12.2	1.30

Table S5. Reaction condition and concentrations. Substrate pro-DNP (**4**) 100 μM, Pd 30 μM, 37 °C, water 3 mL, stirring at 800 rpm. The formation of DNP (**5**) was monitored at λ = 400 nm using UV-Vis spectrophotometer over time.

The catalytic efficiency of the palladium NHC catalyst containing, encapsulated **P1** and covalent **P2** nanoparticles were tested in the depropargylation reaction of pro-DNP (**4**) to DNP (**5**) which absorbs at 400 nm that can be quantified using UV-Vis spectroscopy. Reactions were performed at a preset temperature of 37 ℃, using 100 μM substrate pro-DNP (**4**) and 30 μM Pd concentration in 3 mL water using 10 mm disposable absorbance cuvettes with 800 RPM stirring and the reaction progress was monitored in real-time on Agilent Cary 3500 multicell UV-Vis spectrophotometer.

P1-Pd-Py

Polymer (**P1**) was pre-dissolved in water. Stock solutions of Pd-NHC complex (**2**) was prepared in DMSO (10 mg / mL). Pro-DNP (**4**) stock solution were prepared in DMSO at 50 mM concentration. To a 3 mg of **P1** polymer in 2.988 mL water (1 mg / mL), 5.88 μL DMSO stock of Pd-NHC complex (**2**) was added (for 30 μM Pd) vortexed and sonicated. Then, 6.0 μL DMSO stock of pro-DNP (**4**) was added (100 μM), rapidly mixed and kinetics measurements were immediately performed at a preset 37 ℃ using UV-Vis spectrophotometer. The DMSO content is 0.4 % *v/v* in the final water solution.

P1-Pd-PPh$_3$

Polymer (**P1**) was pre-dissolved in water. Stock solutions of Pd-NHC complex (**3**) was prepared in DMSO (10 mg / mL). Pro-DNP (**4**) stock solution were prepared in DMSO at 50 mM concentration. To a 3 mg of **P1** polymer in 2.987 mL water (1 mg / mL), 7.53 μL DMSO stock of Pd-NHC complex (**3**) was added (for 30 μM Pd) vortexed and sonicated. Then, 6.0 μL DMSO stock of pro-DNP (**4**) was added (100 μM), rapidly mixed and kinetics measurements were immediately performed at a preset 37 ℃ using UV-Vis spectrophotometer. The DMSO content is 0.4 % *v/v* in the final water solution.

P2 particles

The weighed samples of **P2@12% Pd-Py** (0.675 mg), **P2@12% Pd-PPh$_3$** (0.69 mg) and **P2@6% Pd-PPh$_3$** (1.30 mg) polymers were directly dissolved in 2.994 mL water, vortexed, sonicated (for 30 μM Pd). Pro-DNP (**4**) stock solution were prepared in DMSO at 50 mM concentration. Then, 6.0 μL DMSO stock of pro-DNP (**4**) was added (100 μM), rapidly mixed and kinetics measurements were immediately performed at a preset 37 ℃ using UV-Vis spectrophotometer. The DMSO content is 0.2 % *v/v* in the final water solution.

Pd NPs deactivation pathway studies

Pd nanoparticles were prepared as above to which pro-DNP (**4**) (100 μM, DMSO stock) was added followed by 30 μM (stock prepared in milliQ) of various biomolecules like L-glycine, L-cysteine,

L-leucine, L-glutamine, L-histidine, D-glucose, and glutathione were added, rapidly mixed and kinetics measurements were immediately performed at a preset 37 °C using UV-Vis spectrophotometer.

Both the **P1** and **P2** particles lost catalytic activity in the presence of L-histidine, L-cysteine, and glutathione, where free amine and sulphur nucleophiles mostly poison the Pd catalyst while they remained catalytically active in the presence of L-leucine, L-glycine, L-glutamine, and D-glucose (Fig. S48).

Pd NPs reusability studies

Pd nanoparticles were prepared as above to which pro-DNP (**4**) (100 μM, DMSO stock) was added, rapidly mixed and kinetics measurements were immediately performed at a preset 37 °C using UV-Vis spectrophotometer over 15 hours. The reusability of the Pd nanoparticles were evaluated by adding an additional 100 μM of pro-DNP (**4**) substrate to the same reaction after the first catalytic run (15 h) and kinetics measurements were continued further.

The Pd nanoparticles continued to actively cleave the pro-dye even after 30 h. Similarly the reusability studies in the presence of 30 μM L-leucine, L-glycine, L-glutamine, and D-glucose were also performed and found that the Pd nanoparticles remained catalytically active after the first run (Fig. S49).

Pd NPs stability study

Pd nanoparticles were prepared as above and kept aside for 24 hours. To this pro-DNP (**4**) (100 μM, DMSO stock) was added, rapidly mixed and kinetics measurements were immediately performed at a preset 37 °C using UV-Vis spectrophotometer and compared against a freshly prepared Pd NPs.

The catalytic activity of the pre-incubated sample was significantly slower compared to that of a freshly prepared Pd nanoparticles (Fig. S50).

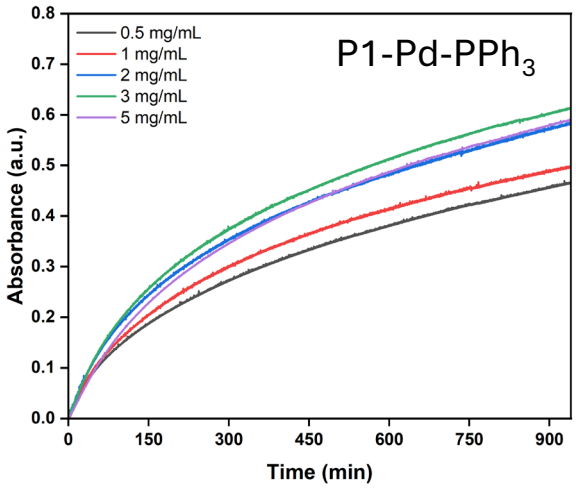

Figure S44. Polymer concentration variation study; pro-DNP (**4**) (100 µM) to DNP (**5**) using 30 µM of **Pd-PPh3** while varying **P1** (0.5, 1, 2, 3 and 5 mg/mL) concentrations in water at 37 °C monitored by UV-Vis spectroscopy over time at λ = 400 nm.

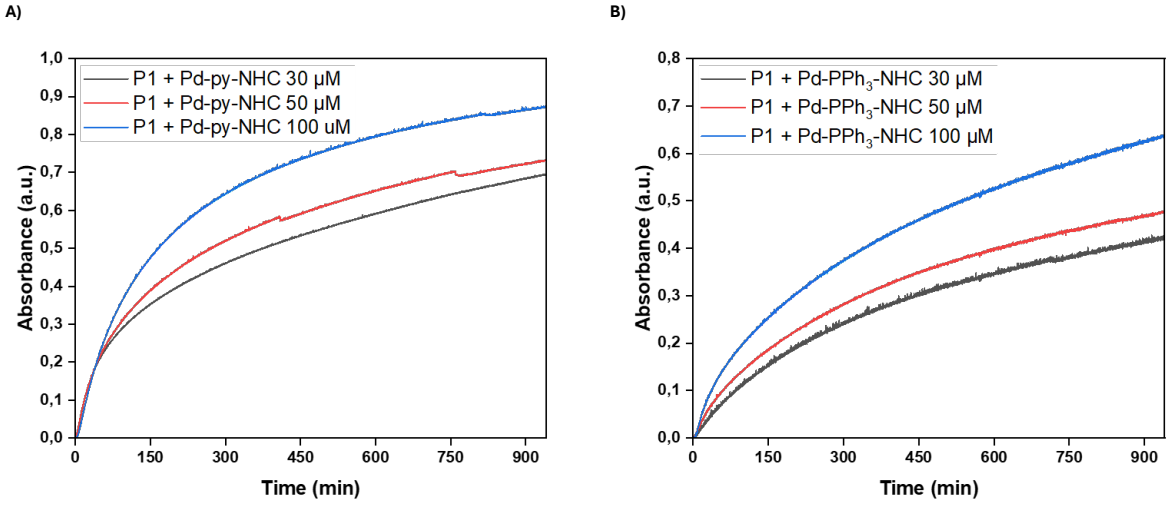

Figure S45. Catalyst concentration variation study; pro-DNP (**4**) (100 µM) to DNP (**5**) using 1 mg/mL **P1**, while varying **Pd** concentrations (30, 50 and 100 µM) in water at 37 °C monitored by UV-Vis spectroscopy over time at λ = 400 nm; A). **Pd-Py**, B). **Pd-PPh3**.

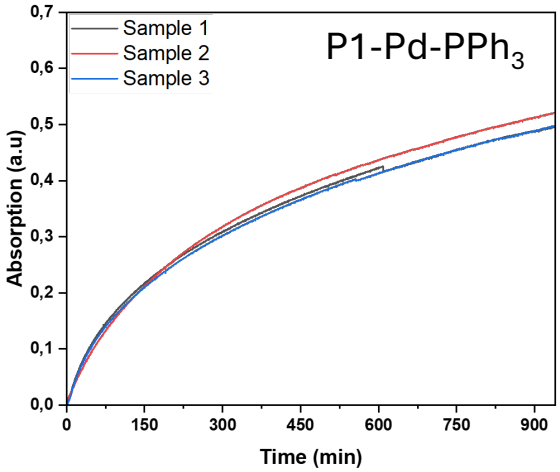

Figure S46. Consistency of the reaction runs; pro-DNP (**4**) (100 µM) to DNP (**5**) using 30 µM of **Pd-PPh3**, 1 mg/mL **P1**, in water at 37 °C monitored by UV-Vis spectroscopy over time at λ = 400 nm.

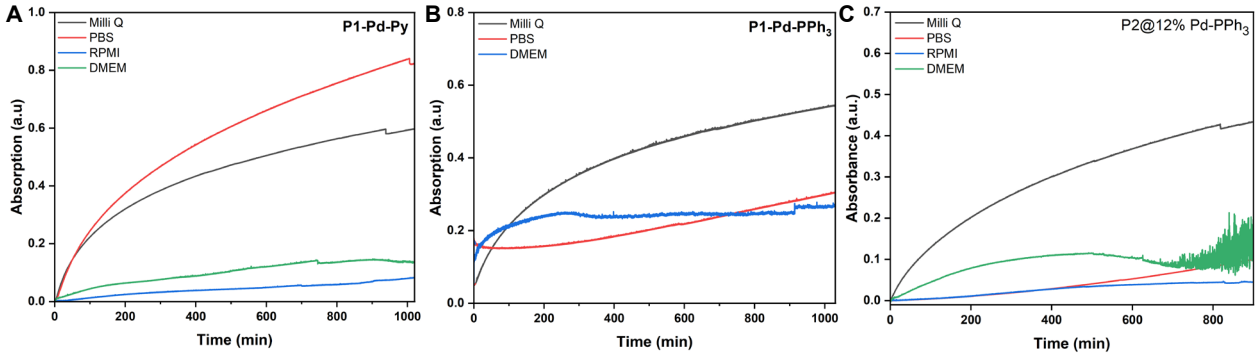

Figure S47. Reaction compatibility in complex media, PBS, RPMI and DMEM; pro-DNP (**4**) (100 µM) to DNP (**5**) using 30 µM of **Pd** at 37 °C monitored by UV-Vis spectroscopy over time at λ = 400 nm; A). **P1-Pd-Py**, B). **P1-Pd-PPh3**, C). **P2@12% Pd-PPh3**.

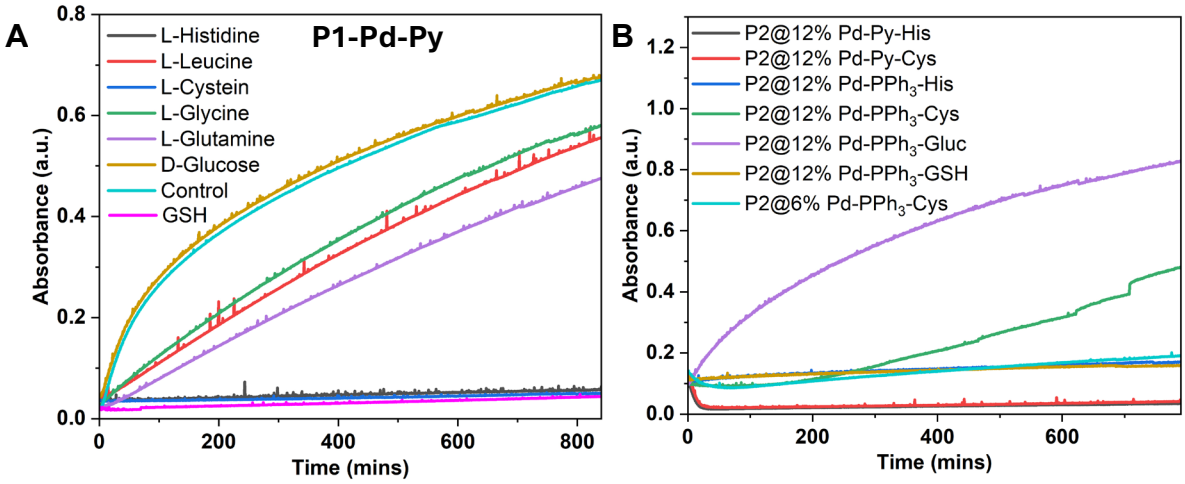

Figure S48. Pd deactivation pathway studies; pro-DNP (**4**) (100 µM) to DNP (**5**) using 30 µM of **Pd** at 37 °C monitored by UV-Vis spectroscopy over time at λ = 400 nm; A). **P1-Pd-Py** against 30 µM of L-glycine, L-cysteine, L-leucine, L-glutamine, L-histidine, D-glucose, and glutathione B). **P2@12% Pd-Py**, **P2@12% Pd-PPh3**, **P2@6% Pd-PPh3**.

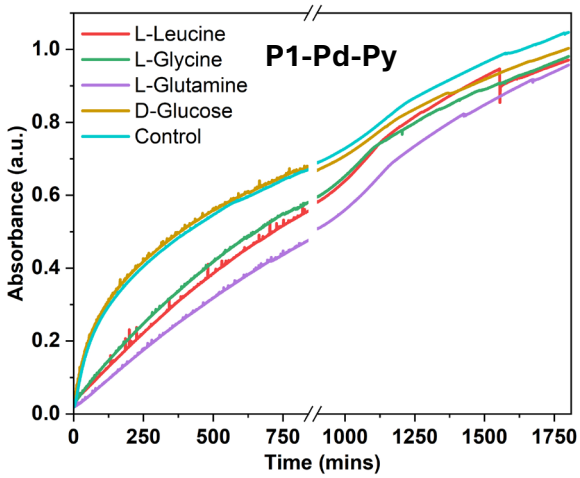

Figure S49. Pd NPs reusability studies; pro-DNP (**4**) (100 µM) to DNP (**5**) using 30 µM of **Pd** at 37 °C monitored by UV-Vis spectroscopy over time at λ = 400 nm; after the first run (15 h), additional 100 µM pro-DNP (**4**) was added and the kinetics were followed continuously. The reusability of the Pd NPs were tested in the presence of 30 µM of L-glycine, L-leucine, L-glutamine and D-glucose as well.

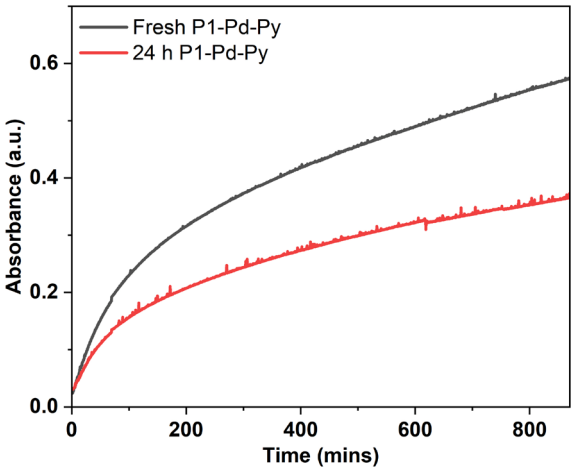

Figure S50. Pd nanoparticles stability (long term pre-incubation) study; pro-DNP (**4**) (100 µM) to DNP (**5**) using 30 µM of freshly prepared **P1-Pd-Py** against 24 h preformed **P1-Pd-Py** particles at 37 °C monitored by UV-Vis spectroscopy over time at λ = 400 nm.

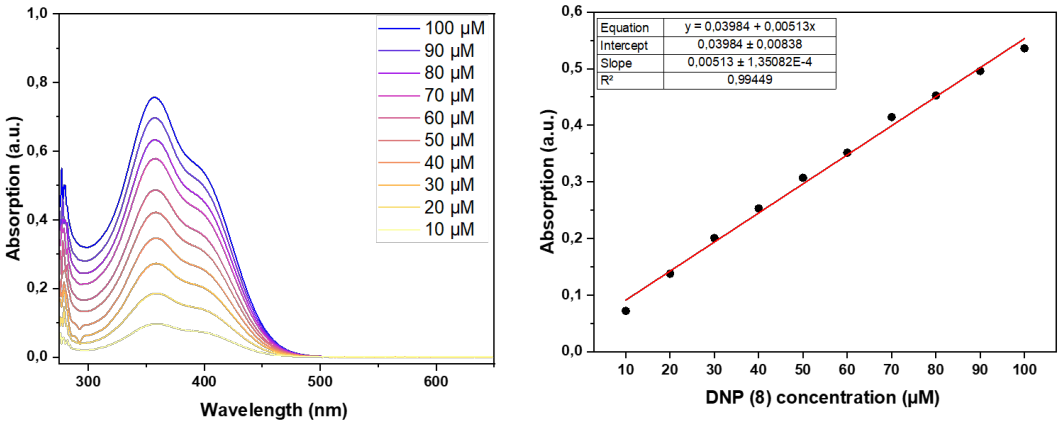

Figure S51. The calibration curve with known concentrations of DNP (**5**) using UV-Vis spectroscopy.

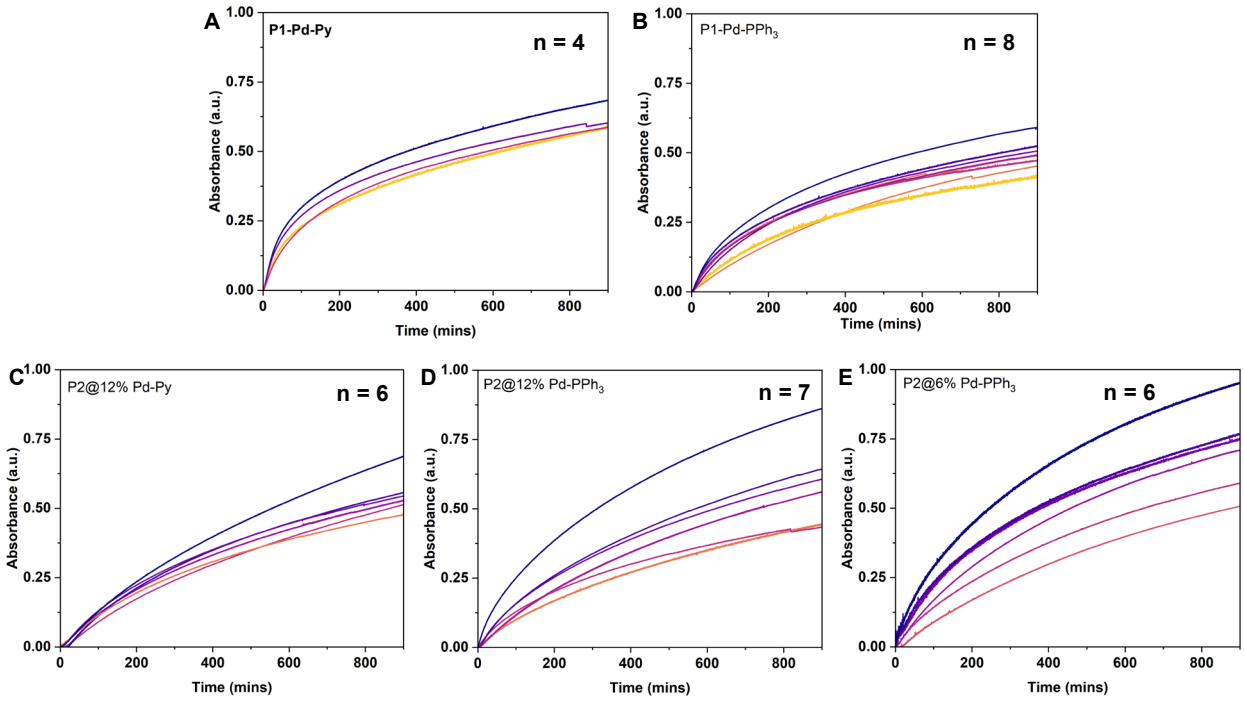

Figure S52. Kinetics profile of the pro-DNP (**4**) (100 μM) to DNP (**5**) monitored by UV-Vis over time at λ = 400 nm in water at 37 °C using 30 μM of Pd performed multiple independent (n) runs; A). **P1-Pd-Py** B). **P1-Pd-PPh$_3$** C). **P2@12% Pd-Py** D). **P2@12% Pd-PPh$_3$** E). **P2@6% Pd-PPh$_3$**.

S. No	Pd nanoparticles	$T_{1/2}$ mean value (mins)	N (number of independent reactions)
1	**P1-Pd-Py**	146	4
2	**P1-Pd-PPh$_3$**	307	8
3	**P2@12% Pd-Py**	338	6
4	**P2@12% Pd-PPh$_3$**	310	7
5	**P2@6% Pd-PPh$_3$**	218	6

Table S6. Determination of $T_{1/2}$ (time taken for 50 % formation of DNP (**5**), approximate time taken to reach 0.3 absorbance based on the calibration curve) for all **P1** and **P2** Pd nanoparticles (30 μM) in the pro-DNP (**4**) (100 μM) activation to DNP (**5**) monitored by UV-Vis over time at λ = 400 nm in water at 37 °C; performed multiple independent (n) runs.

5.2. Pro-DNP (4) activation by HPLC-UV (high-performance liquid chromatography with ultraviolet)

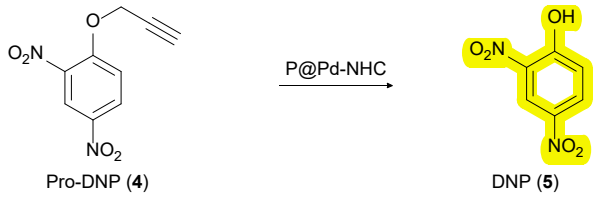

In order to avoid the ambiguities of the absorbance overlap of Pd complexes and/or polymers over the quantification of DNP by UV-Vis study, the formation of the DNP (**5**) was further quantified using HPLC as well. Independent reactions were performed under identical conditions as like UV-Vis experiments except instead of cuvettes, glass vials were used for the reaction. Reactions were performed at 37 ℃ in a pre-heated water bath, using 100 µM substrate pro-DNP (**4**) and 30 µM Pd concentration in 3 mL water. The samples were aliquoted periodically, diluted with 50% ACN by volume which was then injected to HPLC.

HPLC method

High performance liquid chromatography (HPLC) – UV experiments were performed using Shimadzu UFLC-XR with PDA detector with water + 0.1% formic acid (A) and acetonitrile + 0.1% formic acid (B) as eluents on a Kinetex 5 µm EVO C18 100 Å, with an LC column of 50 x 2.1 mm. A/B = 70/30 isocratic for 10 min monitored at λ = 300 nm (flow rate = 0.3 mL/min).

S. No	**Pd nanoparticles**	**Pro-DNP (4) (µM)**	**DNP (5) (µM)**
1	**P1-Pd-Py***	3.1	87.0
2	**P1-Pd-PPh$_3$**	29.4	58.1
3	**P2@12% Pd-Py**	30.1	71.0
4	**P2@12% Pd-PPh$_3$**	10.5	85.4
5	**P2@6% Pd-PPh$_3$**	n.d.	99.3

Table S7. HPLC quantification after 24 h in the pro-DNP (**4**) activation; reaction condition: pro-DNP (**4**) (100 µM), Pd (30 µM), in water (3 mL) at 37 °C; *40 µM of Pd used for the reaction due to a calculation error, n.d. not detected.

S. No	**Pd nanoparticles**	**Pro-DNP (4) (µM)**	**DNP (5) (µM)**
1	**P1-Pd-Py***	80.9	9.4
2	**P1-Pd-PPh$_3$**	91.2	2.2
3	**P2@12% Pd-Py**	106.0	n.d.
4	**P2@12% Pd-PPh$_3$**	92.3	2.0
5	**P2@6% Pd-PPh$_3$**	105.0	2.7

Table S8. HPLC quantification after 24 h in the pro-DNP (**4**) activation; reaction condition: pro-DNP (**4**) (100 µM), Pd (30 µM), in DMEM (3 mL) at 37 °C; *40 µM of Pd used for the reaction due to a calculation error, n.d. not detected.

S. No	DNP (μM) injected	DNP measured (μM)		
		Neat DNP*	DNP in presence of polymer[#]	DNP in presence of polymer[#] + pro-DNP[$]
1	20	19.8	20.9	20.2
2		19.9	21.0	20.4
3	50	50.1	44.3	48.8
4		49.8	45.3	49.8
5	80	79.4	79.4	80.0
6		79.6	80.1	82.0

Table S9. Effect of the presence of polymer and/or pro-DNP in the HPLC quantification of DNP; HPLC measured with known concentration of DNP (**4**)* (20/50/80 μM), and also in presence of 0.69 mg of **P2@12% Pd-PPh$_3$** polymer[#] and pro-DNP (**5**)[$] (80/50/20 μM) to test accuracy of HPLC measurements.

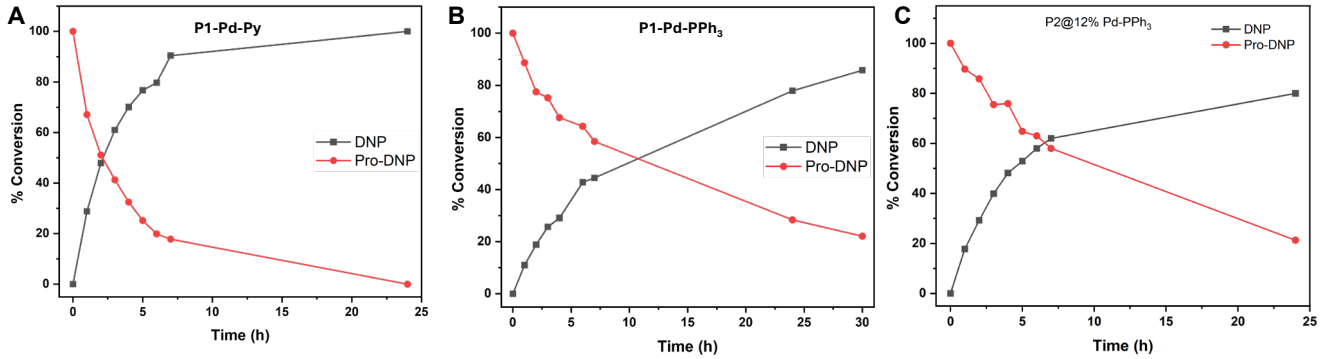

Figure S53. Kinetics profile of the consumption of pro-DNP (**4**) and formation of DNP (**5**) monitored by HPLC over time; reaction condition: pro-DNP (**4**) (100 μM), Pd (100 μM), in water (3 mL) at 37 °C; A). **P1-Pd-Py** B). **P1-Pd-PPh$_3$** C). **P2@12% Pd-PPh$_3$**.

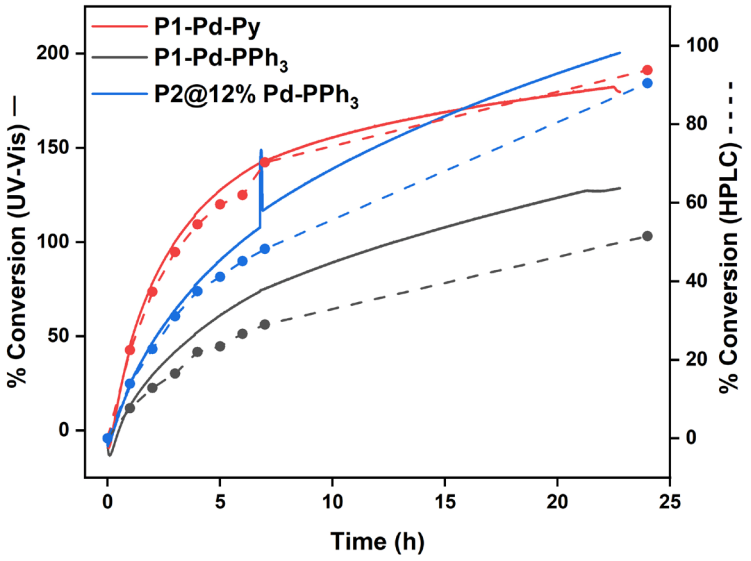

Figure S54. Simultaneous monitoring of the kinetics profile of pro-DNP (**4**) activation in UV-vis spectroscopy and HPLC; reaction condition: pro-DNP (**4**) (100 µM), Pd (100 µM), water (3 mL) at 37 °C, 800 rpm stirring, reaction performed at the UV spectrophotometer, for HPLC samples aliquoted from the same reactions; left axis: UV-Vis conversion (smooth line); right axis: HPLC conversion (dotted line).

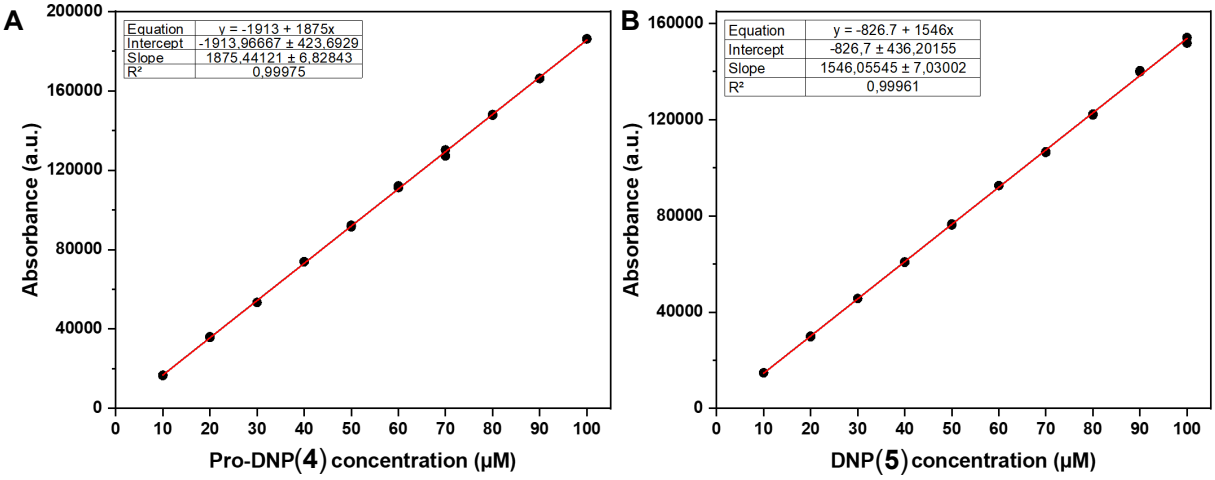

Figure S55. Calibration curves measured in HPLC with known concentrations of A). pro-DNP (**4**) and B). DNP (**5**).

5.3. Pro-cou (6) activation by fluorescence spectroscopy

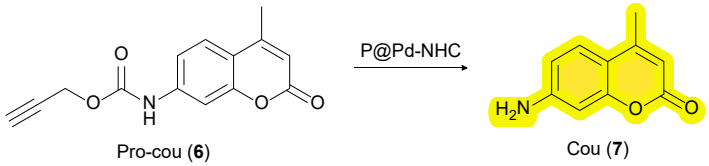

The catalytic efficiency of the palladium NHC catalyst containing, encapsulated **P1** and covalent **P2** nanoparticles were tested in the carbamate cleavage reaction of pro-coumarin (**6**) to coumarin (**7**) which emits at 440 nm (λex = 370 nm) that can be quantified using fluorescence spectroscopy. Reactions were performed at 37 °C, using 100 μM substrate pro-cou (**6**) and 30 μM Pd concentration in 3 mL water using 10 mm fluorescence cuvettes with stirring and the reaction progress was monitored in real-time on Agilent Cary eclipse fluorescence spectrophotometer using 1 cm × 1 cm pathlength quartz cuvettes.

S.No	Nanoparticles	Concentration in 3 mL		P to Pd molar ratio (P:Pd)	Polymer Wt. in 3 mL (mg)
		Polymer (μM)	Pd (μM)		
1	**P1-Pd-Py**	5.29	30	1:5.7	3
2	**P1-Pd-PPh$_3$**	5.29	30	1:5.7	3
3	**P2@12% Pd-Py**	1.23	30	1:24.4	0.675
4	**P2@12% Pd-PPh$_3$**	1.23	30	1:24.4	0.69
5	**P2@6% Pd-PPh$_3$**	2.45	30	1:12.2	1.30

Table S10. Reaction condition and concentrations. Substrate pro-cou (**6**) 100 μM, Pd 30 μM, 37 °C, water 3 mL. The formation of cou (**7**) was monitored at λem = 440 nm (λex = 370 nm) using fluorescence spectrophotometer over time.

P1-Pd-Py

Polymer (**P1**) was pre-dissolved in water. Stock solutions of Pd-NHC complex (**2**) was prepared in DMSO (10 mg / mL). Pro-cou (**6**) stock solution were prepared in DMSO at 50 mM concentration. To a 3 mg of **P1** polymer in 2.988 mL water (1 mg / mL), 5.88 μL DMSO stock of Pd-NHC complex (**2**) was added (for 30 μM Pd) vortexed and sonicated. Then, 6.0 μL DMSO stock of pro-cou (**6**) was added (100 μM), rapidly mixed and kinetics measurements were performed immediately at a preset 37 °C using fluorescence spectrophotometer. The DMSO content is 0.4 % *v/v* in the final water solution.

P1-Pd-PPh$_3$

Polymer (**P1**) was pre-dissolved in water. Stock solutions of Pd-NHC complex (**3**) was prepared in DMSO (10 mg / mL). Pro-cou (**6**) stock solution were prepared in DMSO at 50 mM concentration. To a 3 mg of **P1** polymer in 2.987 mL water (1 mg / mL), 7.53 μL DMSO stock of Pd-NHC complex (**3**) was added (for 30 μM Pd) vortexed and sonicated. Then, 6.0 μL DMSO stock of pro-cou (**6**) was added (100 μM), rapidly mixed and kinetics measurements were performed immediately at a preset 37 °C using fluorescence spectrophotometer. The DMSO content is 0.4 % *v/v* in the final water solution.

P2

The weighed samples of **P2@12% Pd-Py** (0.675 mg), **P2@12% Pd-PPh3** (0.69 mg) and **P2@6% Pd-PPh3** (1.30 mg) polymers were directly dissolved in 2.994 mL water, vortexed, sonicated (for 30 µM Pd). Pro-cou (**6**) stock solution were prepared in DMSO at 50 mM concentration. Then, 6.0 µL DMSO stock of pro-cou (**6**) was added (100 µM), rapidly mixed and kinetics measurements were performed immediately at a preset 37 °C using fluorescence spectrophotometer. The DMSO content is 0.2 % *v/v* in the final water solution.

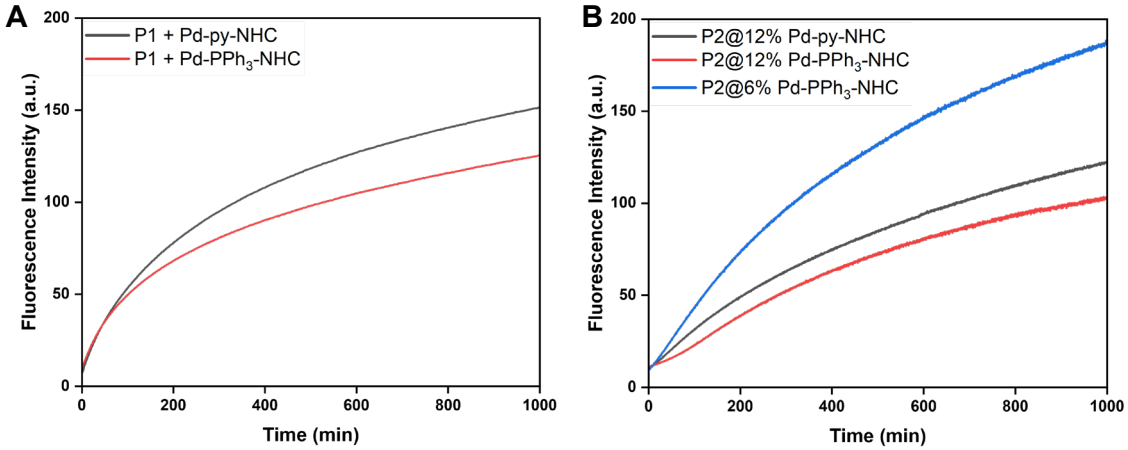

Figure S56. Kinetics profile of the pro-cou (**6**) (100 µM) to cou (**7**) monitored by fluorescence spectroscopy over time at λem = 440 nm (λex = 370 nm) in water at 37 °C using 30 µM of Pd; A). encapsulated **P1-Pd-Py** and **P1-Pd-PPh3** particles B). covalent **P2@12% Pd-Py**, **P2@12% Pd-PPh3** and **P2@6% Pd-PPh3** particles.

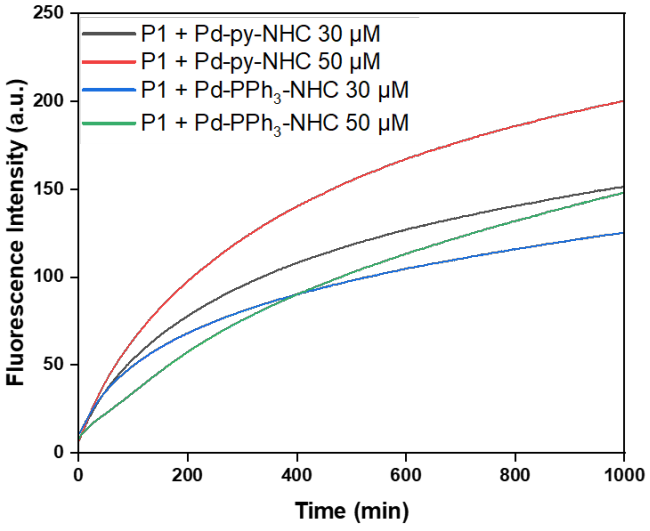

Figure S57. Catalyst concentration variation study; pro-cou (**6**) (100 µM) to cou (**7**) using 1 mg/mL **P1**, while varying **Pd-Py** and **Pd-PPh3**.concentrations (30 and 50 µM) in water at 37 °C monitored by fluorescence spectroscopy over time at λem = 440 nm (λex = 370 nm).

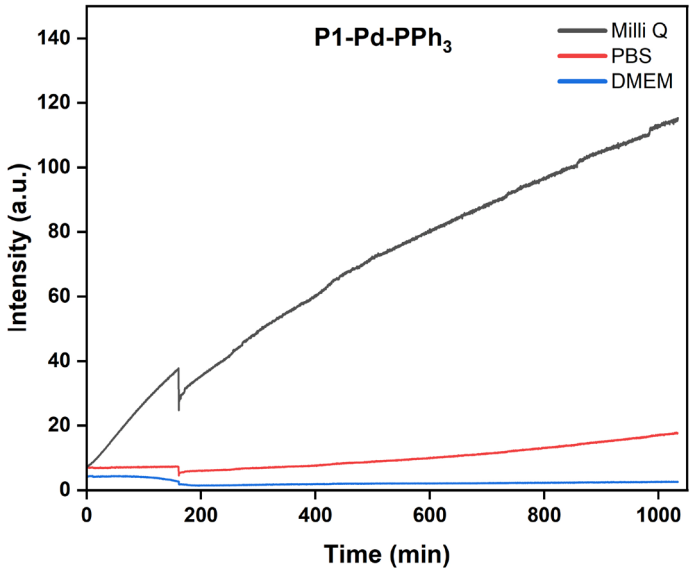

Figure S58. Reaction compatibility in complex media, PBS and DMEM; pro-cou (**6**) (100 µM) to cou (**7**) using 30 µM of **Pd** at 37 °C monitored by fluorescence spectroscopy over time at λem = 440 nm (λex = 370 nm).

5.4. Pro-cou (6) activation by HPLC-UV

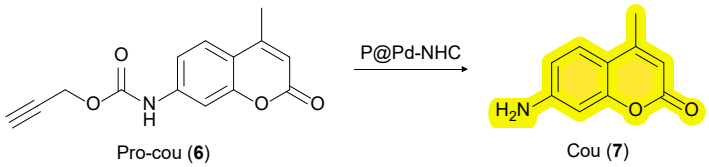

In order to validate the quantification of formed coumarin during catalysis runs, cou (**7**) was further quantified using HPLC as well. Independent reactions were performed under identical conditions as like fluorescence experiments except instead of fluorescence cuvettes, glass vials were used for the reaction. Reactions were performed at 37 °C in a pre-heated water bath, using 100 µM substrate pro-cou (**6**) and 30 µM Pd concentration in 3 mL water. The samples were aliquoted periodically, diluted with 50% ACN by volume which was then injected to HPLC.

HPLC method

High performance liquid chromatography (HPLC) – UV experiments were performed using Shimadzu UFLC-XR with PDA detector with water + 0.1% formic acid (A) and acetonitrile + 0.1% formic acid (B) as eluents on a Kinetex 5 µm EVO C18 100 Å, with an LC column of 50 x 2.1 mm. A/B = 80/20 isocratic for 10 min monitored at λ = 346 nm (flow rate = 0.3 mL/min).

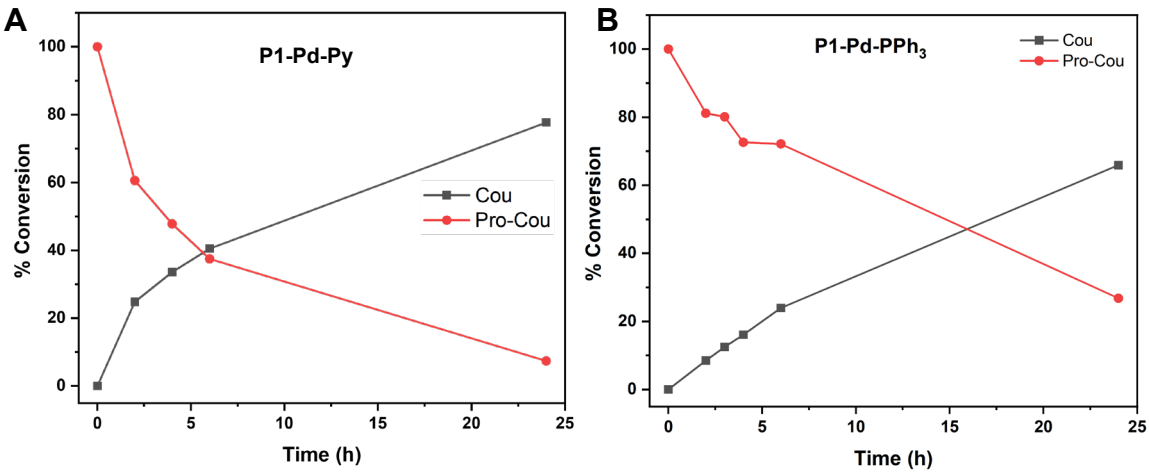

Figure S59. Kinetics profile of the consumption of pro-cou (**6**) and formation of cou (**7**) monitored by HPLC over time; reaction condition: pro-cou (**6**) (100 µM), Pd (100 µM), in water (3 mL) at 37 °C; A). **P1-Pd-Py** B). **P1-Pd-PPh3**.

S. No	Pd nanoparticles	Pro-cou (6) (µM)	cou (7) (µM)
1	**P1-Pd-Py***	40.9	67.5
2	**P1-Pd-PPh3**	37.2	72.8
3	**P2@12% Pd-Py**	69.9	37.3
4	**P2@12% Pd-PPh3**	67.8	39.8
5	**P2@6% Pd-PPh3**	59.3	59.1

Table S11. HPLC quantification after 24 h in the pro-cou (**6**) activation; reaction condition: pro-cou (**6**) (100 µM), Pd (30 µM), in water (3 mL) at 37 °C; *40 µM of Pd used for the reaction due to a calculation error.

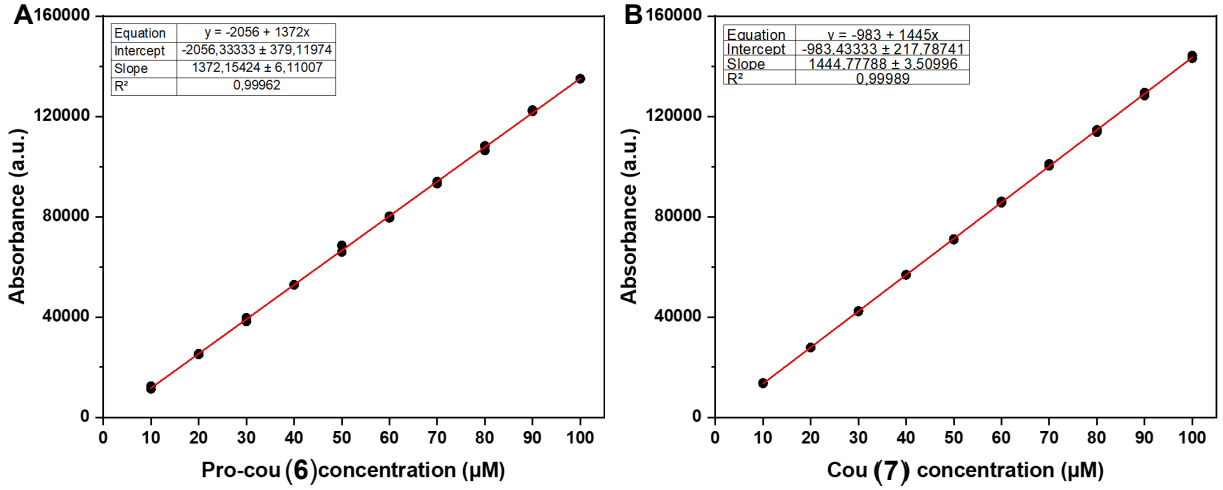

Figure S60. Calibration curves measured in HPLC with known concentrations of A). pro-cou (**6**) and B). cou (**7**).

6. Cell viability study

Cytotoxicity of all the polymeric Pd nanoparticles were evaluated using cell counting kit-8 (CCK-8) assay. 5000 HeLa cells/well were seeded in a 96-well plate in complete DMEM media and cultured for 24 h. Later, the media was replaced with fresh media and varying concentrations of polymeric Pd nanoparticle prepared in fresh media and incubated for 24 h. After that, the media was removed and the cells were washed with PBS followed by addition of media (90 µL) and CCK-8 (10 µL) to each well and incubated further for 3 h at 37 °C. After 3 h, the plate was taken out and absorbance was recorded at 450 nm in a microplate reader to estimate cell viability. For each concentration, three technical replicates were performed.

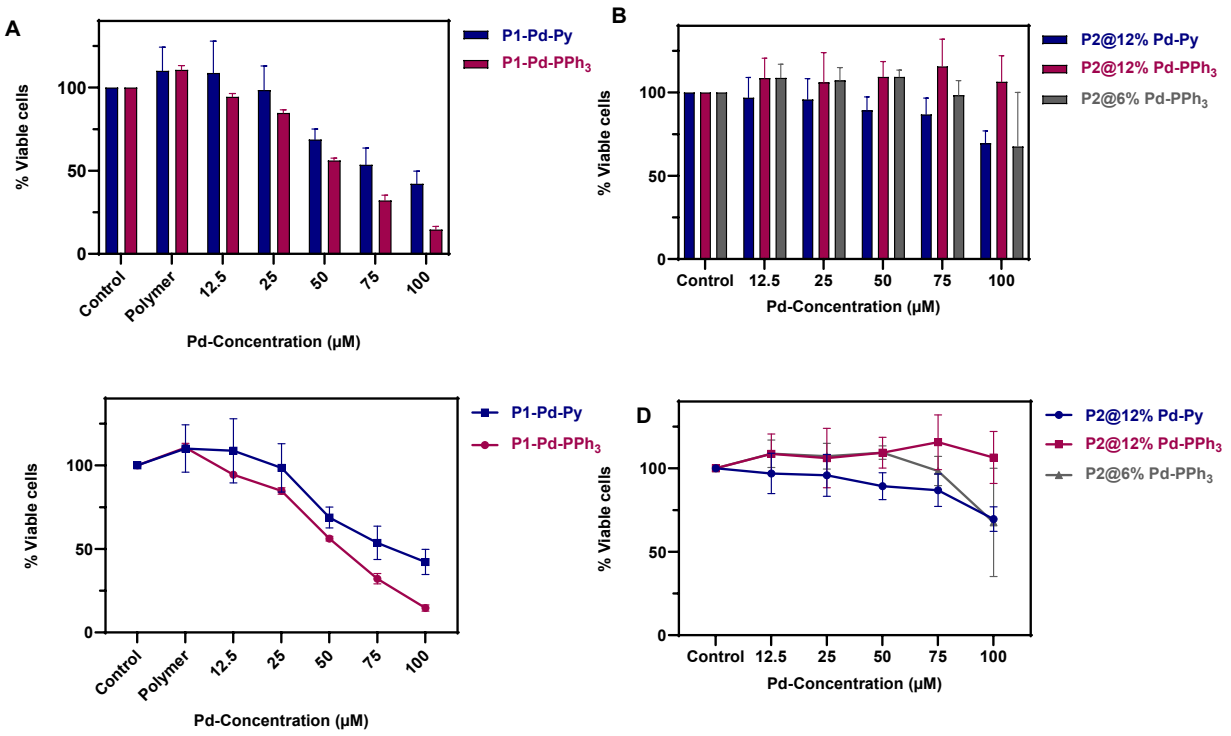

Figure S61. Cell viability assay in HeLa cells with A) Encapsulated **P1-Pd-Py** and **P1-Pd-PPh3** particles B) Covalently attached **P2@12% Pd-Py**, **P2@12% Pd-PPh3** and **P2@6% Pd-PPh3** polymeric nanoparticles C) growth inhibition curve of encapsulated **P1-Pd-Py** and **P1-Pd-PPh3** particles D) growth inhibition curve of covalently attached **P2@12% Pd-Py**, **P2@12% Pd-PPh3** and **P2@6% Pd-PPh3** polymeric nanoparticles; incubation time 24 h; the amount of viable cells was analyzed by CCK-8 assays in replicates of 3; control = 5000 untreated HeLa cells as negative cell control, polymer = 10 µM **P1** as negative polymer control in **P1** particles.

7. Recent Pd mediated bioorthogonal transformations

Table S12. Recent literature overview of Pd mediated bioorthogonal prodye/prodrug activations.

S.No	Catalyst	Carrier	Application	Refs
1	Pd(0) Reduced from K_2PdCl_4	Molecular cage (RCC3)	Activation of coumarin in 3T3 cells Activation of 5-fluorouracil in HeLa cells 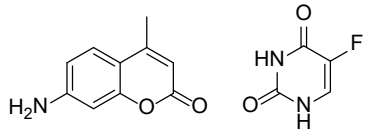	5
2	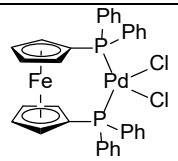	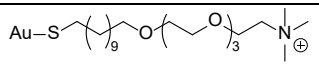 (TTMA)-functionalized gold NPs (encapsulation)	Activation of imiquimod (RAW 264.7 cells) and rhodamine (PBS) 10 μM substrate; 11.6 μM Pd 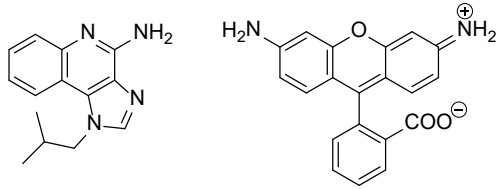	6
3	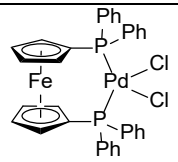	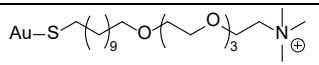 (TTMA)-functionalized gold NPs (encapsulation)	Activation of coumarin in PBS 10 μM substrate; 0.5 μM Pd 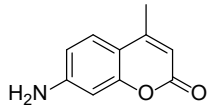	7
4	Pd(0) Reduced from K_2PdCl_4	Extracellular vesicles	Activation of paclitaxel in mice 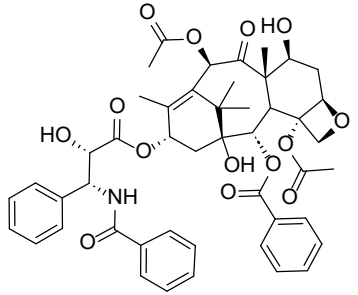	8
5	Pd(0)	Polyvinylpyrrolidone	Activation of coumarin in A549 cells	9

	Reduced from Na_2PdCl_4	Gallium–Indium alloy	Activation of 5-fluorouracil in mice 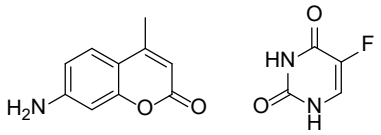	
6	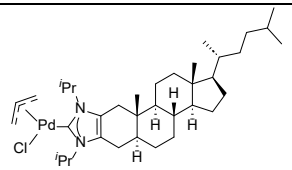	Pd catalyst fused into cholesterol	Activation of umbelliferone in E. coli cells 100 μM substrate; 100 μM Pd 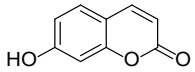	10
7	Pd(0) Reduced form $Pd(NO_3)_2$	Co@ZIF-8 MOF tagged with cDNA and mDNA	Activation of coumarin and 5-fluorouracil in MCF7 cells 5FU in 4T1 tumor-bearing mice 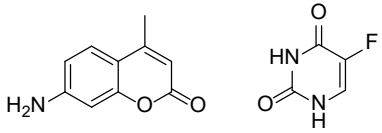	11
8	Pd(0) Reduced from $Pd(PPh_3)_2Cl_2$	Pd catalyst covalently linked to amphiphilic polyacrylamide via phosphine ligand	Activation of rhodamine in HepG2 cells 25 μM substrate; 60 μM Pd Activation of 5-fluorouracil (100 μM substrate; 100 μM Pd) in HepG2 cells Activation of doxorubicin (10 μM substrate; 20 μM Pd) in HepG2 cells 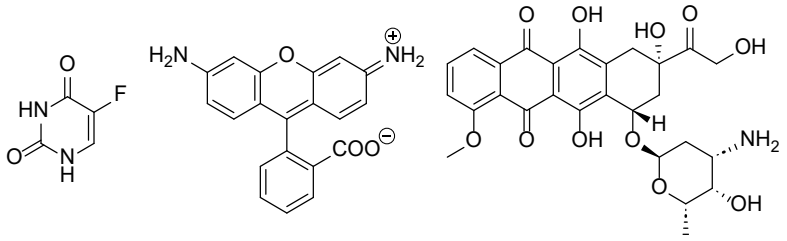	12 (Our group)
9	AuPd alloy NPs	Poly(lactic-co-glycolic acid) PLGA and SiO_2	Activation of rhodamine (100 μM substrate) in PBS Activation of paclitaxel in A549 cells	13

			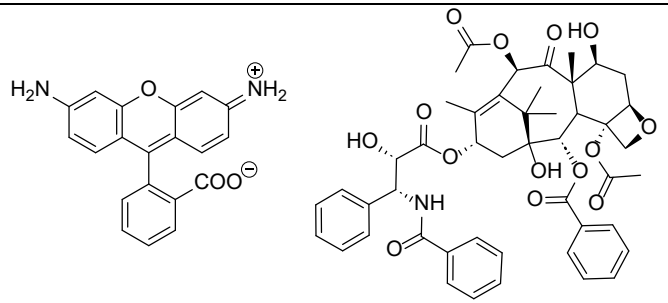	
10	Pd(II)-MOF	Mesoporous MOF	Activation of RNA	14
11	Pd(0) Reduced from H_2PdCl_4	MOF UiO-66	Activation of coumarin, rhodamine in PBS Activation of imiquimod in mice 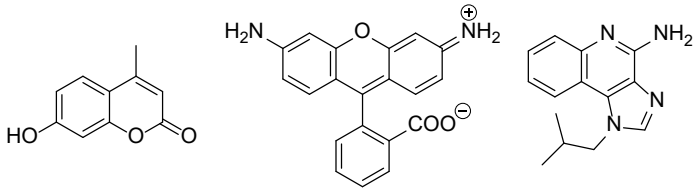	15
12	$Pd(OAc)_2$	Peptide	Activation of paclitaxel and Suzuki synthesis of linifanib in A549 cells 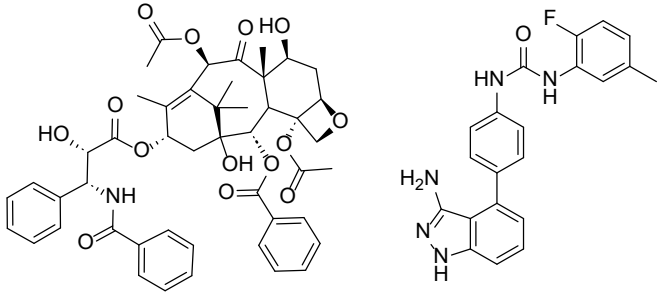	16
13	$Pd(PPh_3)_2Cl_2$	Pd catalyst covalently linked to amphiphilic polyacrylamide via phosphine ligand	Activation of DNP, coumarin, rhodamine in water, PBS, DMEM 100 μM substrate; 30 μM Pd Activation of 5-fluorouracil, paclitaxel, doxorubicin in water, PBS, DMEM	17 (Our group)

			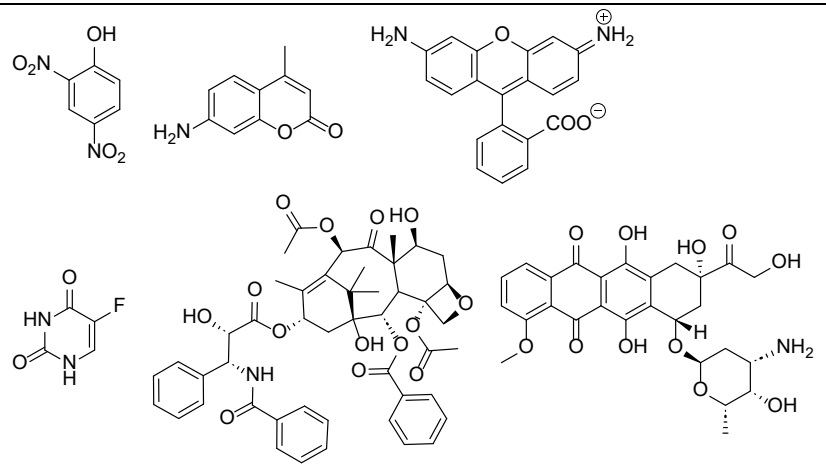	
14	Pd(0) Reduced from K_2PdCl_4	Matérial Institut Lavoisier-101 (MIL-101[Fe])	Activation of coumarin in HeLa cells Activation of 5-fluorouracil in mice 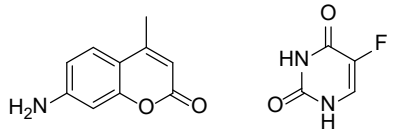	18
15	Pd(0) Reduced from K_2PdCl_4	MOF UiO-66 tagged with AS1411 aptamer	Activation of rhodamine in HEK-293T cells Activation of 4-hydroxytamoxifen in HeLa cells 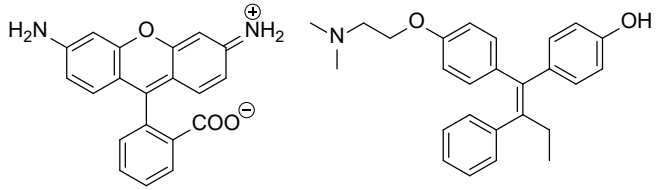	19
16	Pd(0) Reduced from Na_2PdCl_4	Tris(3-sulfophenyl)phosphine trisodium salt (TPPTS)	Activation of duocarmycin, doxorubicin, resorufin and rhodamine in SKBR3 cells	20

			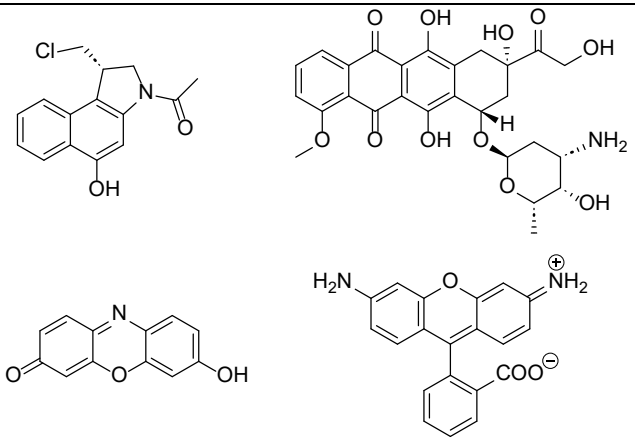	
17	Pd(0)-MOF Reduced from K_2PdCl_4	PMA (poly[isobutylene-alt-maleic anhydride]-graft-dodecyl) polymer	Activation of coumarin, 2-(2′-hydroxyphenyl) benzothiazole, cresyl violet 5 in HeLa cells 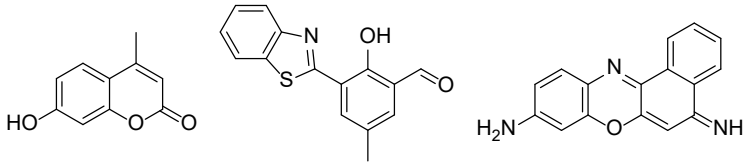	21
18	Pd(ethylenediamine)Cl_2	Peptide (bishistidine)	Activation HBTPQ probe in HeLa cells 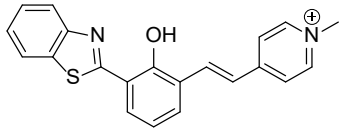	22
19	Pd(0) Reduced from K_2PdCl_4	Exosomes	Activation of resorufin in PBS. Activation of pan-histone deacetylase (HDAC) inhibiting drug in U87 and A549 cells 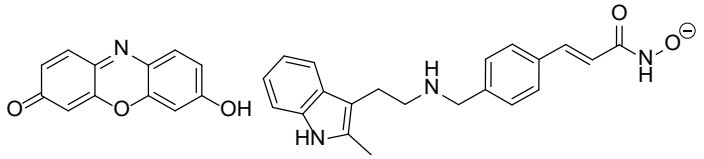	23

20	Pd(0) Reduced from H_2PdCl_4	β-cyclodextrin tagged and silica NPs with azobenzene	Light controlled on-off catalysis Activation of coumarin, rhodamine, 5-fluorouracil and Suzuki reaction in HeLa cells 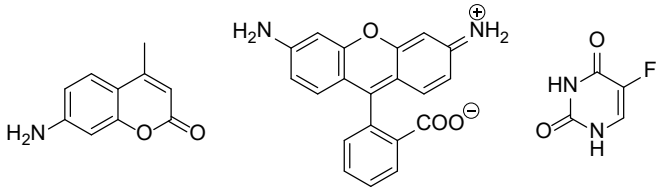	24
21	$Pd(cod)Cl_2$	50% DMSO/H_2O	Doxorubicin release (mediated by 10 Equiv. of $Pd(cod)Cl_2$) from a cysteine bearing protein (nanobody–drug conjugate) in HEK 293 and MCF7 cells 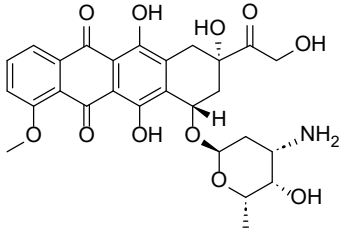	25
22	Na_2PdCl_4	Amphiphilic acrylamide polymer	Activation of rhodamine and PDT in Hela cells 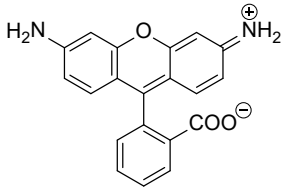	26 Our group
23	Pd(0) Reduced from $Pd(OAc)_2$	Styrene based resin (NovaSyn TG amino resin HL)	Doxorubicin activation in DU145 and U87 cells 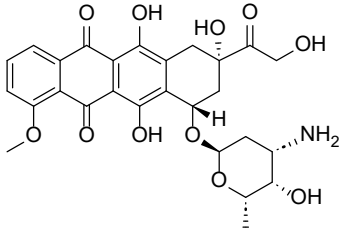	27

24	Pd(0) Reduced from $Pd(OAc)_2$	Styrene based resin (NovaSyn TG amino resin HL)	SN-38 activation in HCT116, U-87, and U-251 cells 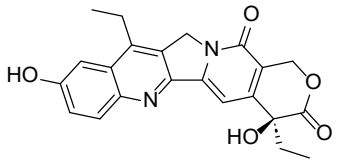	28
25	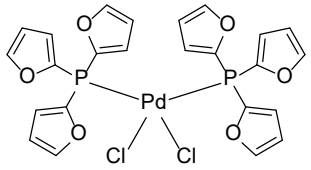	PLGA/PEG	Heck reaction (for coumarin) in HT1080 cells Activation of rhodamine in xenograft model Activation of doxorubicin in HT1080 cells 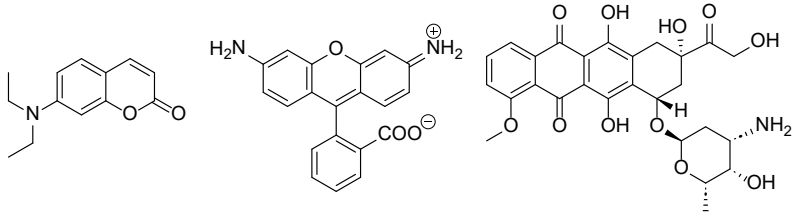	29
26	Pd(0) Reduced from $Pd(OAc)_2$	Polystyrene	Activation of cresyl-violet, 5-fluorouracil and a Suzuki drug synthesis in U87-MG cells 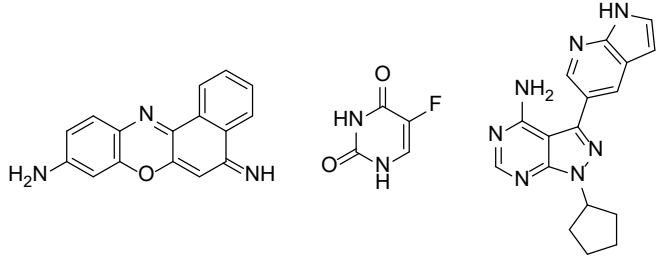	30
27	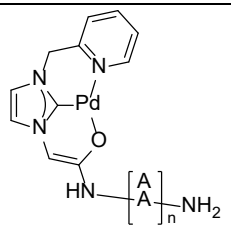	Cell penetrating peptide	Activation of rhodamine in PC-3 cells. 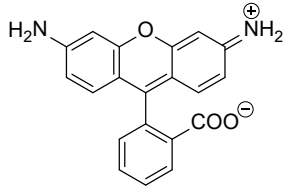	31

28	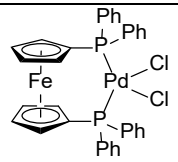	Au NPs	Activation of 5-fluorouracil in HeLa cells 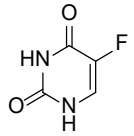	32
29	Pd(0) Reduced from $Pd(OAc)_2$	Polystyrene resin	Activation of floxuridine in BxPC-3 and HCT116 cells 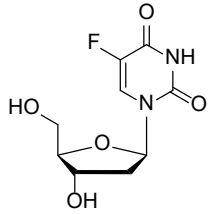	33
30	Pd(0) Reduced from $Pd(OAc)_2$	Polystyrene resin	Activation of 5-fluorouracil in BxPC-3 and HCT116 cells Activation of rhodamine in zebrafish embryo 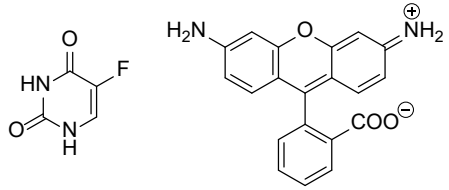	34
31	Pd(0) Reduced from $Pd(OAc)_2$	Polystyrene resin	Activation of gemcitabine in BxPC-3 and Mia PaCa-2 cells 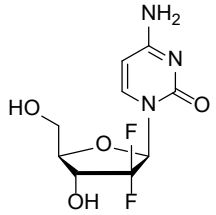	35
32	$Allyl_2Pd_2Cl_2$ $Pd(dba)_2$	-	Activation of rhodamine in HeLa, CHO, HEK293T, NIH3T3, Caco-2 and A549 cells, protein activation (GFP-N149-Lys) in HeLa cells	36

Table S13. Metal nanoparticle mediated synthesis of bioactive molecules.

S.No	Catalyst	Carrier	Application	Refs
1	$NiFe_2O_4$ NPs	Sodium alginate-g-poly(3-aminophenol)	Synthesis of polyhydroquinolines 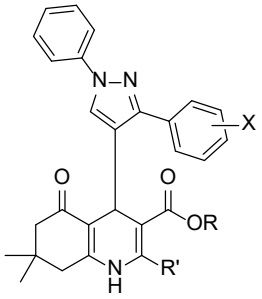	37
2	Fe_3O_4 NPs	Xanthan gum-thiacalix[4]arene	Synthesis of acridindions 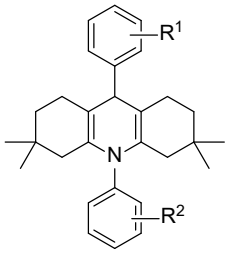	38
3	$ZnFe_2O_4$ NPs	Arabic gum (hydrolyzed)	Synthesis of pyranopyrazoles 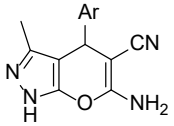	39
4	Fe_3O_4 NPs	Algin-functionalized silica	Synthesis of pyrazolopyridine 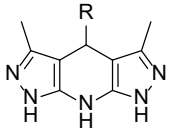	40

8. Well defined mixed NHC-Pd-phosphine complexes

Table S14. Mixed NHC-Pd-phosphine complexes reported in literature.

S.No	Pd-NHC	^{31}P NMR (ppm)	Refs
1	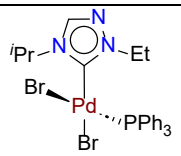	26.5	41
2	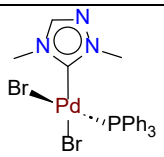	26.9	42
3	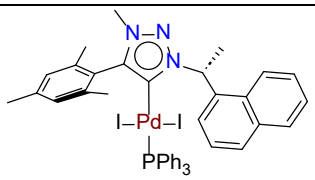	14.56	43
4	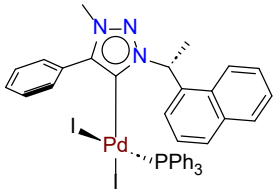	25.03	44
5	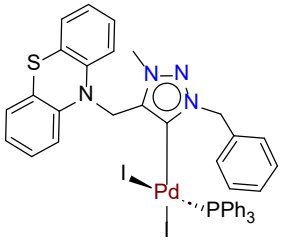	25.01	45
6	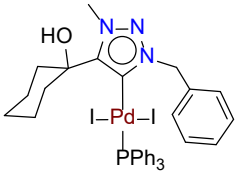	17.00	46
7	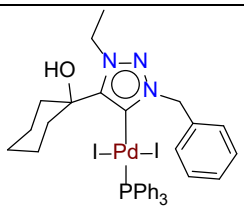	16.97	46

8	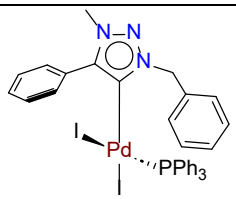	25.19	46
9	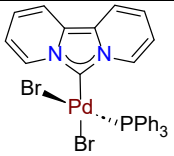	26.5	47
10	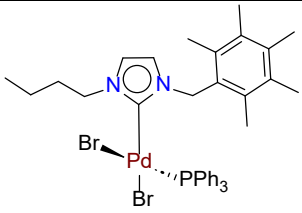	21.6	48
11	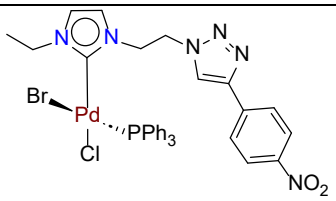	27.0	49
12	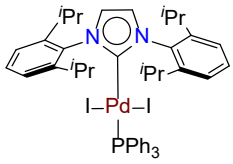	16.2	50
13	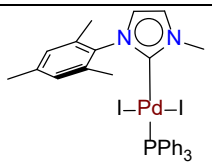	16.2	50
14	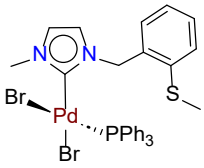	27.13	51, 52
15	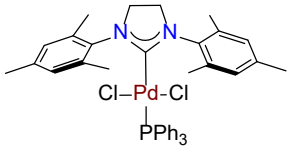	20.88	53
16	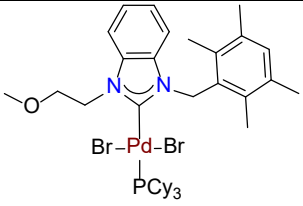	21.6	54

17	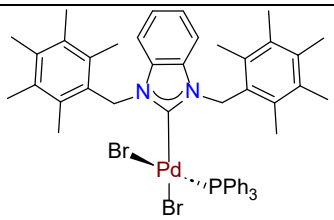	26.7	54
18	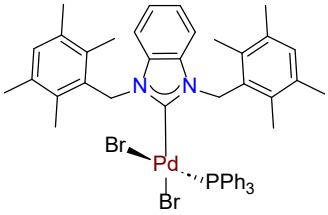	26.8	54
19	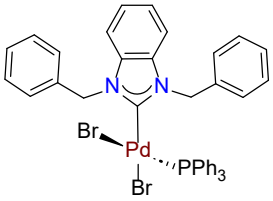	26.6	55
20	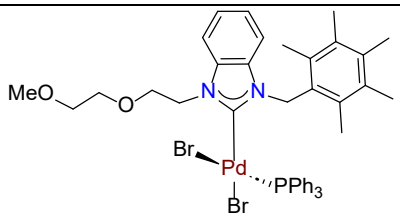	27.13	56
21	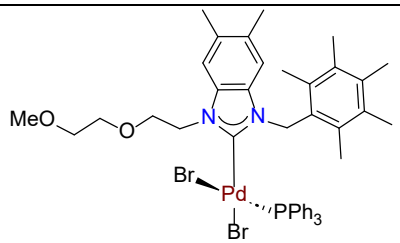	27.20	56
22	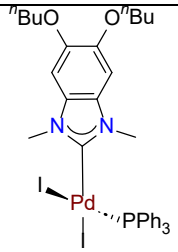	23.5	57
23	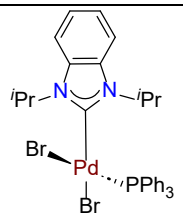	26.6	58

24	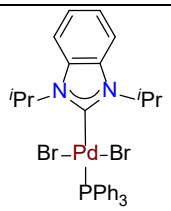	18.0	58
25	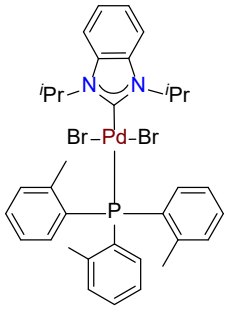	16.27	59
26	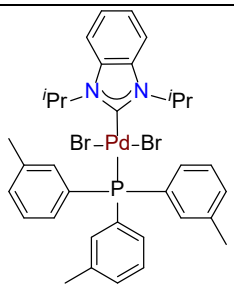	18.8	60

9. References

1 J. Brand, J. Siles and J. Waser, *Synlett*, 2010, 881–884.

2 L. Deng, A. Sathyan, C. Adam, A. Unciti-Broceta, V. Sebastian and A. R. A. Palmans, *Nano Lett.*, 2024, **24**, 2242–2249.

3 A. S. Al-Bogami, T. S. Saleh, A. E. M. Mekky and M. R. Shaaban, *J. Mol. Struct.*, 2016, **1121**, 167–179.

4 S. Wijker, D. Dellemme, L. Deng, B. Fehér, I. K. Voets, M. Surin and A. R. A. Palmans, *ACS Macro Lett.*, 2025, **14**, 428–433.

5 J. Tang, C. Li, W. Ma, Z. Ba, Z. Hu, I. Willner and C. Wang, *Angew. Chem. Int. Ed.*, 2025, **64**, e202503485.

6 X. Zhang, Y. Liu, M. Jiang, J. A. Mas-Rosario, S. Fedeli, R. Cao-Milan, L. Liu, K. J. Winters, C.-M. Hirschbiegel, A. Nabawy, R. Huang, M. E. Farkas and V. M. Rotello, *Chem. Sci.*, 2024, **15**, 2486–2494.

7 L. Liu, X. Zhang, S. Fedeli, Y. A. Cicek, W. Ndugire and V. M. Rotello, *Materials*, 2024, **17**, 1507.

8 M. Sancho-Albero, V. Sebastian, A. M. Perez-Lopez, P. Martin-Duque, A. Unciti-Broceta and J. Santamaria, *Cells*, 2024, **13**, 691.

9 L. Zhang, Y. Sang, Z. Liu, W. Wang, Z. Liu, Q. Deng, Y. You, J. Ren and X. Qu, *Angew. Chem. Int. Ed.*, 2023, **62**, e202218159; *Angew. Chem*. 2023, **135**, e202218159.

10 T. Wegner, A. Dombovski, K. Gesing, A. Köhrer, M. Elinkmann, U. Karst, F. Glorius and J. Jose, *Chem. Sci.*, 2023, **14**, 11896–11906.

11 Y. Zhang, L. Zhang, W. Wang, Q. Deng, M. Liu, Z. Zhu, H. Liu, J. Ren and X. Qu, *Angew. Chem. Int. Ed.*, 2023, **62**, e202306395.

12 L. Deng, A. Sathyan, C. Adam, A. Unciti-Broceta, V. Sebastian and A. R. A. Palmans, *Nano Lett.*, 2024, **24**, 2242–2249.

13 B. Rubio-Ruiz, A. M. Pérez-López, L. Uson, M. C. Ortega-Liebana, T. Valero, M. Arruebo, J. L. Hueso, V. Sebastian, J. Santamaria and A. Unciti-Broceta, *Nano Lett.*, 2023, **23**, 804–811.

14 J. Liu, X. Liu, Q. Liu, J. Cao, X. Lv, S. Wang, T. Tian, X. Zhou and H. Deng, *Angew. Chem. Int. Ed.*, 2023, **62**, e202302649.

15 Y. Wei, G. Qin, Z. Wang, C. Zhao, J. Ren and X. Qu, *ACS Nano*, 2023, **17**, 5808–5820.

16 A. M. Pérez-López, A. Belsom, L. Fiedler, X. Xin and J. Rappsilber, *J. Med. Chem.*, 2023, **66**, 3301–3311.

17 A. Sathyan, S. Croke, A. M. Pérez-López, B. F. M. de Waal, A. Unciti-Broceta and A. R. A. Palmans, *Mol. Syst. Des. Eng.*, 2022, **7**, 1736–1748.

18 S. Wu, L. Zhang, Y. Wei, T. Cui, J. Ren and X. Qu, *Chem. Mater.*, 2022, **34**, 8544–8550.

19 X. Chen, W. Cai, J. Liu, L. Mao and M. Wang, *ACS Appl. Mater. Interfaces*, 2022, **14**, 10117–10124.

20 J. Konč, V. Sabatino, E. Jiménez-Moreno, E. Latocheski, L. R. Pérez, J. Day, J. B. Domingos and G. J. L. Bernardes, *Angew. Chem. Int. Ed.*, 2022, **61**, e202113519; *Angew. Chem*. 2022, **134**, e202113519.

21 R. Martínez, C. Carrillo-Carrión, P. Destito, A. Alvarez, M. Tomás-Gamasa, B. Pelaz, F. Lopez, J. L. Mascareñas and P. del Pino, *Cell Rep. Phys. Sci.*, 2020, **1**, 100076.

22 S. Learte-Aymamí, C. Vidal, A. Gutiérrez-González and J. L. Mascareñas, *Angew. Chem. Int. Ed.*, 2020, **59**, 9149–9154.

23 M. Sancho-Albero, B. Rubio-Ruiz, A. M. Pérez-López, V. Sebastián, P. Martín-Duque, M. Arruebo, J. Santamaría and A. Unciti-Broceta, *Nat. Catal.*, 2019, **2**, 864–872.

24 F. Wang, Y. Zhang, Z. Du, J. Ren and X. Qu, *Nat. Commun.*, 2018, **9**, 1209.

25 B. J. Stenton, B. L. Oliveira, M. J. Matos, L. Sinatra and G. J. L. Bernardes, *Chem. Sci.*, 2018, **9**, 4185–4189.

26 Y. Liu, S. Pujals, P. J. M. Stals, T. Paulöhrl, S. I. Presolski, E. W. Meijer, L. Albertazzi and A. R. A. Palmans, *J. Am. Chem. Soc.*, 2018, **140**, 3423–3433.

27 T. L. Bray, M. Salji, A. Brombin, A. M. Pérez-López, B. Rubio-Ruiz, L. C. A. Galbraith, E. E. Patton, H. Y. Leung and A. Unciti-Broceta, *Chem. Sci.*, 2018, **9**, 7354–7361.

28 C. Adam, A. M. Pérez-López, L. Hamilton, B. Rubio-Ruiz, T. L. Bray, D. Sieger, P. M. Brennan and A. Unciti-Broceta, *Chem. Eur. J.*, 2018, **24**, 16783–16790.

29 M. A. Miller, B. Askevold, H. Mikula, R. H. Kohler, D. Pirovich and R. Weissleder, *Nat. Commun.*, 2017, **8**, 15906.

30 J. Clavadetscher, E. Indrigo, S. V. Chankeshwara, A. Lilienkampf and M. Bradley, *Angew. Chem. Int. Ed.*, 2017, **56**, 6864–6868.

31 E. Indrigo, J. Clavadetscher, S. V. Chankeshwara, A. Megia-Fernandez, A. Lilienkampf and M. Bradley, *Chem. Commun.*, 2017, **53**, 6712–6715.

32 G. Y. Tonga, Y. Jeong, B. Duncan, T. Mizuhara, R. Mout, R. Das, S. T. Kim, Y.-C. Yeh, B. Yan, S. Hou and V. M. Rotello, *Nat. Chem.*, 2015, **7**, 597–603.

33 J. T. Weiss, N. O. Carragher and A. Unciti-Broceta, *Sci. Rep.*, 2015, **5**, 9329.

34 J. T. Weiss, J. C. Dawson, K. G. Macleod, W. Rybski, C. Fraser, C. Torres-Sánchez, E. E. Patton, M. Bradley, N. O. Carragher and A. Unciti-Broceta, *Nat. Commun.*, 2014, **5**, 3277.

35 J. T. Weiss, J. C. Dawson, C. Fraser, W. Rybski, C. Torres-Sánchez, M. Bradley, E. E. Patton, N. O. Carragher and A. Unciti-Broceta, *J. Med. Chem.*, 2014, **57**, 5395–5404.

36 J. Li, J. Yu, J. Zhao, J. Wang, S. Zheng, S. Lin, L. Chen, M. Yang, S. Jia, X. Zhang and P. R. Chen, *Nat. Chem.*, 2014, **6**, 352–361.

37 S. M. Nezhad, A. Rahmavand, A. Kousha, M. M. Salehi, S. A. Pourmousavi, E. N. Zare, A. Maleki and P. Makvandi, *Int. J. Biol. Macromol.*, 2025, **315**, 144406.

38 F. Hassanzadeh-Afruzi, M. M. Salehi, G. Ranjbar, F. Esmailzadeh, P. Hanifehnejad, M. Azizi, F. Eshrati yeganeh and A. Maleki, *Sci. Rep.*, 2023, **13**, 22162.

39 F. Hassanzadeh-Afruzi, M. M. Salehi, G. Heidari, A. Maleki and E. N. Zare, *J. Mol. Struct.*, 2023, **1274**, 134490.

40 F. Hassanzadeh-Afruzi, Z. Amiri-Khamakani, M. Saeidirad, M. M. Salehi, R. Taheri-Ledari and A. Maleki, *RSC Adv.*, 2023, **13**, 10367–10378.

41 A. Kumar, M. K. Gangwar, A. P. Prakasham, D. Mhatre, A. Ch. Kalita and P. Ghosh, *Inorg. Chem.*, 2016, **55**, 2882–2893.

42 S. Guo and H. V. Huynh, *Organometallics*, 2014, **33**, 2004–2011.

43 T. Nath Saha, R. Naskar, A. Adak, B. Mondal and R. Maity, *Eur. J. Inorg. Chem.*, 2024, **27**, e202300630.

44 T. N. Saha, R. Naskar, K. Kundu, N. Yadav and R. Maity, *Appl. Organomet. Chem.*, 2023, **37**(8), e7135.

45 S. Dey and P. Ghosh, *ACS Omega*, 2023, **8**, 11039–11064.

46 S. Modak, M. K. Gangwar, M. Nageswar Rao, M. Madasu, A. Ch. Kalita, V. Dorcet, M. A. Shejale, R. J. Butcher and P. Ghosh, *Dalton Trans.*, 2015, **44**, 17617–17628.

47 V. Gierz, A. Seyboldt, C. Maichle-Mössmer, R. Fröhlich, F. Rominger and D. Kunz, *Eur. J. Inorg. Chem.*, 2012, 1423–1429.

48 R. Fırıncı, M. E. Günay, N. Özdemir and M. Dinçer, *J. Mol. Struct.*, 2017, **1146**, 267–272.

49 G. Gogolieva, J. Durand, O. Dechy-Cabaret and E. Gras, *J. Organomet. Chem.*, 2014, **769**, 7–10.

50 A. Flahaut, K. Toutah, P. Mangeney and S. Roland, *Eur. J. Inorg. Chem.*, 2009, 5422–5432.

51 H. V. Huynh, C. H. Yeo and Y. X. Chew, *Organometallics*, 2010, **29**, 1479–1486.

52 H. V. Huynh, C. H. Yeo and G. K. Tan, *Chem. Commun.*, 2006, 3833.

53 R. Sevinçek, H. Türkmen, M. Aygün, B. Çetinkaya and S. García-Granda, *Acta Crystallogr. C*, 2007, **63**, m277–m279.

54 H. Türkmen, T. Pape, F. E. Hahn and B. Çetinkaya, *Eur. J. Inorg. Chem.*, 2009, 285–294.

55 S. K. Yen, L. L. Koh, H. V. Huynh and T. S. A. Hor, *Aust. J. Chem.*, 2009, **62**, 1047–1053.

56 S. Gülcemal, S. Kahraman, J.-C. Daran, E. Çetinkaya and B. Çetinkaya, *J. Organomet. Chem.*, 2009, **694**, 3580–3589.

57 M. V. Baker, D. H. Brown, P. V. Simpson, B. W. Skelton and A. H. White, *Eur. J. Inorg. Chem.*, 2009, 1977–1988.

58 H. V. Huynh, Y. Han, J. H. H. Ho and G. K. Tan, *Organometallics*, 2006, **25**, 3267–3274.

59 J. N. Leung and H. V. Huynh, *Inorg. Chem.*, 2024, **63**, 18242–18250.

60 H. V. Huynh, Y. Han, R. Jothibasu and J. A. Yang, *Organometallics*, 2009, **28**, 5395–5404.